Numerical modeling of sediment transport over hydraulic structures

MSc Thesis
Vincent Vuik, June 2010

TU Delft

HKV LIJN IN WATER

Numerical modeling of sediment transport over hydraulic structures

MSc Thesis
Vincent Vuik, June 2010

Graduation committee:
Prof. dr. ir. H.J. de Vriend
Dr. ir. W. van Balen
Dr. ir. E. Mosselman
Dr. R.M.J. Schielen
Prof. dr. ir. W.S.J. Uijttewaal

Delft University of Technology
Faculty of Civil Engineering and Geosciences
Section of Hydraulic Engineering
Field of River Engineering

HKV Lijn in Water

TU Delft

HKV LIJN IN WATER

Preface

In this master thesis, a study of the modeling of sediment transport around hydraulic structures is presented. The work has been done at the Faculty of Civil Engineering and Geosciences of the Delft University of Technology and at the consulting company HKV LIJN IN WATER.

I would like to thank the members of my graduation committee, prof. dr. ir. H.J. de Vriend, dr. ir. W. van Balen, dr. ir. E. Mosselman, dr. R.M.J. Schielen and prof. dr. ir. W.S.J. Uijttewaal for your guidance during my graduation period. Your comments concerning content and your practical advices have been highly appreciated. Saskia van Vuren, thank you for sharing your Delft3D experience and giving your plain view on my work. Also thanks to Mathieu Pourquie for your help with the FLUENT sessions, and all others who I have not mentioned here. I would show my gratitude to HKV LIJN IN WATER for giving me the opportunity to do all this work. Finally thanks to all colleagues at HKV for the pleasant companion and nice conversations during the lunches.

Summary

Hydraulic structures are present in the designs of different Room for the River projects in the Netherlands. Examples are longitudinal weirs, groins, summer dikes and weirs in the inlet of a side channel. Morphological simulations with Delft3D are frequently carried out to investigate the effect of such projects on for example hindrance for shipping and dredging costs. It is important that also the physical processes around hydraulic structures are correctly modeled in these situations.

At the upstream slope of a hydraulic structure, the larger depth-averaged velocity causes an increased sediment transport capacity and increased actual bed shear stresses. The latter is reinforced by a change of the velocity distribution over the vertical with respect to uniform flow. Opposite, the gravity component along the slope results in a higher critical bed shear stress than in flat bottom conditions. At steep slopes, (partial) bed-load transport blockage could occur.

Delft3D is meant to model flow phenomena of which the horizontal length and time scales are significantly larger than the vertical scales. Near hydraulic structures, this is generally not the case. These structures are parameterized as weirs in a depth-averaged Delft3D model in engineering practice. The only effect of these weirs is an additional energy loss in the momentum equation. The parameterization aims at representing the influence of the weirs on the flow at larger scales. The local flow around the structures (including turbulence, vertical velocity components and actual shear stresses) is not correctly modeled. Moreover, there is no direct influence of the weir on sediment transport (like increased critical shear stresses and bed-load transport blockage). This inaccurate way of modeling could result in errors in the prediction of the morphological effects of hydraulic structures.

The objectives of this study are:

Current way of Delft3D modeling	Assessing the performance of the current way of Delft3D modeling of sediment transport around hydraulic structures in three-dimensional flows.
Recommended sediment transport modeling	Making recommendations on the modeling of sediment transport around hydraulic structures in hydraulic engineering practice.

The performance of Delft3D has been judged by comparing the results with the results of the numerical model FLUENT. FLUENT is an advanced flow modeling system, in which sediment transport can be studied by analyzing the trajectories of discrete particles. Firstly, some laboratory experiments describing flow and transport over structures have been modeled. In this way, the performance of both models has been investigated and mutually compared. The results of FLUENT gave confidence to use FLUENT as an instrument to judge the performance of Delft3D in modeling three-dimensional flow and transport over hydraulic structures.

A three-dimensional flow situation has been designed, which resembles the flow over a longitudinal weir. In Delft3D, all bed-load transport and suspended-load transport that reaches the weir also passes the weir. In FLUENT, this is not the case. Suspended-load transport is distributed between the main channel and the zone behind the weir in the same ratio as the discharge. The distribution of bed-load transport strongly depends on the particle

diameter. This difference shows that the parameterization of weirs in depth-averaged Delft3D models gives significant errors in the prediction of sediment transport over hydraulic structures, especially when bed-load transport is dominant.

The transport magnitude can be reduced by increasing the bed level points near the weir to crest level. In this schematization, nearly all bed-load transport is blocked and suspended-load transport is reduced. A weir without increased bed level points overestimates the sediment transport over the structure. When the bed level points are increased until crest level of the weir, the sediment transport over the weir is underestimated. The sediment transport over the weir can be tuned by an increased bed level somewhere between zero and crest level.

The distribution of sediment between the main channel (index 1) and the area behind the weir (index 2) can be described with a relation:

$$\frac{S_2}{S_1} = C \cdot \frac{Q_2}{Q_1}$$

The value of C as given by Delft3D can be judged with the following rules of thumb:

Suspended-load transport	Suspended-load transport is distributed between the main channel and the zone behind the weir in the same ratio as the discharge, so $C = 1$.
Bed-load transport	For bed-load transport in three-dimensional situations with clearly oblique flow over the weir, the coefficient C can be related to the excess shear stress $S_\tau = (\theta - \theta_{cr}) / \theta_{cr}$ at the upstream slope, in which the actual Shields parameter θ and the critical Shields parameter θ_{cr} are adjusted for slope effects.
Perpendicular flow	In situations where the flow is directed almost perpendicular to the crest of the structure, the conclusions of LAUCHLAN (2001) are recommended. Nearly all mobile sediment is transported over the structure in these situations.

The coefficient C in Delft3D can be influenced by giving the bed level points near the weir the right height.

Samenvatting

In verschillende Ruimte voor de Rivier projecten zijn kunstwerken aanwezig, zoals langsdammen, kribben, zomerkades en drempels aan de bovenstroomse zijde van nevengeulen. Regelmatig worden er studies verricht met behulp van Delft3D naar de morfologische effecten van dergelijke projecten. Zo kan bijvoorbeeld de hinder voor scheepvaart en de vereiste baggerinspanning worden voorspeld. Het is in dergelijke situaties belangrijk dat de fysische processen ook rond kunstwerken op de juiste wijze worden gemodelleerd.

Bij het bovenstroomse talud van een overlaat zorgen de grotere dieptegemiddelde snelheden voor een toename in sedimenttransportcapaciteit en in schuifspanning die uitgeoefend wordt op de bodem. Het laatstgenoemde effect wordt versterkt door de verandering van de snelheidsprofielen ten opzichte van uniforme stroming: de snelheden nabij de bodem worden relatief groter bij opwaartse taluds. Aan de andere kant zorgt de component van de zwaartekracht langs het talud voor een toename van de kritische schuifspanning ten opzichte van de situatie met een vlakke bodem. Daarnaast kan bij steile taluds een (gedeeltelijke) blokkering van bodemtransport optreden.

Delft3D is bedoeld voor het modelleren van stromingsverschijnselen waarvan de horizontale lengte- en tijdsschalen aanzienlijk groter zijn dan de verticale schalen. Nabij waterbouwkundige kunstwerken is dit in het algemeen niet het geval. Deze kunstwerken worden geparametriseerd als overlaten in een dieptegemiddeld Delft3D model in de ingenieurspraktijk. Het enige effect van deze overlaten is een extra energieverlies in de impulsvergelijking. De parametrisatie is bedoeld om de invloed van loodrechte stroming over overlaten op de stroming op grotere schalen mee te nemen. De lokale stroming rond deze kunstwerken (turbulentie, verticale snelheidscomponenten en schuifspanningen) wordt niet correct gemodelleerd. Daarnaast heeft de overlaat geen directe invloed op sedimenttransport (door bijvoorbeeld toegenomen kritische schuifspanningen of blokkering van bodemtransport). Deze onnauwkeurige manier van modelleren zou kunnen leiden tot verkeerde voorspellingen van het morfologische effect van kunstwerken.

De doelstellingen van deze studie zijn:

Huidige wijze van Delft3D modellering	Het beoordelen van de kwaliteit van de huidige wijze van modelleren met Delft3D van sedimenttransport rond waterbouwkundige kunstwerken in driedimensionale stromingen.
Aanbevolen modellering van sedimenttransport	Aanbevelingen doen over het modelleren van sedimenttransport rond waterbouwkundige kunstwerken in de ingenieurspraktijk.

De prestaties van Delft3D zijn beoordeeld door de resultaten van Delft3D te vergelijken met de resultaten van het numerieke model FLUENT. FLUENT is een geavanceerd stromingsmodel, waarin sedimenttransport kan worden onderzocht door het analyseren van deeltjespaden. Eerst zijn enkele laboratoriumexperimenten gemodelleerd, die stroming en sedimenttransport over kunstwerken beschrijven. Op deze manier zijn de prestaties van beide modellen onderzocht en onderling vergeleken. De resultaten van FLUENT gaven vertrouwen om FLUENT ook te gebruiken als een instrument ter beoordeling van de

prestaties van Delft3D wat betreft de modellering van driedimensionale stroming en transport over kunstwerken.

Een situatie met duidelijk driedimensionale stroming is ontworpen. Dit ontwerp geeft de stroming over een langsdam geschematiseerd weer. Al het sediment dat in Delft3D een overlaat bereikt, passeert deze overlaat ook, ongeacht de transportvorm. In FLUENT is dit niet het geval. Suspensietransport wordt verdeeld tussen de hoofdgeul en de zone achter de dam in dezelfde verhouding als het debiet. De verdeling van bodemtransport is sterk afhankelijk van de korreldiameter. Dit verschil toont dat de parametrisatie van overlaten in dieptegemiddelde Delft3D-modellen significante verschillen oplevert in de voorspelling van sedimenttransport over kunstwerken, vooral als bodemtransport dominant is.

De grootte van het transport kan worden gereduceerd door de bodemhoogtepunten nabij de overlaat omhoog te brengen tot kruinniveau. Bij deze schematisering wordt vrijwel al het bodemtransport geblokkeerd en suspensietransport wordt gereduceerd. Een overlaat zonder verhoogde bodemhoogtepunten zorgt voor een overschatting van het sedimenttransport over het kunstwerk. Als de bodemhoogtepunten worden verhoogd tot het kruinniveau van de overlaat wordt het sedimenttransport over de overlaat onderschat. Het sedimenttransport over de overlaat kan worden gestuurd door het bodemniveau aan weerszijden van de overlaat toe te laten nemen tot een waarde ergens tussen nul en kruinniveau.

De verdeling van sediment tussen de hoofdgeul (index 1) en de zone achter de overlaat (index 2) kan worden beschreven met een splitsingspuntrelatie:

$$\frac{S_2}{S_1} = C \cdot \frac{Q_2}{Q_1}$$

De waarde van C zoals Delft3D die weergeeft, kan worden beoordeeld met de volgende vuistregels:

Suspensietransport	Suspensietransport wordt verdeeld tussen de hoofdgeul en de zone achter de overlaat in dezelfde verhouding als het debiet, dus $C = 1$.
Bodemtransport	Voor bodemtransport in driedimensionale situaties met een duidelijk scheef aangestroomde overlaat kan de coëfficiënt C worden gerelateerd aan het overschot aan schuifspanning $S_\tau = (\theta - \theta_{cr}) / \theta_{cr}$ aan de voet van het bovenstroomse talud. De Shields-parameter θ en de kritische waarde van de Shields-parameter θ_{cr} in deze uitdrukking zijn gecorrigeerd voor hellingseffecten.
Loodrechte aanstroming	In situaties waar de stroming ongeveer loodrecht op de kruin van het kunstwerk aanstroomt, worden de conclusies van LAUCHLAN (2001) aanbevolen. Nagenoeg al het mobiele sediment wordt over het kunstwerk heen getransporteerd in zulke situaties.

De coëfficiënt C in Delft3D kan worden beïnvloed door de bodemhoogtepunten in de nabijheid van de overlaat de juiste hoogte te geven.

Contents

List of symbols

A) Latin symbols

Symbol	Definition	Dimension
A	Wet cross-section	$[L^2]$
a	z-coordinate of the boundary condition near the bed	$[L]$
B	Channel width	$[L]$
C	Chezy coefficient	$[L^{1/2}\ T^{-1}]$
C	Sediment distribution coefficient	$[-]$
c	Mass concentration (of sediment)	$[M\ L^{-3}]$
c	Volume concentration (of sediment)	$[-]$
c	Wave celerity	$[L\ T^{-1}]$
c_a	Reference concentration near the bed (of sediment)	$[M\ L^{-3}]$
C_D	Drag coefficient	$[-]$
c_e	Equilibrium concentration (of sediment)	$[M\ L^{-3}]$
D	Particle diameter	$[L]$
D_*	Dimensionless grain diameter	$[-]$
d	Water depth	$[L]$
E	Specific energy level with respect to local bed level	$[L]$
f	Coriolis parameter	$[T^{-1}]$
$f(\alpha)$	Slope-dependent factor	$[-]$
Fr	Froude number	$[-]$
g	Gravitational acceleration	$[L\ T^{-2}]$
h	Water level	$[L]$
k	Turbulent kinetic energy	$[L^2\ T^{-1}]$
k_s	Nikuradse roughness height	$[L]$
k_s^+	Dimensionless roughness height	$[-]$
L	Characteristic length scale	$[L]$
L_a	Adaptation length of the suspended sediment concentration	$[L]$
l_m	Mixing length	$[L]$
m	Empirical discharge coefficient	$[-]$
p	Pressure	$[M\ L^{-1}\ T^{-2}]$
Pr	Prandtl-Schmidt number	$[-]$
Q	Discharge	$[L^3\ T^{-1}]$
q	Specific discharge Q/B	$[L^2\ T^{-1}]$
q_{ij}	Reynolds stresses, with $i = x,y,z$ and $j = x,y,z$	$[M\ L^{-1}\ T^{-2}]$
Re	Reynolds number	$[-]$
Re_p	Particle Reynolds number	$[-]$
S	Total sediment transport per unit width	$[L^2\ T^{-1}]$
S_τ	Excess shear stress	$[-]$
S_b	Bed-load sediment transport per unit width	$[L^2\ T^{-1}]$
S_s	Suspended-load sediment transport per unit width	$[L^2\ T^{-1}]$
T_a	Adaptation time of the suspended sediment concentration	$[T]$

T_*	Transport stage	[–]
U	Characteristic velocity difference	[L T^{-1}]
U	Depth-averaged velocity (in x-direction)	[L T^{-1}]
u	Velocity (in x-direction)	[L T^{-1}]
u_i	Velocity in x_i-direction, with $x_i = (x_1, x_2, x_3) = (x, y, z)$	[L T^{-1}]
$u_{p,i}$	Particle velocity in x_i-direction, with $x_i = (x_1, x_2, x_3) = (x, y, z)$	[L T^{-1}]
u_*	Shear velocity	[L T^{-1}]
u^+	Dimensionless velocity scale	[–]
V	Depth-averaged velocity in y-direction	[L T^{-1}]
v	Velocity in y-direction	[L T^{-1}]
w	Velocity in z-direction	[L T^{-1}]
w_s	Particle settling velocity	[L T^{-1}]
x	Longitudinal co-ordinate	[L]
y	Transverse co-ordinate	[L]
z	Co-ordinate, perpendicular to the x,y-plane	[L]
z^+	Dimensionless length scale	[–]
z_0	Roughness length $z_0 = k_s / 30$	[L]
z_b	Bed level	[L]

B) Greek symbols

Symbol	Definition	Dimension
α	(Longitudinal) bed slope angle	[–]
α	Coefficient for non-uniformity of the flow	[–]
α	Reflection coefficient	[–]
γ	Transverse bed slope angle	[–]
$\gamma_0, \gamma_1, \gamma_2$	Coefficients in theory of Galappatti & Vreugdenhil (1985)	[–]
Δ	Relative sediment density $(\rho_s - \rho)/\rho$	[–]
ε	Dissipation rate of turbulent kinetic energy	[L^2 T^{-3}]
ε_p	Porosity	[–]
ε_t	Turbulent diffusivity or eddy diffusivity	[L^2 T^{-1}]
η	Kolmogorov micro length scale	[L]
θ	Shields parameter	[–]
θ_{cr}	Critical Shields parameter	[–]
κ	Von Kármán constant	[–]
μ	Dynamic viscosity	[M L^{-1} T^{-1}]
μ	Ripple factor	[–]
μ	Contraction coefficient	[–]
ν	Kinematic viscosity	[L^2 T^{-1}]
ν_t	Turbulent viscosity or eddy viscosity	[L^2 T^{-1}]
ρ	Density of water	[M L^{-3}]
ρ_s	Density of sediment	[M L^{-3}]
σ	Variance of turbulence	[L^2 T^{-2}]
σ	Co-ordinate of sigma co-ordinate system	[–]

τ	Shear stress	[M L^{-1} T^{-2}]
τ	Kolmogorov micro time scale	[T]
τ_b	Bed shear stress	[M L^{-1} T^{-2}]
$\tau_{b,cr}$	Critical bed shear stress	[M L^{-1} T^{-2}]
υ	Kolmogorov micro velocity scale	[L T^{-1}]
ϕ	Angle of internal friction	[–]
φ	Oblique angle of the flow	[–]

1. Introduction

1.1. Context

1.1.1. Room for the River

A new approach in the control of high river discharges in the Netherlands has led to the establishment of the Dutch Policy Document “Room for the River”. In this document, it is stated that the discharge capacity of the Dutch Rhine branches should be enlarged. Dike reinforcements should be limited to a minimum in the future.

At different locations along the Dutch Rhine branches measures will be realized to give the river more space. Examples of Room for the River measures are given in figure 1.1 (taken from www.ruimtevoorderivier.nl).

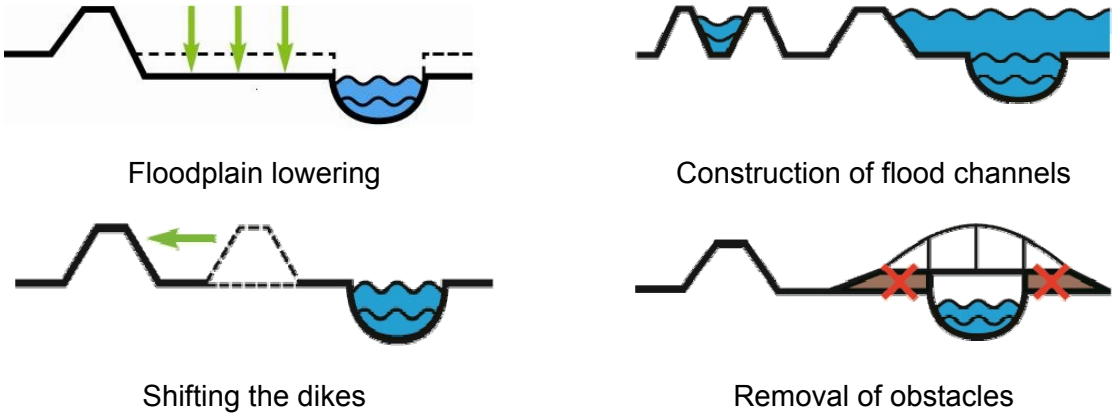

Figure 1.1 – Examples of Room for the River projects

During high discharges, a part of the river water is discharged via the measure area. The relative contribution of the measure to the conveyance of the flood discharge governs the magnitude of the change in flood water levels at the measure and also upstream of the measure.

Such measures have, besides a hydraulic effect, also a morphological effect. An increase of the conveying river width results in a decrease of current velocities. This leads to sedimentation in the main channel, and therefore in the fairway. The distributions of both water and sediment influence the magnitude of the morphological changes in the main channel. This is especially important in larger projects; where due to the (increased) accretion in the main channel (more) hindrance for shipping occurs. More dredging is needed, resulting in higher maintenance costs and (also) hindrance for shipping caused by the dredging vessels in the fairway.

1.1.2. Morphological modeling

Knowledge of morphological effects of a river intervention is necessary to decide whether a project is feasible. As mentioned in the previous section, the morphological changes in the main channel are governing for hindrance for shipping and dredging costs. In the past, expert judgment of experienced engineers has been used in much river projects to predict the

morphological changes. At most, a one-dimensional computer program like SOBEK was used to give an indication of bed level changes.
A substantial improvement of the last years is that (similar to the practice for other river projects in the last decades) morphological modeling of the effects of Room for the River projects is carried out with the help of two-dimensional depth-averaged simulations, for example with the numerical model Delft3D. The complete two-dimensional flow field and bed level changes are calculated. This gives a lot more information than only one representative value for the whole cross-section resulting from a one-dimensional computation. Typical two-dimensional phenomena like meanders, river bifurcations, side channels and bar formation are directly modeled and less inaccurate parameterizations are needed. Vertical division into different computational layers is also possible in Delft3D, although this is hardly ever used because of computational demands. Based on the results of the two-dimensional simulations, predictions can be made about the locations and magnitudes of erosion and sedimentation, navigation depths and required dredging efforts.

1.1.3. Hydraulic structures

In Room for the River projects, different types of hydraulic structures are always present. Examples are longitudinal weirs, groins, summer dikes and weirs in the inlet of a side channel. When the flow goes over or around such structures, a complicated non-uniform and turbulent flow pattern is observed. Because of the effect of the structures on the flow, also the local sediment transport is affected. But by means of sediment blockage and change of bed level slope (which influences the magnitude and direction of the bed-load transport) there is also a direct effect of the hydraulic structure on the sediment motion. When hydraulic structures form an important part of a river project, the water and sediment motion surrounding these structures is of great interest for the morphological effects of the project. This is the case in many projects: for example with longitudinal dams and side channels with a weir in the inlet.

Delft3D is based on the discretized shallow water equations. These equations are based on the Reynolds equations, with different simplifications, including the hydrostatic pressure assumption. Hydraulic structures are represented in Delft3D by a weir on the computational grid. In a depth-averaged computation, the only effect of this weir is an additional energy loss in the momentum equation. There is no direct influence of the weir on the sediment transport.

1.2. Problem description

At the consulting company HKV$_{\text{LIJN IN WATER}}$, different studies have been carried out, to predict the morphological effects of Room for the River projects using Delft3D. In many of these projects, hydraulic structures are important. The suspicion of the HKV engineers is that Delft3D calculates too large sediment transports over these structures, causing sand accumulation for example behind longitudinal weirs or behind the entrance weirs of side channels. This overestimation implies an underestimation of the sedimentation in the main channel, resulting in too low predictions of shipping hindrance and dredging costs.

When hydraulic structures are important, it is necessary to represent the complex water and sediment motion correctly in your numerical model. Delft3D “aims to model flow phenomena of which the horizontal length and time scales are significantly larger than the vertical scales” (Delft3D-FLOW user manual, page 192). When Delft3D is applied to model the flow around hydraulic structures, this is clearly not the case. The model concepts are not fully valid for these situations. This is the case for the three-dimensional version of Delft3D. In river engineering practice, Delft3D is at the moment often applied in depth-averaged mode, resulting in further simplified model concepts.

These shortcomings could result in inaccurate predictions of hindrance for shipping and dredging costs, which pertain to the main components of the maintenance costs. Therefore, it is important to investigate the possible shortcomings of the current modeling of water and sediment motion around hydraulic structures and to improve the model concepts.

1.2.1. Room for the River project Vianen

An example of this problem is found at the Room for the River project near Vianen. To give the river more room, the main channel will be widened with a factor two. The aim is a local lowering of the water level of 20 cm during design conditions. Without taking additional measures, serious siltation in the main channel is expected due to the enormous increase in width, leading to unacceptable hindrance for shipping and dredging efforts. One possibility to prevent these problems is the construction of a longitudinal weir into the river. This weir keeps the flow in the main channel during the periods with lower river discharge. One of the considered designs (not the final design though) of the project is shown in figure 1-2.

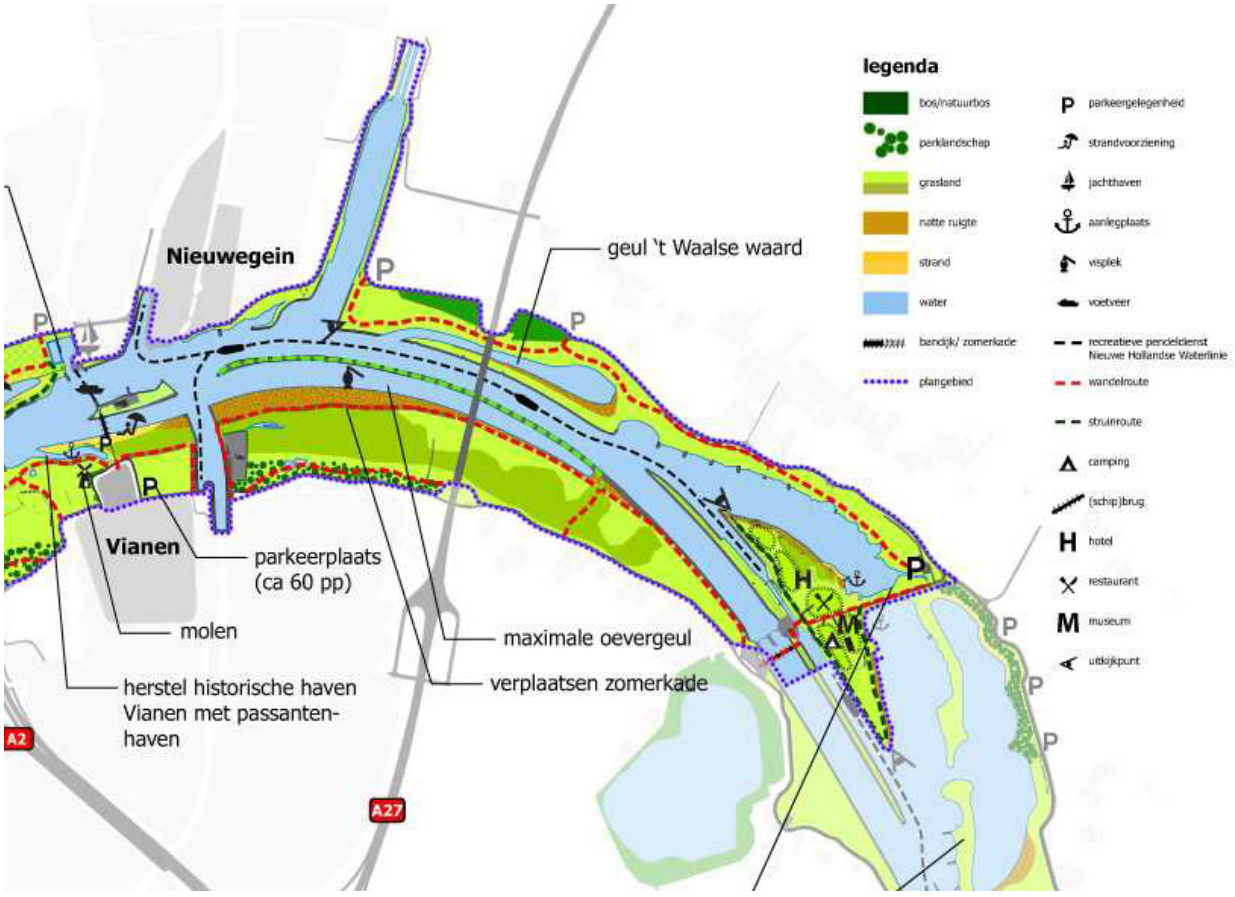

Figure 1.2 – Design of a Room for the River project near Vianen (DN URBLAND, 2009)

When the longitudinal weir is emerged, all the water and sediment remains in the main channel. At high discharges, the weir becomes submerged, and complicated three-dimensional flow patterns come into existence. The sediment load can be divided into a part that remains in the main channel and a part that goes over the structure to the zone behind the weir. In this zone the flow velocities are relatively small, so a considerable part of the entering sediment settles here.

To predict the morphological effects of this design, a depth-averaged Delft3D study has been performed. The computational grid is too coarse to reproduce the details of the cross-section

of the weir. Therefore, the longitudinal weir is considered as a subgrid feature, represented by a 2D-weir in Delft3D. This 2D-weir acts as an impermeable thin dam when the water level is below crest level of the weir. When the weir is submerged, the 2D-weir causes a local energy loss in the momentum equation. This energy loss affects the flow around the structure, and in this way, also the sediment transport is influenced. As aforementioned, there is no direct effect of the weir on the sediment transport. The sediment transport downstream of the weir is set equal to the upstream transport (continuity principle).

The prediction of the change in bed level after 10 years (without dredging) by Delft3D is shown in figure 1.3. The bed level change is scaled between –2 and 2 meter (sedimentation is set positive). The black lines show the weirs in the Delft3D schematization. Substantial sedimentation occurs behind the upstream end of the longitudinal weir and downstream of the longitudinal weir. The large increase in bed level behind the upstream end of the longitudinal weir is questionable. When the weir becomes submerged, the sediment is taken over and also 'through' the weir, and settles behind it. A direct consequence of this sediment withdrawal is a relatively small amount of sedimentation into the main channel.

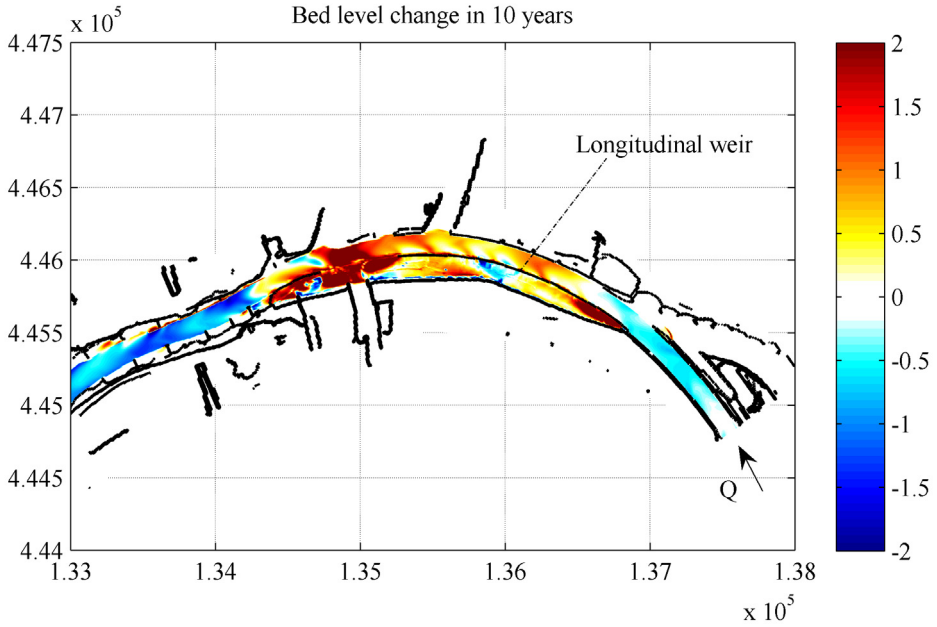

Figure 1.3 – Prediction of bed level change (m) after 10 years by Delft3D

1.2.2. Literature

The limited capacity to model flow and sediment transport around hydraulic structures is also mentioned in literature. A few examples:

- "Christine Lauchlan's experiments as well as parallel numerical simulations have shown that our capacity to model flow and sediment transport over steep slopes and weirs is still very limited." (LAUCHLAN, 2001, an attached memorandum from dr. ir. E. Mosselman)
- In MOSSELMAN (1998), it is stated that knowledge about sediment transport processes is missing, mainly in the case of upward steep slopes, where a part of the sediment is blocked by the obstacle. Different limitations of modeling flow and sediment transport over steep slopes with Delft3D are mentioned.
- RUPPRECHT (2004) performed depth-averaged numerical simulations with Delft3D of experiments concerning morphological processes in groin fields. She concluded:

"Delft3D computes the morphological pattern qualitatively well. When analyzing the details, though, some major differences with the observations occur. Especially the sediment transport into the groin field is not reproduced realistically at the moment".

- MOSSELMAN (2001) explains that application of two- and three-dimensional models is in river engineering practice often limited to processes in the main channel. There is a lack of good submodels for some key processes, including transport of sediment over obstacles and upward slopes (e.g. into a shallower side channel or over a weir at the entrance of a side channel).
- DE VRIEND (2006b) argues that it is time to make a step forward in modeling sediment transport in complex flows. In the currently used models sediment transport formulas are used which are mostly derived from uniform flow experiments. In complex flows, the shallow water approximation for the sediment transport no longer holds, even if the vertical accelerations are small enough for the flow to remain hydrostatic.

1.3. Objectives

The objectives of this study are:

Current way of Delft3D modeling	Assessing the performance of the current way of Delft3D modeling of sediment transport around hydraulic structures in three-dimensional flows.
Recommended sediment transport modeling	Making recommendations on the modeling of sediment transport around hydraulic structures in hydraulic engineering practice.

In this study, sediment transport is restricted to the transport of sand.

1.4. Methodology

In the first stage of the graduation period, a literature study has been carried out, to gain insight in the fundamental hydraulic and morphological processes around hydraulic structures and to collect experimental data to verify the performance of the numerical models used.

There are hardly any data concerning flow and sediment transport around hydraulic structures in fully three-dimensional flow situations. One way to collect this required data is performing a laboratory experiment. An alternative way to judge the performance of the Delft3D model is comparing the results of Delft3D with the results of a (more) detailed numerical model. This approach has been applied in this study. This model should be capable of modeling complex flows reasonably well, and it should be possible to include sediment transport. After comparing different possible software packages, the numerical modeling system FLUENT of the American company Ansys turned out to be the best option. This choice is explained in section 3.1.

Firstly, some experiments from literature are modeled, to gain confidence in the performance of FLUENT. The results of the model are compared with the experimental data. The same simulations are carried out in Delft3D, to compare the representation of different fundamental processes by both models. FLUENT is not able to make fully morphological computations, including bed level change. However, sediment transport patterns can be identified by making use of a discrete particle model.

Subsequently, a three-dimensional flow situation is designed and modeled in FLUENT, including sediment motion. The results of FLUENT are compared with the results of Delft3D for the same situation. This comparison forms the base of a discussion about the modeling of sediment transport in complex flows with Delft3D. Recommendations are given to optimize the performance of Delft3D in engineering practice.

1.5. Thesis outline

Physical processes	In chapter 2, the main physical processes underlying this study are described. Hydraulic and morphological processes are considered, both in general and applied to hydraulic structures.
Model selection and model description	In chapter 3, the choice of the software system FLUENT is founded and the relevant properties of Delft3D and FLUENT are described.
Modeling of laboratory experiments	➢ Chapter 4 deals with the modeling of uniform flow and sediment transport in uniform flow. ➢ In chapter 5, the numerical modeling of laboratory experiments of flow over weirs is discussed. ➢ Chapter 6 describes the modeling of oblique flow over weirs. ➢ In chapter 7, the numerical modeling of laboratory experiments of flow and sediment transport over weirs is described.
3D flow and transport over hydraulic structures	A design is made of three-dimensional flow and transport over hydraulic structures. This design has been modeled with Delft3D and FLUENT. This is treated in chapter 8
Discussion	Chapter 9 contains a discussion about morphological modeling of hydraulic structures in engineering practice.
Conceptual model	Chapter 10 presents a conceptual model to estimate sediment transport around hydraulic structures.
Conclusions and recommendations	This report ends with conclusions and recommendations in chapter 11.

2. Water and sediment motion around hydraulic structures

In this chapter, a description is given of the main physical processes that play a role around hydraulic structures. Turbulence is important in non-uniform flows. Section 2.1 describes turbulence theory and section 2.2 deals with the numerical modeling of turbulence. In section 2.3, a description of sediment transport and morphology is given. In section 2.4, some basic types of hydraulic structures are defined. Section 2.5 describes hydraulic and morphological processes that are specifically related to hydraulic structures. In section 2.6, an analytical formulation of flow over weirs is presented. The chapter ends with a section, in which the relevant processes are briefly summarized.

2.1. Turbulent flow

An important consequence of the non-uniform flow around hydraulic structures is an increase in turbulence intensity. Moreover, turbulence is the main force that keeps sediment in suspension. Finally, turbulent motion near the bottom causes increased erosion of bed material with respect to erosion caused by laminar flow. For these reasons, a general description of turbulence is given in this section. The content is mainly based on UIJTTEWAAL (2003) and NIEUWSTADT (1998). The description of turbulence is also used to explain the turbulence models used in Delft3D and FLUENT.

2.1.1. The nature of turbulence

Turbulent motion is characterized by irregular three-dimensional vorticity fluctuations. Osborne Reynolds (1842-1912) was one of the first researchers who described this phenomenon. Reynolds concluded that the occurrence of turbulence is dependent on the ratio between inertial forces and viscous forces. The dimensionless Reynolds number is based on this ratio:

$$\mathrm{Re} = \frac{UL}{\nu} = \frac{\rho UL}{\mu}, \tag{2.1}$$

with U and L a characteristic velocity difference [m/s] and length scale [m], respectively, and ν is the kinematic viscosity [m^2/s], a fluid property related to the dynamic viscosity μ by $\nu = \mu/\rho$. Turbulent flows are defined as flow with approximately $\mathrm{Re} > 4000$. Flow with $\mathrm{Re} < 2100$ is called laminar flow. The zone in between is called the transition zone. In Civil Engineering practice, almost all flows are turbulent flows, since $\mathrm{Re} >> 10^5$.

Turbulent flows are generally more dissipative than laminar flows. Much (kinetic) energy is lost in the smallest turbulent eddies, where kinetic energy is dissipated into heat by viscous forces. The smallest turbulent length and time scales are larger than the molecular scales. Therefore, turbulent motion can be considered as the flow of a continuum, governed by the equations of fluid mechanics.

Turbulence is created where velocity differences are found, for example near walls and boundaries (wall turbulence), in mixing layers or at locations where the flow is disturbed (free turbulence).

2.1.2. Basic equations

As mentioned in the previous subsection, turbulent flows can be described by the equations of fluid mechanics. These equations are based on the conservation laws for mass and momentum. Combination of these laws results in a system of non-linear partial differential equations. The equations are given for a Cartesian coordinate system, denoted by (x_1, x_2, x_3) or (x, y, z). The corresponding velocity vector is denoted by (u_1, u_2, u_3) or (u, v, w), respectively.

Conservation of mass leads to the continuity equation. Assuming incompressibility of the flow, the continuity equation (2.2) implies a divergence free velocity field.

$$\frac{\partial u_i}{\partial x_i} = 0 \tag{2.2}$$

Conservation of momentum for Newtonian fluids, under the assumption of incompressibility, results in equation (2.3). Equation (2.3) together with equation (2.2) are known as the Navier-Stokes equations, which fully describe fluid motion.

$$\frac{\partial u_i}{\partial t} + \frac{\partial u_i u_j}{\partial x_j} = -\frac{1}{\rho}\frac{\partial p}{\partial x_i} + \frac{\partial}{\partial x_j}\left(\nu \frac{\partial u_i}{\partial x_j}\right) \tag{2.3}$$

The following terms can be recognized in the momentum equation. The left-hand side shows the material derivative of the flow. The right hand side contains a pressure gradient and a (viscous) diffusion term. External source terms (like the Coriolis force) are neglected.

When considering equation (2.3) in dimensionless form by using a characteristic velocity scale U and length scale L, it appears that the Reynolds number is the only remaining parameter. It gives the ratio between advection and viscous stresses. When the viscous stresses are much too small to suppress inertial effects ($\mathrm{Re} >> 1$), the flow can be considered as turbulent.

2.1.3. Reynolds averaging and closure problem

For many applications in civil engineering, an accurate description of the details of the turbulent flow is not very relevant. In this case the mean motion is resolved and the turbulent fluctuations are ignored. The velocity vector and the pressure are separated into an ensemble averaged component (overlined) and a fluctuating component (with prime). Ensemble averaging is used, because averaging in time can lead to interpretation problems when the mean flow varies in time. An ensemble is a number of realizations of the flow under comparable conditions.

$$u_i = \overline{u}_i + u_i' \qquad p = \overline{p} + p' \tag{2.4}$$

This separation is known as Reynolds decomposition. Substitution of (2.4) into the momentum equation (2.3) and ensemble averaging of the different terms leads to the Reynolds equations (2.5). This averaging procedure is called Reynolds averaging. Different terms fall out of the equations, using the Reynolds conditions: $\overline{u'} = 0$ and $\overline{\overline{u}} = \overline{u}$.

$$\frac{\partial \rho \overline{u}_i}{\partial t} + \frac{\partial \rho \overline{u}_i \overline{u}_j}{\partial x_j} + \frac{\partial \rho \overline{u_i' u_j'}}{\partial x_j} = -\frac{\partial \overline{p}}{\partial x_i} + \mu \frac{\partial^2 \overline{u}_i}{\partial x_j^2} \tag{2.5}$$

The fluctuating quantities have disappeared by using $\overline{u'} = 0$, except the non-zero product of the velocity fluctuations $\rho \overline{u_i' u_j'}$. This expression is called the (symmetrical) Reynolds stress tensor, which contains nine elements: normal stresses and shear stresses.

The introduction of the Reynolds stress tensor leads to a closure problem: new unknown variables come into play, for which additional expressions should be found. Due to the symmetry, six independent stresses should be described. Neglecting the three normal stresses leaves us with three unknown shear stresses. Decades of research have not led to an adequate description of the Reynolds (shear) stresses. Many turbulence models are available, all giving approximations of these stresses.

An often-used approach is based on the assumption of gradient-type transport. Turbulent transport of a certain quantity is assumed to be proportional to gradients of this quantity in the mean motion. A well-known assumption for gradient-type transport is the Prandtl mixing length hypothesis. This hypothesis, given in (2.6), states that the velocity that characterizes the turbulent fluctuations is proportional to the velocity difference in the mean flow over a distance l_m over which the transport of momentum takes place. This distance l_m is defined as the mixing length, which can be seen as the distance over which a fluid-particle fully mixes with its surroundings during his motion.

$$U \sim l_m \left| \frac{\partial \overline{u}}{\partial z} \right| \tag{2.6}$$

The turbulent shear stress is considered analogously to the viscous shear stress, with the molecular viscosity replaced by a fictitious turbulent viscosity ν_t, also called eddy viscosity. This eddy viscosity is a product of a characteristic length scale and a characteristic velocity.

$$\nu_t = UL = l_m^2 \left| \frac{\partial \overline{u}}{\partial z} \right| \tag{2.7}$$

An expression for the unknown Reynolds shear stress is found using this eddy-viscosity:

$$q_{zx} = \rho \overline{u'w'} = -\rho l_m^2 \left| \frac{\partial \overline{u}}{\partial z} \right| \frac{\partial \overline{u}}{\partial z} = -\rho \nu_t \frac{\partial \overline{u}}{\partial z}. \tag{2.8}$$

The problem is shifted to a proper description of the mixing length l_m. This description is dependent on the type of turbulence (wall turbulence or free turbulence) and location in the flow domain (e.g. the distance from the wall). The advantage of the Prandtl mixing length approach is the simplicity of its formulation.

The disadvantages of the mixing length approach in complex flows are:

- No turbulent transport can take place where the flow has a zero-gradient.
- The coupling between shear stress and velocity gradient does not hold straightforwardly for recirculation zones.
- Transport of turbulence by advective and diffusive processes is not taken into account.

2.1.4. Turbulent boundary layers

The no-slip condition along wall boundaries gives rise to large velocity gradients perpendicular to the wall. These velocity gradients cause increased turbulence intensity near the wall. These wall shear flows are called boundary layers.

In the wall region, the turbulent shear stress τ is assumed constant perpendicular to the wall. The shear velocity u_* is defined as:

$$\tau = \rho u_*^2 . \tag{2.9}$$

The mixing length close to the wall is proportional to the distance from the wall:

$$l_m = \kappa z , \tag{2.10}$$

where κ is the von Karman constant. The constant shear stress approximation, combined with this definition of the mixing length, leads to a solution of the momentum equation in the form of a logarithmic velocity profile:

$$u(z) = \frac{u_*}{\kappa} \ln\left(\frac{z}{z_0}\right). \tag{2.11}$$

The integration constant z_0 is needed to set the velocity near the wall to a realistic value. Dimensionless variables can be introduced:

$$u^+ = \frac{u}{u_*}, \qquad z^+ = z\frac{u_*}{\nu}. \tag{2.12}$$

The wall region can be divided into three sublayers:

Viscous sublayer ($z^+ \le 5$)	A viscous sublayer closest to the wall, in which viscous shear stress dominates.
Buffer layer ($5 < z^+ < 30$)	A buffer layer, where both viscous and turbulent shear stresses are important.
Inner layer ($z^+ \ge 30$)	A turbulent inner layer, where turbulent shear stresses dominate over viscous stresses.

Table 2.1 – Sublayers in the wall region

The integration constant z_0 depends on the properties of the wall. The wall roughness can be characterized by a Nikuradse roughness height k_s, which has to be determined experimentally. Two limit states can be discerned: hydrodynamically rough walls ($k_s u_* / \nu >> 1$) and hydrodynamically smooth walls ($k_s u_* / \nu << 1$). For both limit states, an expression for z_0 can be given:

$$\begin{aligned} z_0 &\approx \frac{k_s}{30} && \frac{k_s u_*}{\nu} >> 1 \\ z_0 &\approx 0.135\frac{\nu}{u_*} && \frac{k_s u_*}{\nu} << 1 \end{aligned} \tag{2.13}$$

In hydrodynamically rough conditions, the viscous sublayer is not longer distinguishable, because the roughness height exceeds the thickness of the viscous sublayer. The boundary layer flow is in this case independent of the viscosity. In hydrodynamically smooth conditions, the influence of the roughness elements is negligible. When (2.13) and (2.12) are substituted in (2.11), a dimensionless velocity profile is found, depending on the properties of the wall.

The logarithmic velocity profile (2.11) can be used to formulate a relation between the depth-averaged velocity U and the shear velocity u_*. Integration of the logarithmic velocity profile gives:

$$U = \frac{1}{h}\int_0^h \frac{u_*}{\kappa}\ln\left(\frac{z}{z_0}\right)dz \qquad u_* = \frac{U\kappa}{\ln(h/z_0)-1} \tag{2.14}$$

This relation is only valid in fully developed (uniform) flow conditions.

2.1.5. Statistical description

The irregularity or randomness of turbulence requires a statistical approach rather than a deterministic description. In the previous section, the decomposition into a mean value and a turbulent fluctuation has been introduced. An important property of the fluctuating quantity is the variance:

$$\sigma^2 = \overline{u'^2} = \overline{(u-\bar{u})^2}\,. \tag{2.15}$$

For velocities, the variance is a measure of the turbulent kinetic energy. The square root and therefore the standard deviation σ of the velocity is called the turbulence intensity. This intensity can be seen as the mean amplitude of the turbulent fluctuations.

In the previous section the Reynolds shear stress has been introduced, defined in (2.8) as the product of the mass density and the non-zero average product of the velocity fluctuations. This means that the two fluctuating components are correlated. The velocities are irregular, but in some way structured. The mean product of the two velocity components is mathematically defined as covariance, a measure of the degree of correlation and therefore a measure of the Reynolds shear stress.

2.1.6. Energy considerations

In a turbulent motion a macrostructure and a microstructure can be distinguished.

The macrostructure contains the large eddies. Kinetic energy present in the mean motion is entrained in the turbulent motion by deformation work done by the Reynolds stresses. Therefore, the mean motion actively produces turbulent kinetic energy $k = 1/2\,\overline{u_i' u_j'}$ [m^2/s^2]. Viscous effects are negligible at this macro scale, because energy losses due to viscous effects are much smaller than energy losses due to the deformation work done by the Reynolds stresses. In stationary flow, the loss of energy should be balanced by the work done by external forces. The macrostructure of the turbulence depends on the geometry of

the flow domain and is therefore highly anisotropic. The scale parameters for the macro scale are the characteristic velocity scale U and length scale L.

Viscous dissipation of energy (transfer of kinetic energy into heat) can only play a role when the velocity gradients are significantly large. Consider the last term of the momentum equation (2.3). These gradients are large when the length scales are small enough, in other words: viscous dissipation plays only a significant role at the micro scale.

The large turbulent eddies of the macrostructure fall apart into smaller eddies. This process repeats until the viscosity plays a dominant role: the energy cascade. This zone between the macro scale and the micro scale where the energy cascade is found is called the inertial subrange. The (Kolmogorov) micro scales are independent of the scale parameters of the macro scale (U and L). The parameters that are important are the dissipation of kinetic energy ε [m^2/s^3] and the kinematic viscosity ν. Kolmogorov found by dimension analysis the Kolmogorov micro scales η (length scale), υ (velocity scale) and $\tau = \eta/\upsilon$ (time scale).

$$\eta = \left(\frac{\nu^3}{\varepsilon}\right)^{1/4} \qquad \upsilon = (\nu\varepsilon)^{1/4} \qquad \mathrm{Re} = \frac{\upsilon\eta}{\nu} = 1 \tag{2.16}$$

Because the geometry of the flow domain plays no significant role at this level, the micro-structure can be considered as universal and isotropic.

In a few words: the macrostructure is fed by energy extraction from the mean motion via instability processes. Large eddies containing much energy become unstable and drop to smaller eddies by the energy cascade. In this energy cascade no energy is dissipated, but transported to the micro scale, where kinetic energy is dissipated by viscous stresses. Because the dissipation of energy balances with the external forcing, also ε depends on the Reynolds number (the dissipation scales with the macrostructure of the turbulence):

$$\varepsilon = -\frac{dk}{dt} = \nu\frac{\upsilon^2}{\eta^2} \sim \frac{U^3}{L}. \tag{2.17}$$

In this way, the balance between production and dissipation of energy results in a ratio between the micro length scale η and the macro length scale L:

$$\frac{\eta}{L} = \mathrm{Re}^{-3/4}. \tag{2.18}$$

The higher the Reynolds number, the higher the range of turbulent length scales.

2.2. Turbulence modeling

The flow of a continuum can be described by the Navier-Stokes equations (2.2) and (2.3). These equations are a set of non-linear partial differential equations. Finding the analytical solution of the complete system is generally not possible. A solution of this problem could be obtained by solving the discretized version of the equations on a numerical grid. There are several options to deal with the range of turbulent spatial and temporal scales that are present in the flow. An overview of the different types of turbulence simulation is given in figure 2.1.

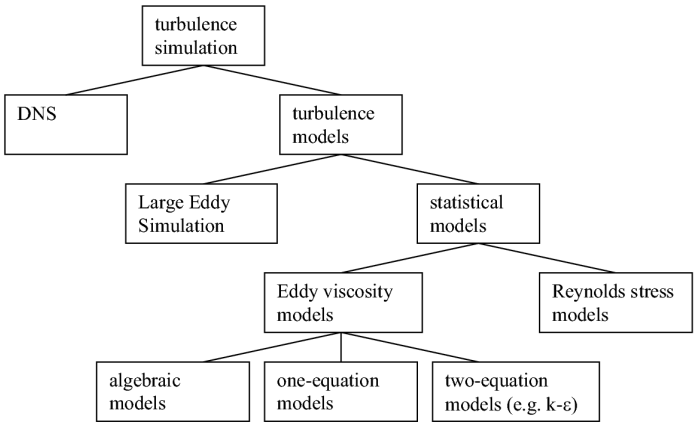

Figure 2.1 – Different types of turbulence simulation (JAGERS & SCHWANENBERG, 2003)

2.2.1. Direct Numerical Simulation

The most straightforward strategy to solve the discretized Navier-Stokes equations is by Direct Numerical Simulation (DNS). To give a correct description of the flow, all the length scales that are present in the flow, should be represented on the numerical grid. The total size of the grid should cover the domain of interest (represented by the macro scale L) and the size of one grid cell should be smaller than the smallest turbulent length scale in the flow (the Kolmogorov length scale η). The number of grid cells is therefore dependent on the ratio between the largest and smallest length scale. This ratio, as given in (2.18), depends on the Reynolds number (NIEUWSTADT, 1998).

Not only the macro scale depends on the Reynolds number, but also the Kolmogorov micro scale. The larger the Reynolds number (an indication of the production of energy), the smaller becomes the smallest length scale of the turbulent motion. In this way, the velocity gradients at the micro scale become larger, causing a larger amount of dissipation by molecular viscosity. The dissipation ε is found by dimension analysis, and given by (2.17). In this way, a balance between production and dissipation of turbulence can be found. This is why the ratio between the length scales depends on the Reynolds number.

This gives an indication for the number of grid points N_g in a three-dimensional space:

$$N_g \sim \left(\frac{\eta}{L}\right)^3 \approx \mathrm{Re}^{9/4} \tag{2.19}$$

With Reynolds numbers found in Civil Engineering practice, this results into huge amounts of grid points. Moreover, the Courant condition requires that the time step should be taken in the order of η / U, to guarantee numerical stability if an explicit time-integration scheme is used (UIJTTEWAAL, 2003). The conclusion is clear: Direct Numerical Simulation in Civil Engineering practice will remain computationally unfeasible in the near future, even with a significant increase in computational power and further efficient parallelization techniques.

2.2.2. Reynolds Averaged modeling

The Reynolds averaged modeling technique makes use of the Reynolds equations, (2.5). All the details of the dynamics of the turbulent motion have disappeared in this Reynolds Averaged Navier Stokes (RANS) modeling. Statistics are applied to the fluctuating quantities,

so models that make use of this technique are indicated as statistical models in figure 2.1. The averaged value of the fluctuating quantities becomes zero, except the mean product of the fluctuating velocities in $\rho\overline{u_i' u_j'}$; see (2.8). This term, originating from the non-linear advection term, is called the Reynolds stress tensor, a symmetric tensor containing nine elements (normal stresses and shear stresses).

As mentioned in section 2.1.3, many turbulence models do exist, to give an approximation of the Reynolds stresses. These turbulence models can be subdivided into eddy viscosity models and Reynolds stress models, following figure 2.1. The main difference between them is the fact that the eddy viscosity models assume a local isotropic turbulence of the flow, which is represented by a scalar eddy viscosity. The Reynolds stress models try to determine the full Reynolds stress tensor, by solving transport equations for all Reynolds stresses, making this kind of models computationally expensive with respect to all types of eddy viscosity models. Reynolds stress models should be more universally applicable, but in wall-bounded shear flows, they are often inferior to two-equation eddy viscosity models (JAGERS & SCHWANENBERG, 2003).

2.2.3. Large Eddy Simulation

Another way of dealing with the discretized Navier-Stokes equations is applying a spatial filter. The large eddies contain much energy and they are highly anisotropic, because they scale with the large-scale geometry. These large eddies are resolved and the isotropic small-scale turbulence is filtered out of the equations: Large Eddy Simulation (LES). Parameterization of this small-scale motion is applied to close the equations. An often-applied closure relation is the Smagorinsky model (NIEUWSTADT, 1998).

2.3. Sediment transport

2.3.1. Transport modes

Sediment transport in rivers can be subdivided into bed-load transport S_b and suspended-load transport S_s. Bed-load transport is related to sediment that predominantly slides or rolls over the riverbed with a velocity significantly lower than the flow velocity. Particles with a relatively smaller weight move in suspension with a velocity comparable to the flow velocity. This transport mode is called suspended-load transport, which is calculated by integration of the product of velocity u and sediment concentration c from a reference height a to the water surface h; see (2.20). The relative contribution of both transport modes depends on sediment properties and flow properties.

$$S = S_s + S_b \qquad S_s = \int_a^h uc\, dz \tag{2.20}$$

Several approaches for the initiation of motion exist. These approaches vary largely in applicability and simplicity. A well-known approach is formulated by Shields. Bed material begins to move when the actual shear stress exceeds a certain critical value. Correction factors exist for e.g. slope effects.

Bed-load, saltation and suspension can be distinguished. Saltation is defined in HARRIS (2003) as transport where individual grains hop along the bed, but reach heights of a few grain diameters above the bed so that they lose contact with bed material. The separation between the different transport modes is dependent on the ratio between settling velocity w_s and shear velocity u_*, defined in (2.9). RAUDKIVI (1998) gives the following indication:

$$\begin{array}{cc} 6 > w_s / u_* > 2 & \text{bed load} \\ 2 \geq w_s / u_* \geq 0.6 & \text{saltation} \\ 0.6 > w_s / u_* & \text{suspension} \end{array} \qquad (2.21)$$

The settling velocity is dependent on sediment characteristics and on the turbulence intensity, represented by the particle Reynolds number $\mathrm{Re_p} = w_s D/\nu$, in which D is a characteristic particle diameter.

$$w_s = \left(\frac{4}{3C_D} \Delta g D \right)^{1/2} \text{, where } \Delta = \frac{\rho_s - \rho}{\rho} \qquad (2.22)$$

The drag coefficient C_D is dependent on the particle Reynolds number $\mathrm{Re_p}$ and can be obtained using diagrams of e.g. ALBERTSON (1953) or analytical relations like the empirical relation of Kazanskij, which holds for $10^{-3} < \mathrm{Re_p} < 3 \cdot 10^4$. This relation can be found in RAUDKIVI (1998).

Equation (2.22) holds for spherical particles, and still requires an expression for C_D. VAN RIJN (1993) gives for natural sediment:

$$\begin{array}{ll} w_s = \dfrac{\Delta g D^2}{18\nu} & 1 < D \leq 100 \text{ µm} \\ w_s = \dfrac{10\nu}{D}\left(\sqrt{1 + \dfrac{0.01 \Delta g D^3}{\nu^2}} - 1 \right) & 100 < D \leq 1000 \text{ µm} \\ w_s = 1.1\sqrt{\Delta g D} & D > 1000 \text{ µm} \end{array} \qquad (2.23)$$

2.3.2. Turbulent diffusion

The turbulent fluctuations in the flow cause a net transport of dissolved material in the presence of a concentration gradient. This can be explained intuitively by the fact that a (turbulent) movement in an arbitrary direction transports a different amount of sediment than the same movement in opposite direction, when a concentration gradient in this direction is present. This gradient type transport is called turbulent diffusion. Molecular diffusion is orders of magnitudes smaller than turbulent diffusion. The suspended sediment concentration can be calculated using a balance equation for the suspended sediment concentration, including turbulent diffusion.

$$\frac{\partial c}{\partial t} + u\frac{\partial c}{\partial x} + v\frac{\partial c}{\partial y} + (w - w_s)\frac{\partial c}{\partial z} - \frac{\partial}{\partial x}\left(\varepsilon_{t,x} \frac{\partial c}{\partial x} \right) - \frac{\partial}{\partial y}\left(\varepsilon_{t,y} \frac{\partial c}{\partial y} \right) - \frac{\partial}{\partial z}\left(\varepsilon_{t,z} \frac{\partial c}{\partial z} \right) = 0 \qquad (2.24)$$

In which $\varepsilon_{t,i}$ in the turbulent diffusion terms is called the eddy diffusivity. The Reynolds analogy states that the eddy diffusivity can be treated in the same way as the eddy viscosity: $\varepsilon_{t,i} \approx \nu_{t,i}$. The ratio is given by the turbulent Prandtl-Schmidt number (2.25). When $\mathrm{Pr} > 1$, it is assumed that the sediment particles cannot fully respond to the turbulent fluid velocity fluctuations (inertia). When $\mathrm{Pr} < 1$, it is assumed that the sediment particles are apparently thrown out of the turbulent eddies. This can be related to the centrifugal forces, which are larger for sediment than for water, due to the higher density of the particles compared to the density of water. Based on laboratory experiments, the latter seems to be dominant.

$$\mathrm{Pr} \equiv \frac{\nu_t}{\varepsilon_t} \tag{2.25}$$

When the turbulence is isotropic, the turbulent diffusion is equal in all directions. In steady ($\partial / \partial t = 0$), uniform flow in x-direction ($\partial / \partial x = 0$, $v = 0$, $w = 0$), (2.24) simplifies to:

$$w_s c + \varepsilon_{t,z} \frac{\partial c}{\partial z} = 0 . \tag{2.26}$$

Following the Reynolds analogy, also the eddy diffusivity has an approximately parabolic distribution over the vertical. When $\mathrm{Pr} = 1$ is assumed, it follows that:

$$\varepsilon_{t,z}(z) \approx \nu_{t,z}(z) = \kappa u_* z (1 - z/h) . \tag{2.27}$$

Integration over the vertical results in the well-known Rouse concentration profile:

$$c(z) = c_a \left(\frac{h - z}{z} \frac{a}{h - a} \right)^{w_s / \kappa u_*} \tag{2.28}$$

In which c_a is a reference concentration near the bed (at $z = a$), and the Rouse parameter $w_s / \kappa u_*$ gives a ratio between the downward (gravitational) and the upward (turbulent) flux. In this way, it becomes clear that turbulence is also of great importance for suspended sediment transport.

2.3.3. Suspended-load transport modeling

Calculating the entire concentration field with the transport equation (2.24) for suspended material is always applicable with Reynolds averaged modeling. However, this approach is also time-consuming. In numerical models, also more simple approaches have been adopted.

Transport formulas for suspended-load transport do exist. These empirical formulas calculate the transport capacity. The actual transport is set equal to the transport capacity, so the sediment is straightforwardly a function of the (depth-averaged) velocity. This approximation holds for uniform flow, or in situations with gradually changing flow properties.

A less simple approach is the application of depth-averaged models. The depth-averaged velocity and concentration are calculated:

$$\frac{\partial (d\overline{c})}{\partial t} + \frac{\partial (\alpha \overline{u} d \overline{c})}{\partial x} = - \left[w_s c + \varepsilon_z \frac{\partial c}{\partial z} \right]_{z=a} . \tag{2.29}$$

The right-hand side gives the vertical flux at the bottom ($z = a$), for which an empirical formulation can be applied. The coefficient α is introduced for considering non-uniform flow conditions. $\alpha = 1$ in uniform flow and $\alpha < 1$ in non-uniform flow conditions.

GALAPPATTI & VREUGDENHIL (1985) give an asymptotic solution for the depth-averaged concentration:

$$T_a \frac{\partial \overline{c}}{\partial t} + L_a \frac{\partial \overline{c}}{\partial x} = \overline{c}_e - \overline{c}\,, \tag{2.30}$$

in which T_a is the adaptation time and L_a is the adaptation length of the concentration field, for which holds:

$$T_a = \frac{\gamma_1}{\gamma_0}\frac{d}{w_s}, \qquad L_a = \frac{\gamma_2}{\gamma_0}\frac{\overline{u}d}{w_s}, \tag{2.31}$$

in which:

$$\gamma_0 = f\left(\frac{w_s}{u_*}, \frac{a}{d}\right), \qquad \gamma_1 = f\left(\frac{w_s}{u_*}, \frac{a}{d}\right), \qquad \gamma_2 = f\left(\frac{w_s}{u_*}, \frac{\overline{u}}{u_*}, \frac{a}{d}\right). \tag{2.32}$$

The ratio w_s / u_* is related to the shape of the equilibrium concentration profile, $\overline{u} / u_*$ depends on the shape of the logarithmic velocity profile and a / d gives the relative elevation of the boundary condition at the bottom.

Depth-averaged models are applicable when the time and length scale of the model are relatively large with respect to T_a and L_a. When T_a and L_a are very small compared to the characteristic time and length of the problem, making use of a transport capacity formulation is sufficient. A rule of thumb is that a capacity formulation can be used when the adaptation length L_a is smaller than 4-5 times the grid cell size. In very local problems, a 2DV or 3D model should be used, and the transport equation (2.24) should be solved.

2.3.4. Bed-load transport

Suspended-load sediment transport can be described with an advection diffusion equation like (2.24). For bed-load transport, this approach is not easily applicable. The interaction between the sediment bed and the sediment in motion is very intense. Particles also slide, roll and jump over the sediment bed. The complexity of bed-load transport results in a great variety of bed-load transport formulas, varying in applicability and physical background. One of the simplest bed-load equations was developed by Meyer-Peter and Müller, with their work starting in 1934. Their work resulted in the well-known Meyer-Peter-Müller formula (MEYER-PETER AND MÜLLER, 1948).

$$S_b = 8\sqrt{\Delta g D^3}\left(\mu\theta - 0.047\right)^{3/2} \tag{2.33}$$

In which μ is a ripple factor, depending on sediment characteristics and the water depth. θ is the Shields parameter: $\theta = u_*^2 / \left(\Delta g D\right)$. The Meyer-Peter-Müller formula is valid for $\mu\theta < 0.2$, $D > 0.4$ mm and $w_s / u_* > 1$.

Other bed-load sediment transport formulas are the more physically and stochastically-based Einstein equation, the process-based (but less widely used) Yalin equation, and the Bagnold equation for sheet flow. HARRIS (2003) gives a description and comparison of these formulas. Other formulas, like the formula of Engelund & Hansen (ENGELUND AND HANSEN, 1967) give an estimation of the total sediment transport. In the formula of Van Rijn (1984), a distinction is made between bed-load and suspended-load. This makes the area of application of this formula quite large. However, all mentioned bed-load transport formulas are derived for uniform flow situations.

Bed slope effects are of great importance in case of sediment transport over hydraulic structures. DEY (2001) gives an empirical formulation for the ratio between the critical shear stress on a sloping bed and on a flat bed:

$$\frac{\tau_{b,cr}}{\tau_{b,cr,0}} = \left(1 - \frac{\tan\alpha}{\tan\phi}\right)^{0.75} \left(1 - \frac{\tan\gamma}{\tan\phi}\right)^{0.37} \tag{2.34}$$

in which α is the longitudinal slope angle, γ is the transverse angle (both defined positive at a downward sloping bed) and ϕ is the angle of internal friction of sand ($\phi \approx 30°$).

2.3.5. Sediment balance and bed level change

The sediment balance describes bed level changes per unit width, caused by a difference in bed-load transport over a control section and an erosion/deposition rate of suspended sediment.

$$\left(1-\varepsilon_p\right)\frac{\partial z_b}{\partial t} + \frac{\partial S_{b,x}}{\partial x} + \frac{\partial S_{b,y}}{\partial y} = \frac{\left(c - c_e\right)d}{T_a} \tag{2.35}$$

In which d is the water depth, ε_p is the porosity, $\left(c - c_e\right)$ the difference between actual and equilibrium sediment concentration, z_b the bed level and T_a an adaptation time of the vertical sediment concentration profile, depending on the sediment settling velocity w_s.

2.4. Hydraulic structures

Two basic types of hydraulic structures are considered to illustrate the behavior of the flow and the sediment transport: a long weir and a vertical wall weir.

A long weir is defined in the left part of figure 2.2 and characterized by a relatively smooth upstream slope, where gradual acceleration occurs. Downstream a backward facing step is located. At this location, abrupt deepening causes flow separation and turbulence.

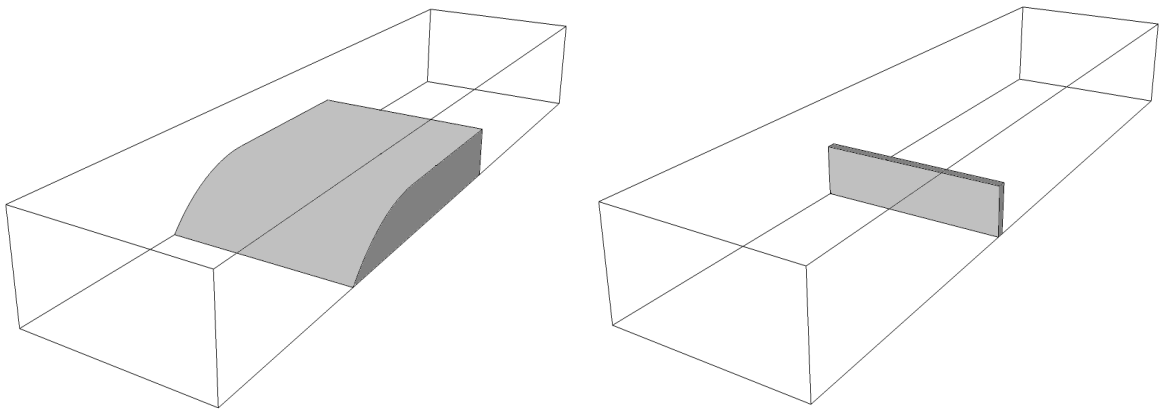

Figure 2.2 – Long weir (left) and vertical wall weir (right)

A vertical wall weir is in this context defined as a vertical plate in the flow, as illustrated in the right part of figure 2.2. Both acceleration and deceleration are caused by an abrupt change in flow geometry.

2.5. Phenomenology

In this section, a general, qualitative description is given of the fundamental processes around hydraulic structures.

2.5.1. Flow regimes

A distinction is made between *drowned overflow* and *free overflow* of a hydraulic structure. A Froude number smaller than one at the weir characterizes drowned overflow (part D of figure 2.3), whereas in the case of free overflow the Froude number exceeds one (parts A and B of figure 2.3). In free overflow conditions, a hydraulic jump can be observed downstream of the structure. This jump can be a surface roller or a submerged roller, depending on the downstream water level. Part C of figure 2.3 shows the transition between both regimes. In this case, surface waves (also known as undulations) are found.

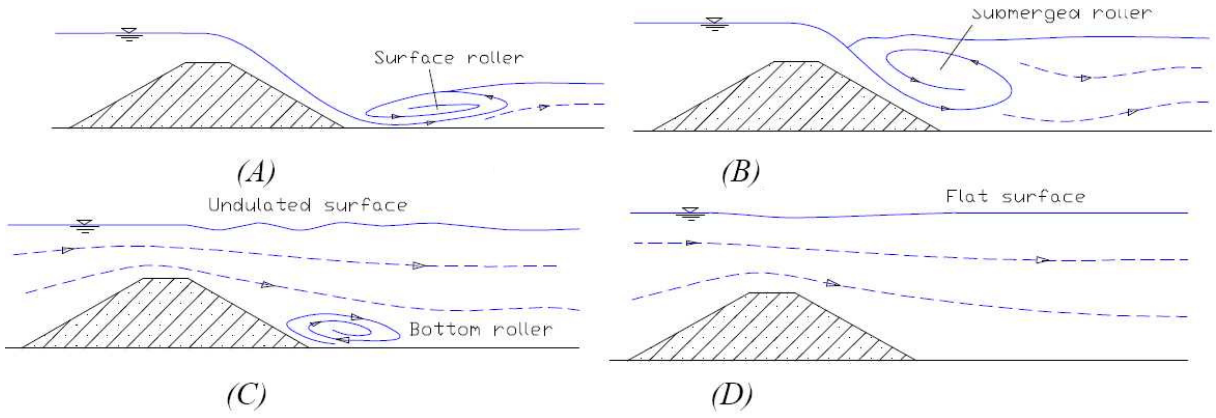

Figure 2.3 – Flow regimes (from NGUYEN, 2006)

In drowned conditions, the wave celerity exceeds the flow velocity; so disturbances are able to propagate upstream. Therefore, both upstream and downstream conditions influence the local flow characteristics. In the case of free overflow, the flow over the weir is fully determined by the upstream conditions.

2.5.2. Acceleration and deceleration zone

At the upstream side of a hydraulic structure, flow contraction occurs, resulting in flow acceleration. In this zone, conservation of energy is assumed, following the Bernoulli principle. The weir forms an obstacle in the flow, causing a momentum loss to the mean flow. In the deceleration zone downstream of the weir, flow separation occurs, resulting in a large amount of turbulence. Conservation of energy is not valid anymore, but conservation of momentum can be assumed.

The behavior of the flow in the deceleration zone depends on the geometry of the downstream part of the structure. The flow is not able to follow abrupt changes in the geometry. In these situations flow separation occurs. An extreme case is a so-called backward facing step, a vertical expansion as shown in figure 2.4.

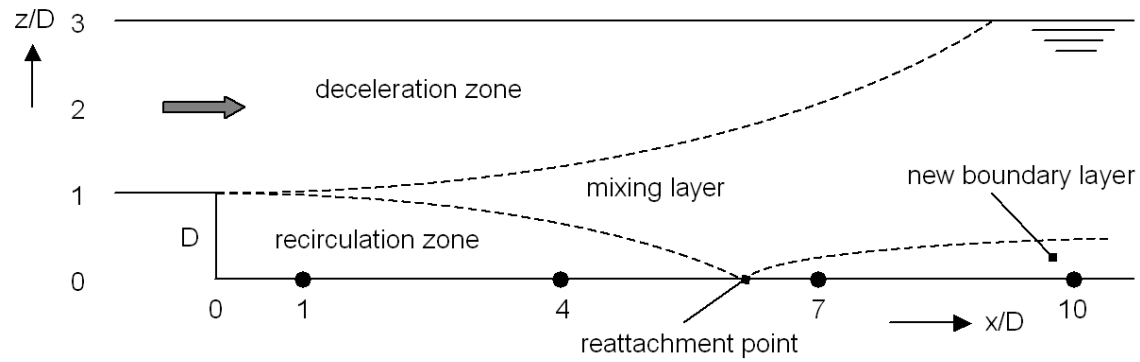

Figure 2.4 – Backward facing step

Directly downstream of the backward facing step, a recirculation zone is found, characterized by a wake with relatively low flow velocities. A mixing layer comes into being between the parts of the flow with different flow velocities. High levels of turbulence are found into this mixing layer. The main flow reaches the bed again at the reattachment point, located at 5 to 7 times the stepheight downstream of the step (SCHIERECK, 2004).

2.5.3. Sediment transport over hydraulic structures

Sediment transport over hydraulic structures depends on the flow over these structures and the geometry of the structure. A structure can roughly be subdivided into an upstream and a downstream slope.

At the upstream slope, flow acceleration is found. Physical processes at the upstream slope are mentioned below.

Increased depth-averaged velocity	The larger depth-averaged flow velocity leads to an increase in both sediment transport capacity and actual bed shear stress.
Velocity profiles	Also the velocity distribution over the vertical changes. The standard logarithmic velocity profiles for uniform flow are not valid anymore. The velocities near the bed increase, causing an increased actual bed shear stress.
Critical shear stress	At the other side, the gravity component along the slope results in a higher critical bed shear stress than in flat bottom conditions. This is formulated by (2.34).
Bed-load transport blockage	Bed-load transport blockage can occur at steep slopes.

The effect of slope angle on the critical shear stress can be adequately described, but the effects on actual shear stress are less clear.

LAUCHLAN (2001, 2004) performed laboratory experiments of sediment transport over vertical wall weirs and sloped (1:4) weirs. She concluded that for vertical wall weirs, a strong vortex upstream of the weir entrains all bed-load and suspended-load material and transports it over the weir. For sloped weirs, the strongly accelerating flow entrains all sediment as it attempts to move up the slope. In both cases, no deposition occurs upstream of the weir. The interaction between bed-load and suspended-load transport around the weir appears to be very important.

At the downstream slope, all the sediment passes the slope. The morphological processes downstream of this slope are comparable to sedimentation in a sand trap or scour effects around structures (MOSSELMAN, 1998).

Observations in the field contradict the conclusions of Lauchlan. At high flood events, significant deposition is observed at the upstream slopes of e.g. summer dikes.

The following reasons can be put forward:

The time scale of the flood event	It is possible that at some point, the flow conditions over the weir in the field allow deposition on the slope. In the experiment, the flow conditions are kept constant.
The effect of flow angle	The effect of flow angle can change the results. In the field, the flow is oblique rather than perpendicular to the slope (as in the experiments).
Sediment non-uniformity	Sediment non-uniformity in the field can result in preferential movement and deposition of material. This phenomenon was not taken into account in the experiments.
Three-dimensionality	The experiments are highly two-dimensional. All the approaching water is forced to move over the weir by the sidewalls of the flume. The conditions in the field are clearly three-dimensional. A part of the water flows over the weir, a part flows parallel to the weir.
Possible scale effects	It is possible that deposition occurs at relatively large water depths above the weirs in the field. In this case, also the acceleration of the flow is relatively small.

Unfortunately, no information is available about the conditions in the field when deposition occurs. At the downstream slope, the observed deposition in the experiments agrees with the observations in the field.

2.6. Depth-averaged analytical description

For the case of a (long) sill, simplified analytical descriptions of the flow are available (BATTJES, 2002). Two flow regimes are distinguished in the previous section: drowned overflow and free overflow.

An analytical description of *drowned overflow* is obtained using the conservation laws, as indicated in section 2.5.2.

Acceleration zone:

Continuity $$q = U_1 d_1 = U_2 d_2 \tag{2.36}$$

Conservation of energy $$d_1 + \frac{U_1^2}{2g} = h_{sill} + d_2 + \frac{U_2^2}{2g} \tag{2.37}$$

Deceleration zone:

Continuity $$q = U_2 d_2 = U_3 d_3 \quad (2.38)$$

Conservation of momentum $$\frac{1}{2}\rho g h_2^2 + \rho U_2^2 d_2 = \frac{1}{2}\rho g h_3^2 + \rho U_3^2 d_3 \quad (2.39)$$

In the case of *free overflow* ($\mathrm{Fr} > 1$), the flow is fully determined by the upstream boundary conditions. A (further) decrease of the downstream water level does not affect the discharge over the structure anymore.

$$q = m\frac{2}{3}E_2\sqrt{\frac{2}{3}gE_2}\,, \quad (2.40)$$

in which E_i is the energy height with respect to bed (if $i = 1$ or $i = 3$) or sill level (if $i = 2$) and m is an empirical discharge coefficient depending on weir shape (-). With this simple set of equations, it is possible to check the results of a numerical simulation of flow over a (long) sill roughly.

2.7. Summary

The *turbulent non-uniform flow* around hydraulic structures can be described with the *Navier-Stokes equations*, which are based on conservation of mass and momentum. In calculation models, not all the details of the turbulent flow can be resolved. For that reason, a statistical approach is frequently used, in which mean components and fluctuating components of the velocity and the pressure are distinguished. Ensemble averaging simplifies the Navier-Stokes equations to the *Reynolds equations*. These Reynolds equations are used in Reynolds Averaged Navier Stokes (RANS) modeling. Additional *turbulence models* are introduced to close the set of equations.

Sediment transport in rivers can be subdivided into *bed-load transport and suspended-load transport*. The separation between the different transport modes is dependent on the ratio between settling velocity w_s and shear velocity u_*. Suspended-load transport can be described by a transport equation, which contains (turbulent) advection and diffusion and a settling velocity caused by gravity. Bed-load transport is usually estimated with empirical formulas. A sediment balance can be used to determine *bed level changes*.

A distinction is made between *drowned overflow and free overflow* of a hydraulic structure, with Froude numbers smaller than one and greater than one, respectively.

At the *upstream slope* of a hydraulic structure, acceleration occurs. The depth-averaged velocity increases, resulting in larger equilibrium sediment concentrations and increased bed shear stresses. The effect of increasing bed shear stresses is reinforced by a deformation of the velocity profiles with respect to uniform flow. The increased bed shear stress indicates increased bed-load transports. However, the component of gravity along the slope results in a higher critical bed shear stress than in flat bottom conditions. This effect counteracts the increased actual bed shear stress. At steep slopes, bed-load transport blockage can occur. Laboratory experiments have shown that the interaction between bed-load and suspended-load transport around the structure is important. Sediment that approaches the structure as bed-load transport can be entrained by the reinforced flow forces, and brought into suspension over the structure.
At the *downstream slope*, all the sediment passes the slope. Depending on the geometry, sedimentation and/or scouring can occur. High levels of turbulence are found in this zone. Flow separation is found when the geometry contains abrupt changes. In extreme situations, a recirculation zone could come into play.

3. Model selection and model description

This chapter focuses on the theoretical background and the properties of the Computational Fluid Dynamics (CFD) software that has been used in this study. Firstly, the selection of the numerical flow model FLUENT is founded. After that, the relevant properties of Delft3D and FLUENT are described. In section 3.4, the differences between Delft3D and FLUENT are briefly summarized. The chapter ends with a section about computational grids.

3.1. Model selection

A model has to be chosen to simulate flow and sediment motion around hydraulic structures. This model should be capable of reproducing experimental data. When the results of the computational model agree with the experimental data, we have gained confidence to use this model in situations that are more complex. The outcomes of the simulations of these more complex situations will be compared with the results of Delft3D for the same situations. The results of this comparison will be used to assess the quality of the Delft3D computations.

Different Computational Fluid Dynamics (CFD) packages are available to simulate flow over hydraulic structures. The CFD package should preferably fulfill the following requirements:

- Available for use during the graduation period
- Non-hydrostatic flow calculations
- Possibility to simulate sediment transport
- Advanced turbulence modeling
- Free surface modeling.
- Relatively easy to use
- Technical support available
- Limited computation times

The experimental TU-Delft packages FINLAB and Large Eddy Simulation and the commercial packages CFX and FLUENT have been compared.

Available for use

FINLAB and Large Eddy Simulation are experimental packages of the Environmental Fluid Mechanics group of the Civil Engineering faculty of Delft University of Technology.

CFX is not available at TU-Delft. Deltares has one license available, but this license is used too intensively at this institute. FLUENT is available at the Mechanical, Maritime and Material engineering faculty of TU-Delft.

Non-hydrostatic flow calculations

All packages considered are capable of making non-hydrostatic calculations.

Possibility to simulate sediment transport

The four considered models are not meant to make fully morphological computations. In the packages CFX and FLUENT it is possible to release discrete particles in the flow. The particle motion is calculated by a stochastic analysis of the amount of turbulence and the gravitational forces on a particle. Also a continuous representation of sediment transport is possible, by means of an advection-diffusion consideration. This approach is applicable to

suspended sediment transport, but it does not hold for bed-load transport. In FINLAB only this continuous advection-diffusion modeling is available, though, this concept has not been validated yet. In the Large Eddy Simulation package, sediment transport modeling is not possible.

Advanced turbulence modeling

A correct representation of the turbulence in the complex flow around hydraulic structures is important. The Large Eddy Simulation package makes use of a high-quality Large Eddy Simulation code. In FINLAB, only RANS turbulence models are available. In CFX and FLUENT a RANS turbulence model is the default option, but also Large Eddy Simulation has been implemented. In LES, the macro structure of the turbulence is directly calculated; in RANS models, the turbulence is modeled by means of a mixing length hypothesis (as given in section 2.2).

Free surface modeling

Mainly in free overflow situations, the deformation of the surface behind a hydraulic structure is important. The LES package makes use of a rigid-lid assumption. Free surface calculations are therefore not possible. The other three models are capable of calculating the free surface. In CFX and FLUENT, also the air phase should be taken into account for free surface calculations (multiphase flows).

Relatively easy to use

A distinction is made between experimental, semi-commercial and commercial packages. Experimental means that there are numerous options to alter the code to meet the demands of the problem on hand. Altering is a specialized job that takes considerable time. FINLAB and Large Eddy Simulation are experimental packages of the Environmental Fluid Mechanics group of the Civil Engineering faculty of Delft University of Technology. Both packages have no user interface; the modeling is based on generating or altering FORTRAN code.
CFX and FLUENT are both commercial packages of the American company Ansys. These packages cover a wide range of applications in modeling fluid motion. The main part of the modeling can be done using the user interface. Modification of certain details is possible by making use of User Defined Functions (C++ code). Extended user guides are available, also for using the User Defined Functions.
Commercial software should always work, also when the user is not very competent. This is an advantage, because you cannot easily make big mistakes. At the other side, it can be disadvantageous, because the source code of commercial models is sometimes slightly adapted, so that it becomes e.g. unconditionally stable. This can influence the accuracy of the results.

Technical support available

CFX is not available at TU-Delft, which means that technical support is not available, in case educational licenses can be arranged. FLUENT is available at the Mechanical, Maritime and Material engineering faculty of TU-Delft. At this faculty, there is a FLUENT user group, so technical support is well available.
FINLAB and LES are products of the Civil Engineering faculty of the TU-Delft. Technical support of the developers is available.

Limited computation times

LES models require a dense grid and a small time step. Therefore, LES requires more computational resources than RANS models. Furthermore, in the LES model, 2DV simulation

is not possible, which is possible in the other models (though not combined with LES in CFX and FLUENT). Simulation of a free surface in CFX and FLUENT increases the computation time, because also the air phase should be taken into account and a grid refinement is needed at the interface of both phases. Parallel computations are possible with all models. Use could be made of a computer cluster at TU-Delft to run large FLUENT simulations. In general, it can be stated that the computation time of the simulations is dependent on the complexity of the problem. In LES, fewer simplifications are possible, so the computation time is always larger than in the other models considered.

The comparison between the four models is summarized in table 3.1.

Requirement	FINLAB	LES	CFX	FLUENT
Available for use	yes	yes	no	yes
Non-hydrostatic flow calculations	yes	yes	yes	yes
Possibility to simulate sediment transport	limited	no	yes	yes
Advanced turbulence modeling	no	yes	yes	yes
Free surface modeling	yes	no	yes	yes
Relatively easy to use	no	no	yes	yes
Technical support available	yes	yes	no	yes
Limited computation times	yes	no	yes	yes

Table 3.1 – Comparison of FINLAB, LES, CFX and FLUENT

Based on this comparison, FLUENT is chosen to use in this graduation study.

At Deltares, sediment transport modeling with FLUENT has been assessed (MEIJER, 1994). The sediment distribution between two branches at a river bifurcation has been modeled. The results of FLUENT are “qualitatively satisfying”. “On this ground it can be expected that FLUENT is a suitable instrument for solving more complicated problems”. No quantitative judgment has been made in this study.

This study supports the decision to use FLUENT for researching the sediment motion around hydraulic structures.

3.2. Delft3D

In this section, the relevant properties of Delft3D are described. For a more comprehensive overview of the physical processes that are included in Delft3D, reference is made to the User Manual (DELTARES, 2009).

3.2.1. General

Delft3D is a software system of the Dutch institute Deltares, developed for numerical modeling of flow and transport. Delft3D is meant for applications in coastal, river and estuarine areas. The package is able to model flow and transport phenomena of which the horizontal length and time scales are significantly larger than the vertical scales. Currents, waves, sediment transport, water quality and morphological development can be calculated.

Delft3D consists of several modules. Both 2D-horizontal and 3D computations are possible. Rectilinear and curvilinear, boundary fitted meshes can be used. In 3D computations, the

vertical is subdivided into different computational layers, following the sigma co-ordinate approach or the Cartesian co-ordinate approach. In the sigma-coordinate approach, the thickness of the layers depends on the distance between the free surface and the bed level. The number of layers is constant. In the Cartesian co-ordinate approach (called Z-grid mode), the layers are strictly horizontal. The number of layers depends on the local bed level. The transformation of z-coordinates to sigma-coordinates is given by:

$$\sigma = \frac{z - \zeta}{d} \tag{3.1}$$

The spatial schematization in Delft3D is based on the finite difference concept. The water level points, bed level points and velocity points are located at different positions on the numerical grid. The resulting pattern is known as a staggered grid. Several interpolation techniques are available to combine values of the different variables in the equations. For all details of the numerical aspects of Delft3D, reference is made to chapter 10 of the Delft3D-FLOW User Manual.

3.2.2. Assumptions

The following assumptions are made in the numerical code of Delft3D:

Incompressibility	The flow is assumed to be incompressible
Hydrostatic pressure assumption	The vertical momentum equation is reduced to the hydrostatic pressure relation (the hydrostatic pressure assumption). This implies that vertical accelerations are assumed negligible with respect to the gravitational acceleration. Vertical accelerations are therefore neglected. This assumption is not made when making use of the optional Non-Hydrostatic Pressure Model, which is only available in Z-grid mode. The hydrostatic pressure assumption simplifies the Reynolds equations to the shallow water equations.
Boussinesq approximation	The density is assumed constant in all terms of the flow equations, except the pressure term.
Reynolds averaging	The flow equations are Reynolds averaged, as described in section 2.1.3. This procedure introduces Reynolds stresses, which are related to the Reynolds-averaged flow quantities by a turbulence closure model. The treatment of turbulence in Delft3D will be described in section 3.2.5.
Boussinesq hypothesis	The Reynolds stresses affect the mean flow in the same way as viscous stresses.
Wall boundaries	At the bottom, a slip boundary condition is assumed. A quadratic bed shear stress formulation is applied.
Eddy viscosity and diffusivity	The effect of both 3D turbulent eddies and horizontal motions that are smaller than the horizontal grid size are taken into account by horizontal viscosity and diffusivity coefficients.

Table 3.2 – Assumptions underlying Delft3D that are relevant for this study

3.2.3. Flow equations

The *Reynolds equations* are simplified to the *shallow water equations* by the introduction of the *hydrostatic pressure assumption*. Integration of the shallow water equations over the water depth gives the 2D-horizontal shallow water equations. These equations contain depth-averaged velocities U and V.

$$\frac{\partial h}{\partial t} + \frac{\partial}{\partial x}(U \cdot d) + \frac{\partial}{\partial y}(V \cdot d) = 0 \tag{3.2}$$

$$\begin{aligned}
&\frac{\partial U}{\partial t} + U\frac{\partial U}{\partial x} + V\frac{\partial U}{\partial y} = -g\frac{\partial h}{\partial x} + fV + \nu_t^H\left[\frac{\partial^2 U}{\partial x^2} + \frac{\partial^2 U}{\partial y^2}\right] - \frac{gU\sqrt{U^2+V^2}}{C^2 d} \\
&\frac{\partial V}{\partial t} + U\frac{\partial V}{\partial x} + V\frac{\partial V}{\partial y} = -g\frac{\partial h}{\partial y} - fU + \nu_t^H\left[\frac{\partial^2 V}{\partial x^2} + \frac{\partial^2 V}{\partial y^2}\right] - \frac{gV\sqrt{U^2+V^2}}{C^2 d}
\end{aligned} \tag{3.3}$$

The continuity equation (3.2) contains one term representing the storage and two terms representing the net inflow in a control section, respectively. The momentum equations (3.3) contain a material derivative of the depth-averaged velocities (left hand side) and forcing terms (right hand side). The forcing terms represent a water level gradient, the Coriolis effect, diffusion depending on the horizontal eddy viscosity and bottom friction, respectively. The non-dimensionless Chézy coefficient C is used in the Delft3D formulations.

The 3D shallow water equations are given in terms of the velocity components u, v and w.

$$\frac{\partial u}{\partial x} + \frac{\partial v}{\partial y} + \frac{\partial w}{\partial z} = 0 \tag{3.4}$$

$$\begin{aligned}
&\frac{\partial u}{\partial t} + u\frac{\partial u}{\partial x} + v\frac{\partial u}{\partial y} + w\frac{\partial u}{\partial z} = -g\frac{\partial h}{\partial x} + \nu_t^H\left[\frac{\partial^2 u}{\partial x^2} + \frac{\partial^2 u}{\partial y^2}\right] + \frac{\partial}{\partial z}\left(\nu_t^V\frac{\partial u}{\partial z}\right) \\
&\frac{\partial v}{\partial t} + u\frac{\partial v}{\partial x} + v\frac{\partial v}{\partial y} + w\frac{\partial v}{\partial z} = -g\frac{\partial h}{\partial y} + \nu_t^H\left[\frac{\partial^2 v}{\partial x^2} + \frac{\partial^2 v}{\partial y^2}\right] + \frac{\partial}{\partial z}\left(\nu_t^V\frac{\partial v}{\partial z}\right) \\
&\frac{\partial p}{\partial z} = -\rho g
\end{aligned} \tag{3.5}$$

The Coriolis effect and baroclinic effects have been kept out of the equations. The hydrostatic pressure assumption results in the very simple momentum equation in vertical direction.

The position of the free surface is determined using a Height Function method. In this approach, a single-valued height function describes the position of the free surface as a function of the horizontal co-ordinate directions. In Z-grid mode the position of the surface is tracked using a Eulerian approach. When using the sigma co-ordinate system, a Lagrangian approach is adopted, where the grid is adapted with the movement of the free surface. The position of the free surface is calculated by solving a separate depth-integrated continuity equation.

The shallow water equations together with the free-surface equation form the basis of the Delft3D code (JAGERS & SCHWANENBERG, 2003).

3.2.4. Stability and accuracy

The Delft3D code uses an implicit numerical scheme, resulting in unconditional stability. However, too large time steps cause inaccurate results. This can be checked using the *Courant wave number* and the *Courant advection number* (COURANT AND HILBERT, 1962).

The Courant wave number is related to the propagation of energy through the system. During one time step Δt, energy is moved over a distance $c\Delta t$. The Courant wave number,

$$c\frac{\Delta t}{\Delta x}, \tag{3.6}$$

gives the number of cells over which the energy is moved within one time step. When the wave celerity $c=\sqrt{gd}$ changes gradually, large Courant wave numbers can be applied, in the order of 60. When sudden depth changes occur, the Courant wave number should be decreased.

The Courant advection number is related to the advection of water with the flow velocity U. The main importance of this number is the accuracy of the drying and flooding algorithm. During one time step Δt, water is moved over a distance $U\Delta t$. The Courant advection number,

$$U\frac{\Delta t}{\Delta x}, \tag{3.7}$$

gives the number of cells per time step that is skipped during drying or flooding with a velocity U.

3.2.5. Turbulence modeling

The Reynolds averaging procedure introduces Reynolds stresses into the momentum equations, as mentioned in the sections 2.1.3 and 2.2.2. A formulation for the Reynolds stresses in terms of an eddy viscosity is given in equation (2.8). This formulation is used in the diffusion terms of (3.5).

Delft3D uses anisotropic turbulence modeling: the horizontal and vertical eddy viscosity are treated separately. The *horizontal eddy viscosity* ν_t^H is usually set constant. This is physically incorrect, because the horizontal eddy viscosity is a property of the flow. However, in many cases a constant ν_t^H gives sufficiently accurate results. The horizontal eddy viscosity should be equal to the product of the velocity scale and length scale of the large momentum transferring eddies. When this approach is not sufficiently accurate, Horizontal Large Eddy Simulation (HLES) can be used, which is a special modified version of LES for shallow flows. A disadvantage of this approach is a stringent restriction of the time step.

A turbulence closure model is applied to calculate the *vertical eddy viscosity* ν_t^V. Four different options (in order of increasing complexity) are included in Delft3D:

- A user-defined constant vertical eddy viscosity.
- The Algebraic Eddy viscosity closure Model (AEM)
- The k-L turbulence closure model
- The k-ε turbulence closure model

The models give a relation between the turbulent kinetic energy k, the dissipation rate ε, the mixing length l_m and the vertical eddy viscosity ν_t^V.

A constant vertical eddy viscosity is the simplest concept, resulting in a parabolic velocity distribution over the vertical. This approach is very inaccurate. The other three models make use of the eddy viscosity concept of Kolmogorov and Prandtl, as described in section 2.1.3. This kind of models is indicated as eddy viscosity models in figure 2.1. The Algebraic Eddy viscosity closure Model uses analytical formulations to calculate k and l_m. The k-L turbulence closure model uses an analytical expression for the mixing length and a transport equation for the turbulent kinetic energy. The k-ε model uses transport equations for both k and ε.

3.2.6. Sediment transport and morphology

Delft3D supports both bed-load transport and suspended-load transport for non-cohesive material. Complications if compared to modeling of constituents like heat are for example the exchange of sediment with the sediment bed and the settling velocity caused by gravity. Exchange of sediment with the sediment bed causes changes in bed level, which results in changes in hydrodynamic behavior. In this way, the interaction between flow, sediment transport and morphology is taken into account.

Three-dimensional *suspended-load transport* is calculated using a three-dimensional advection diffusion equation, as given in (2.24). When using Delft3D in depth-averaged mode, also (2.24) is averaged over the water depth. The flow velocities and eddy diffusivities are based on the results of the hydrodynamic calculation (using the Reynolds analogy as described in section 2.3.2). The settling velocity is determined by the formulations of Van Rijn (1993) by default; see (2.23). The transport equation is not used when sediment type “bedload” is defined or when a transport formula is chosen that calculates a total transport, for instance Engelund & Hansen or Meyer-Peter-Müller.

Bed-load transport is calculated by transport formulas. These formulas give the magnitude of the transport. Subsequently, the sediment transport rates at the cell interfaces are determined, and corrected for slope effects, bed composition and sediment availability. Several bed-load formulations are available in Delft3D, varying in complexity and applicability. Bed-load transport is corrected for slope effects by a rotation of the transport vector.

At the boundaries, morphological boundary conditions should be defined. Sediment transports, bed levels and bed level changes can be prescribed. An alternative approach is the use of a Neumann boundary condition, which sets the inflow sediment concentration equal to the concentration calculated in the interior.

A number of standard sediment transport formulas is available in Delft3D, including Engelund & Hansen, Meyer-Peter-Müller (which both give a total transport rate) and Van Rijn (1993), which gives both suspended-load and bed-load transport rates. The more advanced formulas in Delft3D also include effects of for instance waves.

Because morphological processes take place at significantly larger time scales than the flow, a morphological acceleration factor can be used. The calculated bed level change within one time step is simply multiplied with this factor. In this way, computation times are decreased.

3.2.7. Hydraulic structures

In Civil Engineering practice, the domain of interest has often dimensions in the order of kilometers. To limit computation demands, a coarse computational grid is often chosen. The consequence is that not all details of the hydraulic structures present in the domain can be resolved onto the horizontal grid. That is why the structures are treated as subgrid features in Delft3D. A parameterization is applied to account for the force on the flow generated by the structure. The hydraulic structures are placed on velocity points of the staggered grid. The width of the hydraulic structures is set to zero. In this section, the different types of hydraulic structures in Delft3D are described.

Four types of parameterization are possible.

1. Partial blockage of the flow by a *3D gate*. The velocities and transport fluxes perpendicular to the hydraulic structure are set to zero. Both movable and fixed gates can be selected.
2. The second type of parameterization is *quadratic friction*. The flow through a hydraulic structure is related to the difference between the upstream and downstream water levels h by a Q-H relationship (3.8), in which μ is a dimensionless contraction coefficient, depending on the kind of hydraulic structure and A is the wet cross-section. A local equilibrium between the force on the flow due to the obstruction and the local water level gradient is assumed. An additional quadratic friction term is inserted into the momentum equations, depending on the contraction coefficient.

$$Q = \mu A \sqrt{2g\left|h_u - h_d\right|} \tag{3.8}$$

3. Thirdly, Delft3D offers the possibility of adding a *linear friction* term to the momentum equations, to reduce the flow rate through a certain cross-section. This kind of hydraulic structure is also known as a rigid sheet. The user should define the loss coefficients manually.
4. Finally, *floating structures* can be defined.

All energy loss formulations assume subcritical flow, except for the 2D-weir, for which an empirical formulation for supercritical flow has been implemented. The table below gives an overview of the relevant types of hydraulic structures. For a complete overview, reference is made to the Delft3D-FLOW user manual (DELTARES, 2009).

3D-gate	Represents small obstacles in the flow by inserting a vertical plate in one of the grid directions over one or more computational layers. (3D).
Barrier	A barrier restricts the flow area from above by blocking a part of the water depth. Combination of a movable gate and a quadratic friction term (3D) or only quadratic friction (2D).
Current deflection wall	Combination of a fixed gate and a quadratic friction term. A current deflection wall can be seen as a “plate on piles” in the flow. (3D)
Thin dam	All the velocities and transport fluxes perpendicular to this type of hydraulic structure are set to zero over the complete water depth. (2D and 3D)
Weir	Weirs are fixed structures, causing a local energy loss to the flow. They are commonly used to model sudden depth changes due to the presence of for example roads, dikes and groins. 2D-weirs are used in 2D-horizontal mode, local weirs in 3D mode.
2D-weir	The user-defined crest level is only used to determine whether the weir is emerged or submerged in the drying and flooding algorithm. When the weir is emerged, it acts as a thin dam. In a submerged state, a quadratic friction formulation is used. For supercritical flow, the discharge is completely determined by the upstream energy head. For subcritical flow, the energy loss is determined by a Carnot loss or using experimental data from tables. The choice depends on the local flow velocity. (2D)
Local weir	The water depth at the weir point is decreased, depending on the crest height. A part of the energy loss is computed directly by the discretization of the convection terms in the momentum equations and the bottom friction term. (3D)
Culvert	Intake / outlet coupling structure. The discharge through the culvert depends on the water level difference over the culvert. A quadratic friction term is applied. (3D).

Table 3.3 – Overview of types of hydraulic structures in Delft3D

3.3. FLUENT

FLUENT is a Computational Fluid Dynamics (CFD) package from the American company Ansys. A brief description of this model is given in this section. For more detailed information, reference is made to the FLUENT User Guide; see FLUENT INC. (2005). The content of this section is partly based on this User Guide.

3.3.1. General

FLUENT is capable of simulating both *two-dimensional and three-dimensional situations*. Both structured and unstructured *meshes* are possible. Different types of elements are permitted such as quadrilaterals and triangles for 2D simulations and hexahedra, tetrahedra, polyhedra, prisms and pyramids for 3D simulations. The geometry, mesh, boundary types and volume types can be specified in the preprocessor Gambit.

3.3.2. Turbulence modeling and wall treatment

Inside FLUENT different *turbulence models* are available, including various k-epsilon models, k-omega models, a Reynolds stress model (RSM), Detached Eddy Simulation (DES) and Large Eddy Simulation (LES). DES and LES are only available in the 3D version of FLUENT.

There are two approaches to model *boundary flows*. In one approach, the viscosity-affected region (the viscous sublayer and the buffer layer, as described in section 2.1.4) is not resolved. Instead, semi-empirical formulas called *wall functions* are used to bridge the viscosity-affected region between the wall and the fully turbulent region.

Three types of wall functions have been implemented in FLUENT:

Standard wall functions	A standard solution is prescribed for the flow near the wall, assuming flow parallel to the wall surface. Wall functions can be used when the distance z_p of the first velocity point from the wall satisfies approximately $z_p^+ > 20$.
Non-equilibrium wall functions	Non-equilibrium wall functions are modified standard wall functions, which have been implemented in FLUENT for non-uniform flow situations.
Enhanced wall treatment	Enhanced wall treatment makes use of enhanced wall functions, in which also an expression for the laminar sublayer is included. This approach can only be used when the grid resolution near the wall is high enough to discern the laminar sublayer, so $z_p^+ < 5$.

When the mesh near the wall is fine enough to resolve the laminar sublayer, the velocity in point p (in which $z = z_p$) of the wall-adjacent grid cell is calculated by:

$$u^+ \left(z = z_p \right) = z_p^+ . \tag{3.9}$$

If the grid resolution is too small to resolve the laminar sublayer, a logarithmic law-of-the-wall is adopted:

$$u^+\left(z = z_p\right) = \frac{1}{\kappa}\ln\left(Ez_p^+\right), \tag{3.10}$$

in which the empirical constant $E = 9.793$.

This approach is valid for hydrodynamically smooth walls. When a Nikuradse roughness height k_s is introduced (which is only possible when using wall functions), a law-of-the-wall modified for roughness is employed:

$$u^+\left(z = z_p\right) = \frac{1}{\kappa}\ln\left(Ez_p^+\right) - \Delta B. \tag{3.11}$$

This expression has (when plotted in a semi-logarithmic way) the same slope ($1/\kappa$) but another intercept than the standard law of the wall (3.10). This shifted intercept is given by ΔB. This ΔB has been found to be correlated with the dimensionless roughness height:

$$k_s^+ = k_s\frac{u_*}{\nu}. \tag{3.12}$$

Three different regimes can be discerned, based on k_s^+: hydrodynamically smooth conditions, a transition regime and fully rough conditions, respectively.

$$\begin{aligned}
&\Delta B = 0 && k_s^+ \le 2.25 \\
&\Delta B = \frac{1}{\kappa}\ln\left(\frac{k_s^+ - 2.25}{87.75} + C_s k_s^+\right)\cdot\sin\left(0.4258\left\{\ln\left(k_s^+ - 0.811\right)\right\}\right) && 2.25 < k_s^+ \le 90 \\
&\Delta B = \frac{1}{\kappa}\ln\left(1 + C_s k_s^+\right) && k_s^+ > 90
\end{aligned} \tag{3.13}$$

The roughness constant C_s is 0.5 by default, which corresponds to Nikuradse's resistance data for pipes. For non-uniform sand grains, a higher value is more appropriate ($C_s = 0.5 \sim 1.0$), but no clear guideline for choosing a proper value is available (FLUENT INC, 2005).

It is not physically meaningful to have a mesh size such that the wall-adjacent cell is smaller than the roughness height. The best results are obtained when the distance from the wall to the centre (velocity point) of the wall-adjacent cell is greater than k_s.

3.3.3. Multiphase flows

With multiphase modeling, flows that contain more than one phase can be modeled, for example a flow with both liquid and gas. The range of multiphase flows, which are of interest in this study, is limited to free surface flows and sediment transport.

Free surface flows are treated as immiscible fluids, separated by a clearly defined interface. An Euler-Euler approach is used to calculate this interface. In the Euler-Euler approach, the different phases are treated mathematically as interpenetrating continua. Since the volume of a phase cannot be occupied by the other phases, the concept of phasic volume fraction is introduced. The sum of the volume fractions of both phases (water and air) in a grid cell equals one. The volume fractions are assumed to be continuous functions of space and time. Conservation equations for both phases are used to calculate the multiphase flow.
Three Eulerian approaches are available in FLUENT: the Volume of Fluid (VOF) model, the Mixture model and the Eulerian model. In this study the VOF model is used, designed for two or more immiscible fluids where the position of the interface between the fluids is of interest. In the VOF model, the fluids share a single set of momentum equations, and the volume fraction of each of the fluids in each computational cell is tracked throughout the domain. Initial conditions and boundary conditions should be prescribed for the different phases.

Sediment transport is modeled using an Euler-Lagrange approach. The flow of the fluid phase is calculated by solving the discretized Reynolds equations. The discrete phase (the sediment particles) is solved by tracking the particles through the calculated flow field: a Lagrangian approach. An important condition for using the discrete phase model is that the discrete phase occupies a small volume fraction (below 10-12%). Exchange processes between the phases are taken into account, using one-way coupling (when the influence of the particle motion is negligible for the fluid motion) or two-way coupling. A particle trajectory is determined by considering the balance between gravitational forces and forces resulting from the turbulent motion around a particle:

$$\frac{du_{p,i}}{dt} = F_D\left(u_i - u_{p,i}\right) + \Delta g_i + F_{ext,i}\,, \tag{3.14}$$

in which $\vec{u}_p$ is the particle velocity, F_D is a drag force per unit particle mass, $u_i = \overline{u}_i + u_i'$ and F_{ext} is an additional acceleration force per unit particle mass. For spherical particles, the drag coefficient C_D as a function of the particle Reynolds number is determined by the relation of MORSI AND ALEXANDER (1972).

Two methods are available for taking the turbulent fluctuations u_i' into account: the random walk model and the particle cloud model. In the random walk model, the particle motion is calculated, including the effect of instantaneous turbulent velocity fluctuations by making use of stochastic methods. In the particle cloud model, the evolution of a cloud of particles is tracked, by discerning a mean trajectory and a Gaussian probability density function, representing the position of individual particles into the cloud. In this study, only the random walk model is used.
Both steady and unsteady discrete phase calculations are possible. In a steady calculation, the fluid motion is calculated first. When the flow field is in a steady state, the particles are inserted. The particle motion is calculated, based on the steady state turbulence properties. In an unsteady calculation, the fluid motion and the particle motion are alternately calculated. This approach requires more computational time; so unsteady particle tracking is only used when the temporal evolution of the flow is important for the sediment transport.

3.3.4. Boundary conditions

Many types of *boundary conditions* are available in FLUENT. Only the boundary conditions, which are used in this study, are listed in this section.

Wall	A no-slip or partial-slip condition is imposed, all fluxes perpendicular to the wall are set to zero. For turbulent flows, roughness conditions can be specified. A law-of-the-wall modified for roughness is used, in which three regimes can be discerned: hydrodynamically smooth conditions, fully rough conditions and a transitional regime. See sections 2.1.4 and 3.3.2 for more information. The roughness conditions influence the velocity profile in the wall region.
Symmetry	A free-slip condition is imposed, all fluxes perpendicular to the wall are set to zero. Symmetry conditions are applied to all equations. A symmetry boundary is used to define the water surface in rigid-lid calculations.
Velocity inlet	The velocity components, turbulence properties and other scalar properties are prescribed at the inlet boundary. When the density is constant, the velocity inlet fixes the mass inlet. With the help of User Defined Functions (C++ code), a function can be defined, coupling the inlet velocity to the location at the inlet boundary. In multiphase calculations, also the inlet volume fraction of the considered phases must be defined.
Outflow	This type of boundary condition is used at outlet boundaries, when the details of the flow velocity and pressure are not known beforehand. They are only appropriate in (nearly) uniform (fully-developed) flow regions, since an outflow boundary assumes zero normal gradients for all flow variables except pressure. FLUENT extrapolates the required information at the outlet from the interior. Therefore, the conditions at the outflow boundary have no impact on the upstream flow.
Pressure outlet	The static (gauge) pressure is defined at an outlet boundary. When using User Defined Functions, a hydrostatic pressure distribution can be prescribed, which is equivalent to a certain water level at the outlet boundary. Also realistic backflow quantities (and backflow phasic volume fractions in the case of multiphase flows) can be specified, leading to faster convergence with respect to outflow boundaries when reversed flow at the outlet boundary occurs during the iteration procedure.
Periodic	This type of boundary conditions is used when the geometry and the flow have a periodically repeating nature. It can for example be used to model the flow in an infinitely long channel. The outflow quantities at the outlet boundary are continuously imposed as inflow quantities at the inlet boundary. With this approach, you can save enormous amounts of grid cells. A longitudinal pressure gradient can be imposed in a periodic simulation to drive the flow.
Interior	This type of boundary conditions does not influence the flow at all.

Table 3.4 – Boundary condition types in FLUENT that are used in this study

When using discrete phase models, discrete phase boundary conditions should be defined at all boundaries. When a particle hits a boundary face, different scenarios are possible. A particle can be reflected by an elastic or inelastic collision, slide along the wall, escape through the boundary or be trapped at the boundary.

3.4. Comparison of Delft3D and FLUENT

In this section, the differences between Delft3D and FLUENT are summarized.

	Delft3D	**FLUENT**
Zone of application	Numerical modeling of currents, waves, sediment transport and morphology in shallow flows.	Numerical modeling of various kinds of flows.
Flow equations	Shallow water equations, which are the Reynolds equations, in which the vertical momentum equation is reduced to the hydrostatic pressure relation.	Filtered or Reynolds Averaged Navier Stokes (RANS) equations.
Turbulence modeling	Separated treatment of the horizontal and vertical eddy viscosity: *Horizontal*: user-defined constant eddy viscosity or Horizontal Large Eddy simulation. *Vertical*: k-ε turbulence model, more simple turbulence models or a user-defined constant eddy viscosity.	Reynolds Averaged Navier Stokes (RANS) modeling with different options for turbulence models: for example several types of k-ε and k-ω models and the Reynolds stress model (RSM). Large Eddy Simulation (LES), Detached Eddy Simulation (DES).
Sediment transport	Suspended-load transport and bed-load transport due to waves and currents.	Discrete phase modeling, with which particle trajectories can be calculated, based on gravity and steady state flow and turbulence properties.
Free surface modeling	Single-valued height function method.	Multiphase modeling, in this study with the Volume of Fluid method.
Grid generation	Horizontal grid: rectilinear or curvilinear. Vertical layers: z-grid or sigma-grid approach.	Very flexible. Structured and unstructured grids. Several element types like quadrilaterals and triangles for 2D simulations and hexahedra, tetrahedra, polyhedra, prisms and pyramids for 3D simulations.

Table 3.5 – Comparison of Delft3D and FLUENT

3.5. Computational grids

The appropriate generation of a computational grid is of great importance for the quality of the results of the flow simulation. The grid points are densely distributed in regions where the flow changes a lot, for example near wall boundaries and behind separation points. In the ideal case, the properties of the grid should have no influence on the final solution.

In good grids, the transition of one element to the other will be gradual. Quads (four-sided elements) are the preferred elements (in two-dimensional grids), as much like a square as possible. This means that the aspect ratio of a cell should be less than 1:10, except for the boundary layer very close to the wall. When triangular elements are needed, the triangles should preferably have as much equal sides as possible. At the wall rectangles perpendicular to the wall are preferred; triangles at the wall are not preferable.

One has to choose between a *structured grid* and an *unstructured grid*. The simplest approach is using Cartesian or rectilinear grids, for example the Z-grid mode in Delft3D. The staircase approximation of inclined boundaries can introduce significant errors. For that reason, curvilinear orthogonal grids are frequently used, in which also curved grid lines are present. Curvilinear grids are the default in Delft3D. Both grid types can be used in collocated (all variables in one point) or staggered (different locations for pressure points and velocity points) arrangement of variables. More flexibility is obtained by using domain decomposition, where the domain is split up into different mutually linked grids (JAGERS & SCHWANENBERG, 2003).

	Advantages	Disadvantages
Structured grids	✓ Good control over grid near walls or corners ✓ Fast numerical schemes	× More work for user, more surfaces should be created × Possible wasting grid points, when you have fine grids where it is not necessary
Unstructured grids	✓ Less work for user to create the grid, also for complex geometries ✓ Applicable in almost all situations	× The software has more work to create the grid × Less control over the region near the wall or an obstacle × When use of triangles is needed, the computations are less accurate and the simulation needs more memory and computation time. × Need for a more complex data structure and numerical schemes.

Table 3.6 – Advantages and disadvantages of structured and unstructured grids

Considering these advantages and disadvantages, structured grids are preferable when the geometry is not very complex.

4. Uniform flow and sediment transport

Several situations from literature have been modeled with the modeling systems FLUENT and Delft3D, to gain confidence in the performance of FLUENT (also in more complex situations) and to judge the representation of fundamental processes by both models. These situations are briefly described in this section. For information that is more detailed, reference is made to the corresponding literature.

The modeling of the situations from literature is treated in the chapters 4 to 8:

- Uniform flow and sediment transport: chapter 4
- Flow over weirs: chapter 5
- Flow over oblique weirs: chapter 6
- Sediment transport over weirs: chapter 7
- Three-dimensional flow and transport over hydraulic structures: chapter 8

Every chapter contains a description of the situation, a description of the model set-up in Delft3D and FLUENT and a presentation and discussion of the results. Also this chapter 4 has this structure. The section with results is subdivided in a part about hydrodynamic aspects of uniform flow and a part about sediment transport in uniform flow.

4.1. Simulation description

The representation of various fundamental processes can be judged by modeling uniform turbulent flow. The main results are vertical velocity profiles and the distinction between bed-load transport and suspended-load transport (section 2.3.1). A straight channel with a uniform depth of 5 meter is modeled. In addition, different sediment transport modes are investigated.

4.2. FLUENT model set-up

Because the geometry of the uniform flow has an infinite character, periodic boundary conditions can be used, see section 3.3.4. This results in a very short grid in flow direction. In this case, 10 grid points have been chosen, but even less cells is possible. In vertical direction, 25 intervals have been chosen, with smaller dimensions near the bed. The uniform flow character allows a rigid-lid approximation, so a symmetry boundary condition has been defined at a water level of 5 meter. The flow is driven by a constant pressure gradient $\partial p / \partial x$. This pressure gradient is related to the shear velocity by (VAN BALEN, 2005):

$$\frac{\partial p}{\partial x} d = \rho u_*^2 \tag{4.1}$$

The pressure gradient equals 0.18 Pa/m, resulting in $u_* = 0.030$ m/s and $U \approx 1$ m/s. The roughness height has been set at 0.2 mm.

Several runs have been performed with discrete phase modeling, to investigate the reproduction of sediment transport in uniform flow by FLUENT. The particle diameter has been varied in these runs.

4.3. Delft3D model set-up

A straight channel section with a constant depth of 5 meter, a width of 10 meter and a length of 100 meter has been modeled on a grid with 100x10 grid cells. The vertical has been

subdivided into 10 layers. At the inlet, a total discharge of 50 m^3/s has been imposed, resulting in a depth-averaged velocity of 1 m/s. The vertical profile for hydrodynamics has been set on “logarithmic”. At the downstream boundary, a water level has been prescribed, corresponding with the water depth of 5 meter. For the bottom roughness, $z_0 = k_s / 30 = 2 \cdot 10^{-4} / 30 = 6.6667 \cdot 10^{-6}$ m has been defined. At the sidewalls, a free-slip condition has been chosen. The k-epsilon turbulence model calculates the vertical eddy viscosity.

The Courant advection number $U\Delta t / \Delta x \leq 1$ has been used, which results in $\Delta t \leq 1$ s. The Courant wave number $c\Delta t / \Delta x$ with $c = \sqrt{gd}$ equals 4.2 in this case. Because an implicit numerical scheme is used in Delft3D, this is no problem for stability. A Courant wave number of this order of magnitude gives sufficiently accurate results in a simulation with a smoothly varying water depth. For more information about the Courant conditions, reference is made to section 3.2.4. The Courant numbers have also been used in all other simulations to choose an appropriate time step. Therefore, the choice of the time step is not explicitly mentioned in the following sections.

4.4. Results

4.4.1. Velocity profiles

The distribution of velocity over the vertical for Delft3D and FLUENT is given in figure 4.1 in dimensionless form. The vertical ax is logarithmically distributed in the lower subplot.

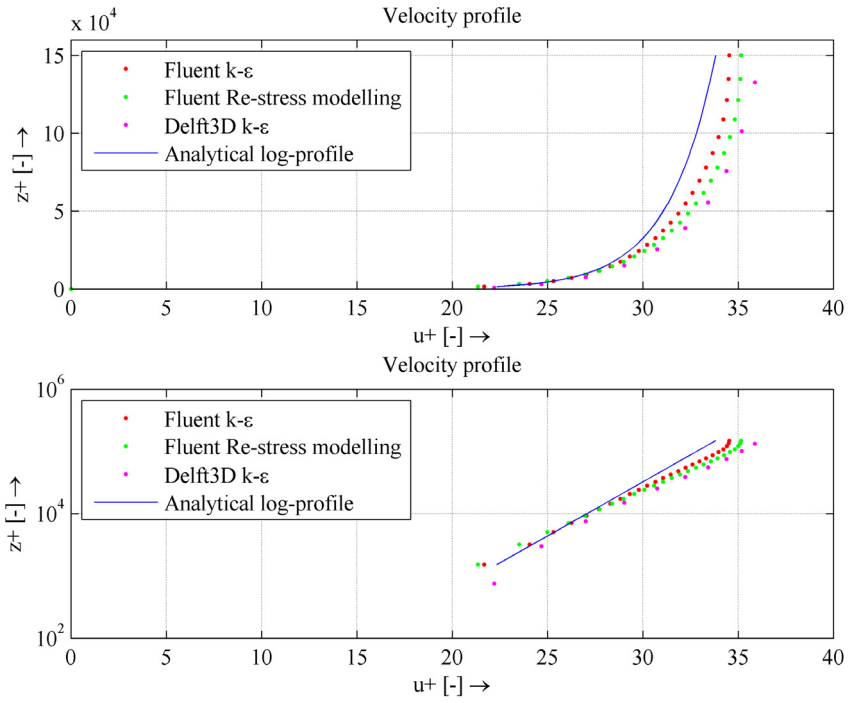

Figure 4.1 – Velocity profiles in uniform flow conditions

The analytical logarithmic profile has been obtained by using expression (2.11) in dimensionless form. The parameter z_0 is based on the Nikuradse roughness height; see (2.13). The remark should be made that the value 30 in this expression is an empirical value. Other textbooks recommend other values. Therefore, the shown analytical profile is not infallible. Furthermore, the discharge is not equal in the different simulations. This is because

a pressure gradient has been defined instead of a discharge. The different turbulence models give different relations between the pressure gradient, the shear velocity and the depth-averaged velocity.

The deviation in the FLUENT results in the upper part of the flow shows that the boundary flow has not been fully developed yet. In Delft3D, a logarithmic velocity profile has been imposed at the upstream boundary. The flow is immediately in a near-equilibrium state. Both models show the same trend.

It is important for sediment transport to investigate the reproduction of shear stress by FLUENT. Three situations have been considered, also in this case with $d = 5$ m and $U = 1$ m/s. Firstly, flow over a smooth bed has been modeled with enhanced wall treatment. $z_p^+ \approx 2.5$ has been chosen for the wall-adjacent velocity point p. In the second case the same flow has been calculated with standard wall functions, where $z_p^+ \approx 77$. Thirdly, a rough bed with $k_s = 0.03$ m has been considered, which is clearly in the fully rough regime ($k_s^+ > 90$). The mesh near the wall fulfills $z_p^+ > k_s$ corresponding to section 3.3.2.

In table 4.1, these three situations are shown. In the second column the shear velocity as calculated with equation (2.14) is shown. The third column gives the shear velocity based on the wall shear stress output of FLUENT.

Situation	**Shear velocity** *analytical*	**Shear velocity** *FLUENT*
Enhanced wall treatment, $k_s = 0$ m	0.0309 m/s	0.0298 m/s
Wall functions, $k_s = 0$ m	0.0309 m/s	0.0295 m/s
Wall functions, $k_s = 0.03$ m	0.0532 m/s	0.0532 m/s

Table 4.1 – Shear velocity in different FLUENT simulations

It can be concluded that both enhanced wall treatment and wall functions give a good reproduction of the wall shear stress in uniform flow conditions. This conclusion gives confidence for modeling situations that are more complex. This result has been obtained with a default roughness constant $C_s = 0.5$. Because the exact value of this constant is uncertain, we choose $C_s = 0.5$ in the subsequent chapters.

4.4.2. Sediment transport in uniform flow

In FLUENT, sediment transport is taken into account by making use of a discrete phase model. The performance of this approach has been investigated by considering the difference between suspended-load and bed-load transport.

Equation (2.14) gives $u_* = 0.0319\,\text{m/s}$ when $U = 1\,\text{m/s}$, $k_s = 0.2 \cdot 10^{-3}\,\text{m}$ and $d = 5\,\text{m}$.

Three types of sediment have been considered; see table 4.2. The settling velocity has been determined using (2.22). The distinction between the transport modes is based on (2.21).

Particle diameter *D* (μm)	**Settling velocity w_s (m/s)**	**Ratio w_s / u_***	**Transport mode**
100	0.0083	0.26	Suspension
250	0.0334	1.05	Saltation
500	0.0785	2.46	Bed-load

Table 4.2 – Types of sediment in FLUENT simulations

FLUENT represents the difference between suspended-load transport and bed-load transport correctly. Figure 4.2 shows suspended sediment transport at the downstream boundary, 300 meter from the upstream boundary.

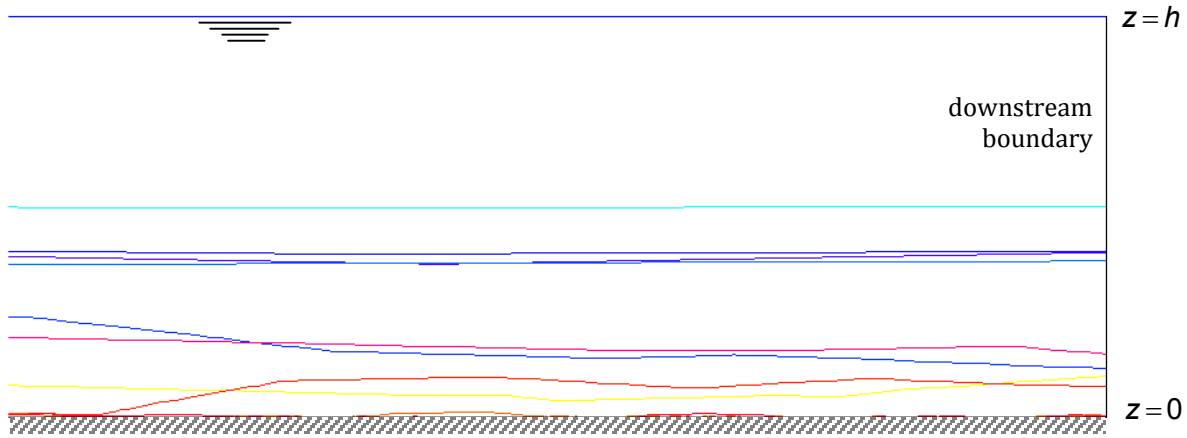

Figure 4.2 – Suspended sediment transport in FLUENT (D = 100 μm), particle trajectories at the downstream boundary. At the upstream boundary, 10 particles are linearly released from the bed (red) to the water surface (blue).

Saltation and bed-load transport look almost identical: particles move in an almost straight line (with slope w_s / u) to the bed. When the particles reach the bed, they begin to slide along the bed with a velocity significantly lower than the flow velocity. Bed-load material moves a bit slower than saltating material. As described in section 2.3.1, saltation is characterized by grains that jump and slide over the sediment bed, and reach heights of several grain diameters above the bed. Vertical movements are therefore negligible. Both Wall Functions and Enhanced Wall Treatment have been compared. This gave no difference for sediment transport in uniform flow.

It seems that FLUENT is not able to reproduce incipient motion. For large values of w_s / u_*, vertical movements reduce to zero, but particles keep sliding over the bed. This is also the case when the critical shear stress exceeds the actual bed shear stress. Expressions for incipient motion or roughness effects are not taken into account in equation (3.14). When a particle is on the bed, the gravitational force is balanced by the reaction force of the bottom. The only remaining term is the drag term. This term causes acceleration of the particle, until the particle velocity equals the local flow velocity. For this reason, results for large values of w_s / u_* should be treated carefully.

4.5. Conclusions

Delft3D and FLUENT both show correct logarithmic profiles, which belong to uniform flow conditions. Shear velocities, as calculated analytically, are represented well by FLUENT. This holds both for hydrodynamically rough and smooth beds. FLUENT represents the difference between suspended-load transport and bed-load transport correctly. It seems that FLUENT is not able to reproduce incipient motion. Particles keep sliding over the bed when the critical shear stress exceeds the actual bed shear stress. For this reason, results for large values of w_s / u_* should be treated carefully.

5. Flow over weirs

The flow over weirs has been studied by STOLKER (2005ab). In his report, the flow over a groin section in a laboratory flume is described.

This chapter deals with this laboratory experiment. The situation is described, the model set-up in FLUENT and Delft3D is treated and the results are presented.

5.1. Simulation description

STOLKER (2005ab) describes the results of laboratory experiments of flow over different groin sections. The experiments have been performed in a flume of the laboratory of Deltares. The reports contain detailed data of water levels, velocity components and turbulence quantities. The flow over the groin section is in the drowned overflow regime in all cases.

In this study, the groin section T6, given in figure 5.1, has been modeled.

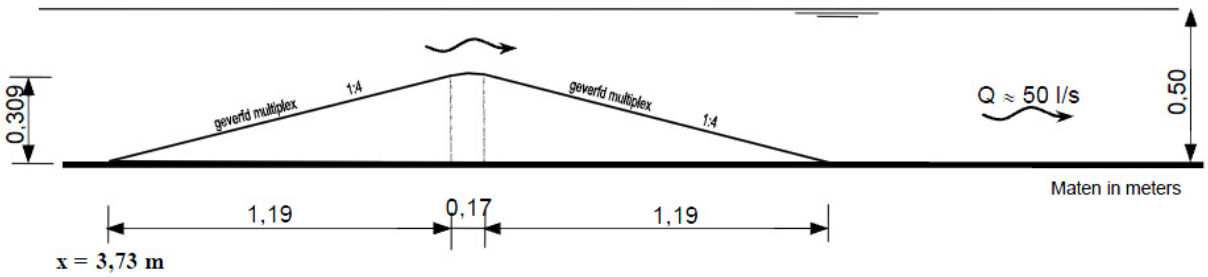

Figure 5.1 – Properties of groin section T6 (STOLKER, 2005b)

The 1:4 slopes of the groin had been made of painted multiplex, the groin crest of curved aluminum. The crest level is 0.309 m above the flume bottom. The downstream water depth equals approximately 0.503 m (averaged over time). The time-averaged discharge is 50.3 l/s. The width of the flume equals 0.5 m. The locations of the monitoring points for velocity and turbulent kinetic energy are indicated in figure 5.2.

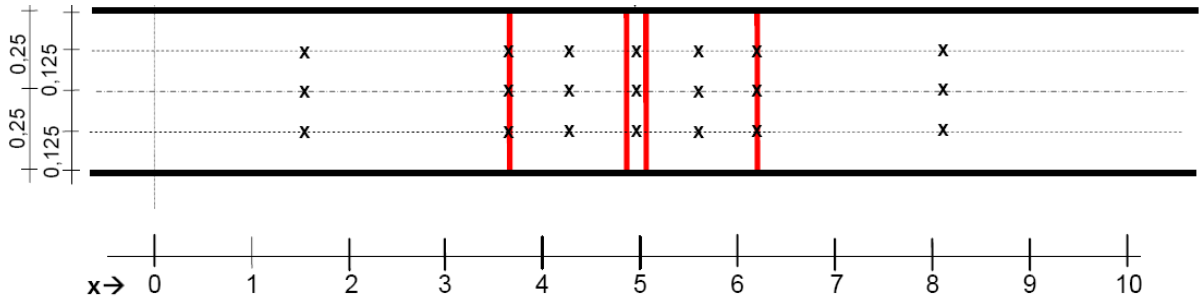

Figure 5.2 – Location of monitoring points in the experiment of STOLKER (2005b)

SCHWANENBERG (2006) performed 3D non-hydrostatic numerical simulations of the groin sections T6, T7 and T8 with the CFD package CFX to develop generic knowledge on the numerical computation of flow about hydraulic structures. His findings can be used to

optimize the way in which the flow is simulated, and to compare them with the results of FLUENT and Delft3D.

Groin section T3 from STOLKER (2005a) has also been modeled. The results of these simulations lead to the same conclusions as following from section T6. For that reason, the results of the modeling of section T3 are not shown in this report.

5.2. FLUENT model set-up

A brief description of the groin section has been given before. Only 2DV computations are performed. Data are used from the experimental investigation of this groin section to compare different modeling options:

- Rigid-lid computations or free-surface computations with the Volume of Fluid method
- Steady solver or non-steady solver
- Grid density
- Different turbulence models: k-epsilon model and Reynolds stress modeling
- Angular or rounded weir crest
- Wall functions or enhanced wall treatment
- Boundary condition types

Rigid-lid computations

The domain has a length of 12.55 meter and a height of 0.5 meter. The groin section is located between 5 and 7.55 meter. The final curvilinear 2DV grid contains 1000x40 elements. The choice for a curvilinear grid has been motivated in section 3.5. The density of the grid has been enlarged near the walls and in the flow separation zone. In the final model, the steady solver, the k-epsilon turbulence model, a rounded weir crest and non-equilibrium wall functions have been used. The boundary conditions are listed in table 5.1.

Location	Type	Characteristics
Bottom flume	WALL	Roughness height 0.2 mm*
Groin section surface	WALL	Roughness height 0.6 mm*
Inlet	VELOCITY INLET	Velocity: UDF **, $k = 0.0002$ m^2/s^2, $\varepsilon = 0$ *
Outlet	OUTFLOW	
Rigid-lid water surface	SYMMETRY	

Table 5.1 – Boundary conditions for rigid-lid FLUENT computations of the groin section

* Roughness heights and inflow turbulence quantities are adopted from SCHWANENBERG (2006).
** A logarithmic velocity profile is defined at the inlet, using a User Defined Function (UDF).

Free-surface computations

The domain has a length of 12.55 meter and a total height of 3 meter (containing approximately 0.5 m water phase and 2.5 m air phase). The groin section is located between

5 and 7.55 meter. The final 2DV grid contains 154x70 elements. In the final model, the steady solver, the k-epsilon turbulence model, a rounded weir crest and enhanced wall treatment have been used. The boundary conditions are listed in table 5.2.

Location	Type	Characteristics
Bottom flume	WALL	Roughness height 0.2 mm*
Groin section surface	WALL	Roughness height 0.6 mm*
Inlet water	VELOCITY INLET	Velocity: UDF **, $k = 0.0002$ m^2/s^2 *, $\varepsilon = 0$ *, Volume fraction water = 1
Outlet water	PRESSURE OUTLET	Pressure: UDF ***, Backflow equal to inflow at inlet boundary water phase
Water surface	INTERIOR	Initial water surface
Inlet air	VELOCITY INLET	$u = 0$, $k = 0.0002$ m^2/s^2 *, $\varepsilon = 0$ *, Volume fraction water = 0
Outlet air	PRESSURE OUTLET	$p = 0$. Backflow equal to inflow at inlet boundary air phase
Upper boundary	SYMMETRY	

Table 5.2 – Boundary conditions for free-surface FLUENT computations of the groin section

* Roughness heights and inflow turbulence quantities are adopted from SCHWANENBERG (2006).
** A logarithmic velocity profile is defined at the inlet, using a User Defined Function (UDF).
*** A hydrostatic pressure profile is defined at the inlet, using a User Defined Function (UDF).

The user-defined velocity profiles have the form of (2.11). They are based on the roughness height of the flume (via the integration constant z_0, see (2.13)) and the depth-averaged velocity, as given in STOLKER (2005b). The depth-averaged water flow velocity U is taken into account in the formulation of the shear velocity u_* by integrating the velocity profile over the water depth d. The relation between U and u_* is given by (2.14).

5.3. Delft3D model set-up

The flow over the groin sections has been modeled on a 552x2 grid with 20 sigma-layers. The height of the layers is smaller near the bed. Free slip has been chosen at the sidewalls. This is practically equivalent to a 2DV simulation. The weir shape has been taken into account in the depth file of Delft3D. At the inlet boundary, a depth-averaged velocity magnitude of 0.2012 m/s has been imposed, with a logarithmic distribution over the vertical. At the outlet boundary, the depth has been set to 0.5 meter. Nikuradse roughness lengths have been prescribed for the bottom roughness by a z_0-formulation, in which $z_0 = k_s / 30$. The Nikuradse roughness lengths are equal to the values in FLUENT, as shown in table 5.2. The k-epsilon turbulence model calculates the vertical eddy viscosity. The background vertical eddy viscosity has been set equal to the kinematic viscosity ν.

5.4. Results

The groin section of Stolker (2005b) has been modeled in FLUENT and Delft3D.

The following results are analyzed:

- Horizontal component of the velocity
- Vertical component of the velocity
- Turbulent kinetic energy
- Free-surface position

In the figures below, the experimental results (dots), the results of FLUENT with a rigid lid (green line, RL), the results of FLUENT with a free surface (red line, FS) and the results of Delft3D are shown (pink line). The locations are shown in figure 5.2. The Electromagnetic (EMS) velocity measurements are considered inferior to the Laser Doppler (LDS) measurements (STOLKER, 2005). Not all results are shown, mainly the results at the locations where the model results differ from the experimental values. Both horizontal and vertical velocity components are scaled with the mean inflow velocity at the upstream boundary (0.2 m/s).

It can be concluded that upstream of the weir crest, the results of both models are in good agreement with the measurements. Above the weir crest, the velocities are larger near the groin surface, due to acceleration of the flow. FLUENT reproduces this phenomenon well; Delft3D does not. This is shown in figure 5.3. This difference could result in a deviation of the prediction of bed-load transport over hydraulic structures in Delft3D. In the measurements, the flow is again horizontal above the weir crest. Both models show a significant upward velocity; see figure 5.4. The deviation is larger in Delft3D than in FLUENT.

Downstream of the weir, both FLUENT and Delft3D do not reproduce the flow separation very well. The distribution of the velocity over the vertical differs from the measurement. The downward movement of the flow behind the structure is too small in the model results. This is illustrated by the vertical velocity (also scaled with the mean total inflow velocity of 0.2 m/s) above the downstream slope in figure 5.5. Delft3D reproduces the vertical velocity a little better than FLUENT, in spite of the simplified formulations for the vertical velocity component. This result is related to the vertical velocity component above the weir crest, as shown in figure 5.4.

The following remarks can be made:

- Flow separation is a very complex process. Numerous studies have been carried out to describe this phenomenon with numerical models. The results are very sensitive to the turbulence model used, the treatment of the wall and the exact geometry of the structure. The reproduction of the flow separation in FLUENT appeared to be very sensitive to the exact groin shape. Tests with relatively more angular or more rounded crests showed significant differences in the results of FLUENT. The exact crest shape was not described in STOLKER (2005).
- In FLUENT, the velocities are systematically smaller than the measured values in the flume axis, because in the 2DV simulation the redistribution of the discharge over the width of the flume (due to the influence of the side walls) is not taken into account.
- The measurements in the flume axis (as shown in the figures) show significant differences with the measurements between the axis and the sidewalls. Clearly, three-dimensional effects are important.

- The velocity measurements near the free surface are systematically smaller than further down in the water column. This is due to secondary circulations in the flume. The models do not show this effect.
- In the separation zone, the turbulent kinetic energy differs significantly from the measured data. This is due to the limitations of the k-epsilon turbulence model. Delft3D showed larger errors, because only the vertical component of the eddy viscosity is modeled. The horizontal component is equal to the user-defined value everywhere. It should be mentioned that choosing the Reynolds stress turbulence model in FLUENT does not improve the results, in spite of the increased calculation time per iteration and the slower convergence.
- The Volume of Fluid multiphase simulation with FLUENT showed strange velocity values near the wall when the empirical non-equilibrium wall functions are used. Therefore, enhanced wall treatment (EWT) has been chosen, as described in section 3.3.2. In the rigid-lid (RL) simulations, the use of the wall functions (WF) gave no problems. The rigid-lid simulation results are not inferior to the multiphase simulation results in this case. Because multiphase modeling is very time-consuming (both in model set-up and calculation times), rigid-lid simulation is used in subsequent simulations, where the deformation of the surface remains relatively small.

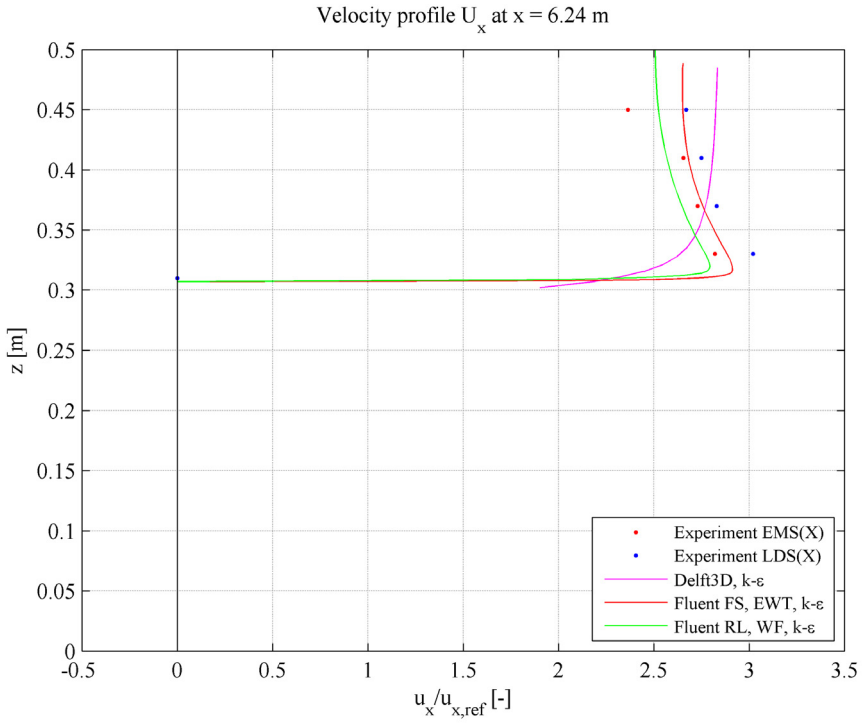

Figure 5.3 –Horizontal velocity above the groin crest, scaled with inflow velocity of 0.2 m/s FS = free surface, RL = rigid lid, EWT = enhanced wall treatment, WF = wall functions.

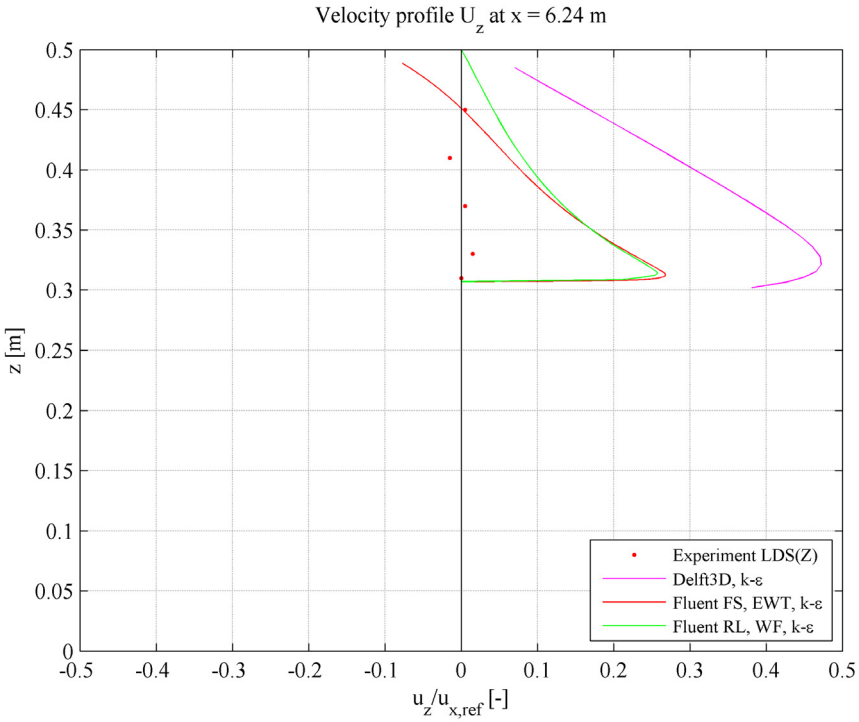

Figure 5.4 – Vertical velocity above the groin crest, scaled with inflow velocity of 0.2 m/s FS = free surface, RL = rigid lid, EWT = enhanced wall treatment, WF = wall functions.

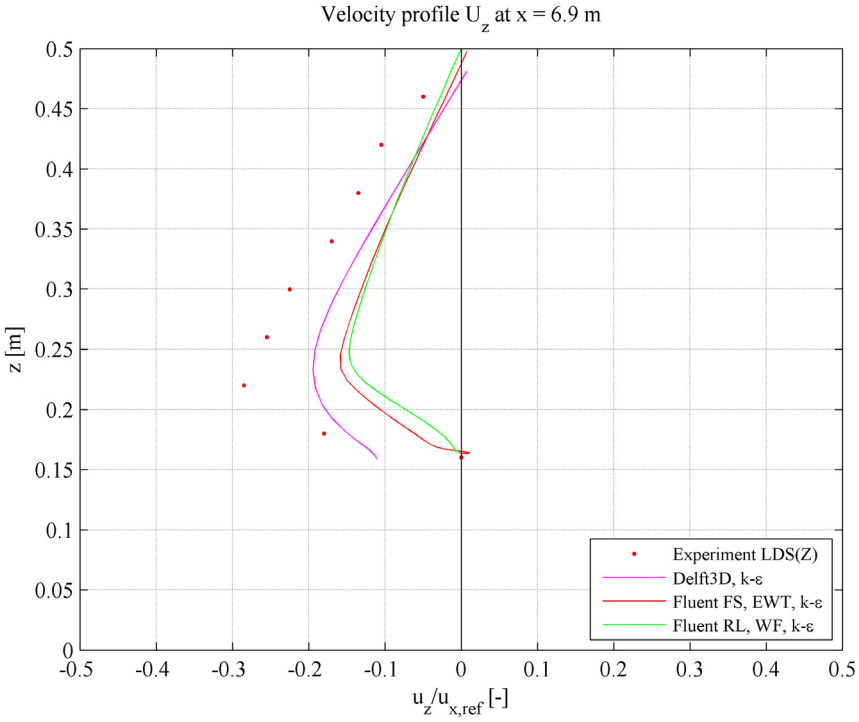

Figure 5.5 –Vertical velocity above the downstream slope, scaled with inflow velocity of 0.2 m/s FS = free surface, RL = rigid lid, EWT = enhanced wall treatment, WF = wall functions.

The position of the free surface in both models is compared to the measurements in figure 5.6. Delft3D calculates the free surface position using the single-valued height function method. It should be mentioned that FLUENT gives no exact position of the free surface. The Volume of Fluid method has been used, resulting in a gradual transition between the water and air phase. The blue line in figure 5.6 has been obtained by selecting the position with the largest (vertical) density gradient. The more continuously shaped red line shows a moving average of this free surface.

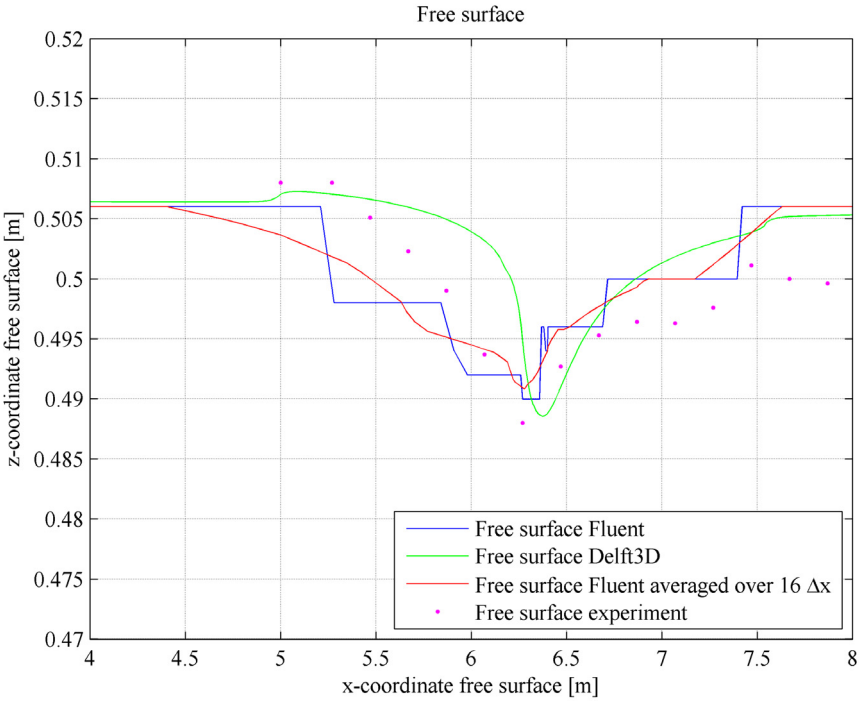

Figure 5.6 – Elevation of the free surface (m) above the weir crest

Both models reproduce the free surface very well, considering the free surface deformation in the order of two centimeters. The scaling of both axes is very different. The groin section is located between 5.00 and 7.55 m.

The results of both models can also be compared with the results of a Rigid-lid simulation (also using the k-epsilon turbulence model) of the same groin section with the Computational Fluid Dynamics package CFX, as described in SCHWANENBERG (2006). The deviations with the measurements as observed in the results of FLUENT and Delft3D, have qualitatively also been found in the results of CFX.

Concerning the aim of this study: the prediction of sediment transport over hydraulic structures, the results downstream of the groin crest are of less importance compared to the upstream side. The results of both models at the upstream side of the groin section are satisfying. In 3D situations, the errors downstream of a hydraulic structure do not influence the modeling of the sediment distribution between both sides of the structure. What happened with the sediment downstream of the structures (sedimentation patterns, scouring et cetera) is outside the scope of this study.

5.5. Conclusions

A laboratory experiment about flow over a 1:4 sloped weir has been modeled with Delft3D and FLUENT. The grid in both models has been refined to such an extent, that the details of the weir geometry can be taken into account correctly. It can be concluded that upstream of the weir crest, the results of both models are in good agreement with the measurements. Downstream of the weir, both FLUENT and Delft3D do not reproduce the flow separation very well. The statistical turbulence models in both numerical models (k-ε and in FLUENT also Reynolds Stress Modeling) are not able to describe flow separation correctly. Delft3D (with the height function method) and FLUENT (with the Volume of Fluid method) are able to describe the deformation of the free surface, as measured in the experiment. When the deformation of the surface remains relatively small, the differences between rigid-lid computations and free-surface computations with FLUENT are negligible. Concerning the aim of this study: the prediction of sediment transport over hydraulic structures, the results at the upstream slope are of main importance. What happens with the sediment downstream of structures (sedimentation patterns, scouring et cetera) is outside the scope of this study.

6. Flow over oblique weirs

Experiments of oblique weirs, which had been performed by NGUYEN (2006), have been modeled with FLUENT and Delft3D. This chapter deals with three of this laboratory experiments. The situations are described, the model set-up in FLUENT and Delft3D is treated and the results are presented.

6.1. Simulation description

When a weir is placed under an angle to the flow, the flow becomes three-dimensional. Experiments of oblique weirs have been performed by NGUYEN (2006). I have taken three situations with a trapezoidal weir at an oblique angle of 45 degrees. All the experiments of Nguyen have been listed in appendix B.2 of his report. I have simulated the situations 32, 35 and 38 of this list. The relevant properties of these experiments are listed in table 6.1.

Property	**Experiment no. 32**	**Experiment no. 35**	**Experiment no. 38**
Oblique angle (degrees)	45	45	45
Weir type	Trapezoidal	Trapezoidal	Trapezoidal
Weir crest height (m)	0.102	0.102	0.102
Discharge (l/s)	30	30	30
Water level above bed: upstream (h_0) (m)	0.1402	0.1691	0.1406
Water level above bed: downstream (h_2) (m)	0.1073	0.1684	0.1260
Froude number above weir	0.97	0.22	0.91
Submergence h_2/h_0	0.14	0.99	077

Table 6.1 – Characteristics of the modeled experiments of NGUYEN (2006)

6.2. FLUENT model set-up

A multiphase model has been made in FLUENT, to investigate the flow in different flow regimes over the oblique weirs. The boundary conditions have been defined in the same way as for the free-surface computations of the groin section of the previous section; see table 5.2. The structured grid contains 20x20x100 elements. The k-epsilon turbulence model has been used.

6.3. Delft3D model set-up

To simulate the flow over the oblique weirs of the experiments of Nguyen, a 200x40 grid has been chosen, with 10 computational layers. The height of the layers is smaller near the bed. The shape of the weirs has been included in the depth file. At the inlet boundary, a total discharge has been prescribed, with a logarithmic distribution over the vertical. At the outlet boundary, a water level boundary condition forces the water depth to the value from the experiment. The roughness of the bottom and the walls corresponds to $k_s = 0.2$ mm. Nguyen did not give a value of the roughness of the flume and the weirs in his report.

The k-epsilon turbulence model calculates the vertical eddy viscosity. The background vertical eddy viscosity has been set equal to the kinematic viscosity ν. The horizontal eddy viscosity has been set to 0.005 m^2/s. This value has been calculated with $\nu_t = \kappa u_* h / 6$. Delft3D is often applied in situations where the horizontal eddy viscosity is much larger than the vertical eddy viscosity. Because the flow is bounded by the flume walls in this situation, the anisotropy of the turbulence is not very large in this particular case.

6.4. Results

6.4.1. FLUENT

Quantitative reproduction of the experiments of Nguyen is difficult, because it is not clear in which experiment certain phenomena had been observed. Three situations are selected with different expected flow regimes. This expectation is based on the Froude number on top of the weir and the submergence. Figures 6.1 to 6.3 give the free surface position for the experiments with numbers 35 (drowned overflow expected), 32 (free overflow expected) and 38 (in which maybe undulations are visible).

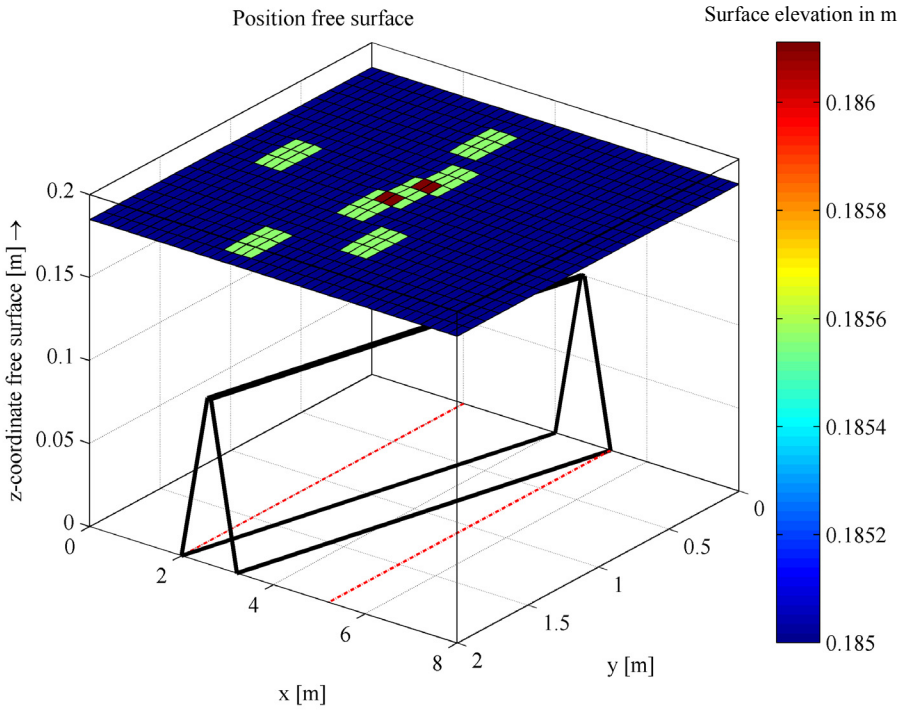

Figure 6.1 – Position (z-coordinate) of the free surface in FLUENT (m), experiment Nguyen no. 35 with drowned overflow

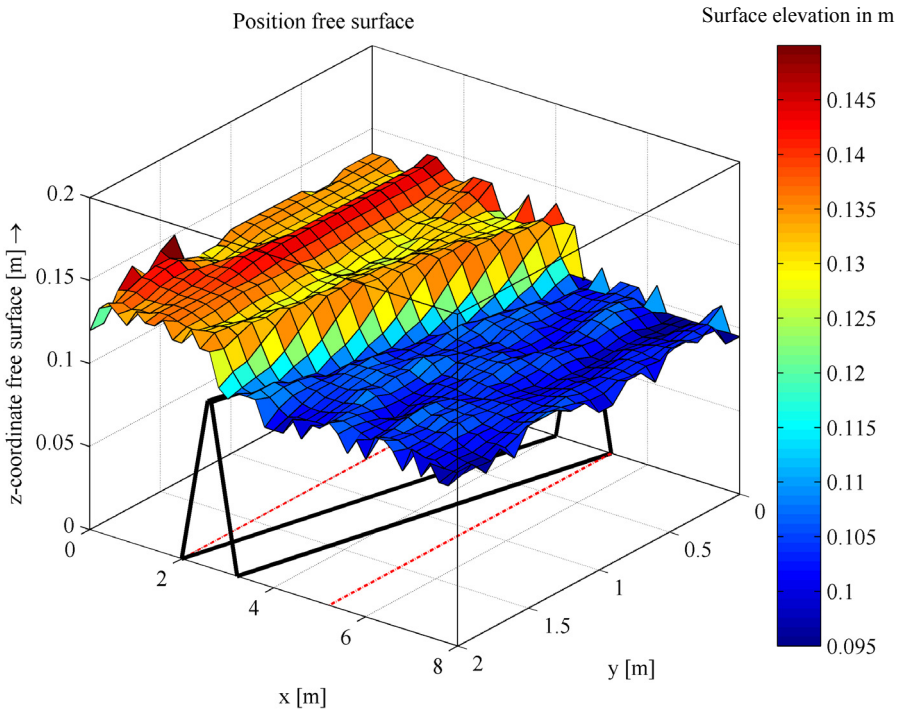

Figure 6.2 – Position (z-coordinate) of the free surface in FLUENT (m), experiment Nguyen no. 32 with free overflow

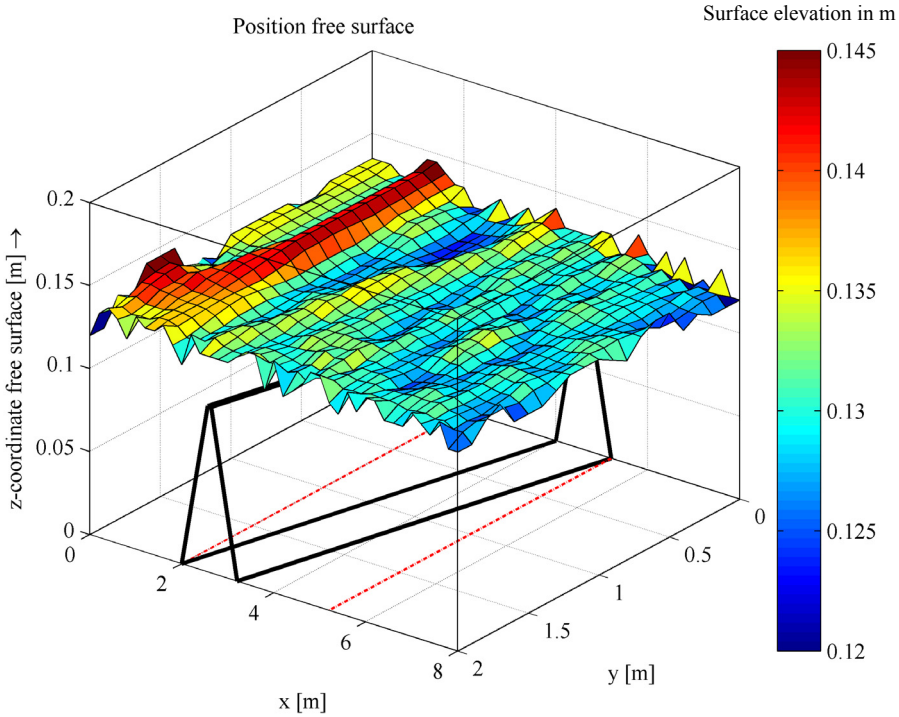

Figure 6.3 – Position (z-coordinate) of the free surface in FLUENT (m), experiment Nguyen no. 38 with undulated flow

FLUENT gives hardly any deformation of the free surface in the situation number 35 with a Froude number on top of the weir of 0.22 and a submergence of 0.99. This behavior clearly indicates drowned overflow. The water level as defined at the downstream boundary is dominant in the complete domain. The magnitude of the flow velocities on top of the weir is

approximately 0.2 m/s. This gives a Froude number of 0.24, which corresponds to the measured value. The flow downstream of the weir is more concentrated at the right side of the flume. This is because the flow on top of the weir turns in the direction perpendicular to the crest. This phenomenon was also observed in the experiment.

The simulation of situation number 32, with a Froude number on top of the weir of 0.97 and a submergence of 0.14, shows a hydraulic jump. Surface waves are visible, which indicates very turbulent flow. The water depths (and therefore the submergence) correspond with the values of the experiment. Flow velocities on top of the weir in FLUENT have a magnitude of approximately 0.9 m/s. Downstream of the weir, the flow is strongly concentrated at the right side of the flume. Nguyen observed a horizontal recirculation cell at the left side of the flume, but it is not clear in which situation with free overflow he observed this behavior. FLUENT does not show reverse flow.

The experiment with number 38 has a Froude number on top of the weir of 0.91 and a submergence of 0.77. Nguyen has not been described the observed flow regime in this situation. FLUENT shows a free surface without a hydraulic jump, but with small surface waves. These surface waves indicate undulated flow. The flow velocities on top of the weir are approximately 0.45 m/s.

The modeling of the oblique weirs shows that the Volume of Fluid method in FLUENT is able to reproduce free surface deformations, also in free overflow conditions.

6.4.2. Delft3D

Delft3D is not meant for non-hydrostatic flows over hydraulic structures. Correct modeling of the experiments with free overflow (number 32) and undulated flow (number 38) is not possible in Delft3D.

Non-hydrostatic effects are of less importance in drowned overflow conditions (number 35). Delft3D gives a Froude number on top of the weir of 0.21, which corresponds to the measured value of Nguyen. The deformation of the free surface is only 1-2 mm. This is qualitatively in accordance with the measurements and the results of FLUENT. The flow on top of the weir is not fully perpendicular to the crest. This is shown in figure 6.4. The flow in Delft3D has an angle of 21 degrees with respect to the flume axis (x-axis), while in the experiments nearly perpendicular flow over the crest was observed (45 degrees with respect to the flume axis).

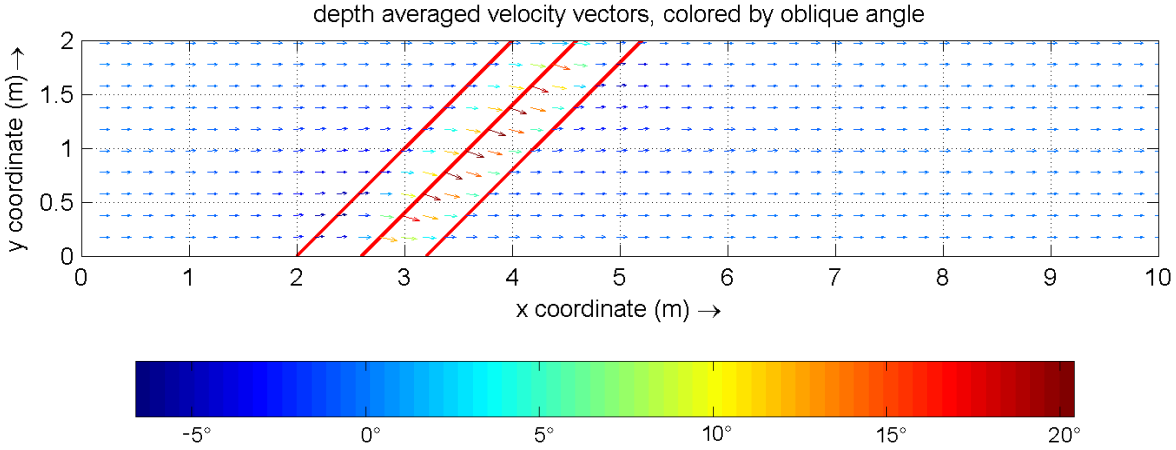

Figure 6.4 – Depth-averaged velocity vectors in Delft3D, colored by the angle of obliqueness (degrees) with respect to the x-axis. Experiment Nguyen no. 35, drowned overflow.

In spite of the non-valid hydrostatic flow assumption, the flow in the other two experiments also looks realistic. The experiment with number 32 gives a drop in water level of approximately six centimeter. Vertical velocities are limited to realistic values. The velocity magnitude on top of the weir is approximately 0.9 m/s, which is equal to the value from FLUENT. The same conclusion can be drawn for experiment with number 38.

6.5. Conclusions

Three oblique weir experiments have been modeled with drowned overflow, free overflow and a situation in between. Quantitative reproduction of the experiments of Nguyen is difficult, because it is not clear in which experiment certain phenomena were observed.

FLUENT reproduces the deformation of the surface qualitatively right in all situations. The hydrostatic pressure assumption in Delft3D makes correct numerical modeling of free overflow impossible. Therefore, the experiment with free overflow has not been modeled in Delft3D. A difference between the experimental results and the results of Delft3D is the oblique angle of the flow. The flow in Delft3D has an angle of 21 degrees with respect to the flume axis, while in the experiments nearly perpendicular flow over the crest has been observed (45 degrees with respect to the flume axis).

7. Sediment transport over weirs

Laboratory experiments of sediment transport over weirs have been performed by LAUCHLAN (2001, 2004). Transport over sloped weirs and vertical wall weirs have been investigated.

In this study, the experiments have been modeled with FLUENT and Delft3D. In this chapter, the situations are described, the model set-up in FLUENT and Delft3D is treated and the results are presented.

7.1. Simulation description

LAUCHLAN (2001, 2004) describes the results of experiments that have been carried out in a flume at the Fluid Mechanics Laboratory of the Delft University of Technology in 2001. In this experiments, flow and sediment transport over a sloped (1:4) and vertical wall weir were studied. Also the resulting bed levels and bed forms have been described.

In this study, the situations w1b (vertical wall weir) and w2b (sloped weir) are modeled. The characteristics of the sediment used are: $D_{10} = 0.112$ mm, $D_{50} = 0.164$ mm, $D_{90} = 0.238$ mm. The combination of flow and sediment characteristics results in the appearance of both bed-load and suspended-load transport. Some relevant characteristics of the experiments w1b and w2b are listed in table 7.1. All levels are measured with respect to the flume bottom. The width of the flume equals 0.80 m.

Property	Experiment w1b	Experiment w2b
Weir type	Vertical wall weir	Sloped weir, slopes 1:4, crest length 0.06 m
Flow regime	Submerged	Submerged
Water level upstream (m)	0.51	0.45
Water level downstream (m)	0.51	0.45
Average bed level upstream (m)	0.10	0.10
Average bed level downstream (m)	0	0
Weir crest level (m)	0.20	0.25
Depth-averaged velocity upstream (m/s)	0.43	0.35
Time averaged discharge (m^3/s)	0.141	0.098
Total sediment transport rate (kg/h)	40	9
Bed-load transport (kg/s)	0.0026	0.0011
Suspended-load transport (kg/s)	0.0086	0.0013

Table 7.1 – Characteristics of the modeled LAUCHLAN (2001) experiments

Lauchlan suggested that with the information from her experiments the following development can be undertaken:

- Calibration and validation of the existing Delft3D model concept for bed-load transport over weirs.

- The development of Delft3D model concepts for suspended sediment transport over weirs.

Lauchlan also tried to model the flow over the weirs with a non-hydrostatic and a hydrostatic two-dimensional vertical flow model, and to model the morphological development of the bed around the weirs with the help of Delft3D. Only a very brief qualitative description of the results of these models has been given in the report.

7.2. FLUENT model set-up

The experiments w1b and w2b of LAUCHLAN (2001) have been modeled. The final computations are 2DV with a rigid lid. For the case of a vertical wall weir (w1b), also 3D computations have been carried out, both with the k-epsilon turbulence model and with Large Eddy Simulation. The length of the domain equals 10 meter, with the weir in the middle of the domain. The height and (in 3D) the width are equal to the experimental values. The 2DV grid contains 700x80 (LxH) grid points, the 3D grid 500x15x40 (LxBxH) grid points. The density of the grid has been enlarged near the walls and around the weir. The boundary conditions are listed in table 7.2.

Location	Type	Characteristics
Sediment bed	WALL	Roughness height 0.714 mm ($3D_{90}$)
Weir surface	WALL	Roughness height 0.6 mm
Inlet	VELOCITY INLET	Velocity: UDF, $k = 0.0002$ m^2/s^2, $\varepsilon = 0$
Outlet	OUTFLOW	
Rigid-lid water surface	SYMMETRY	

Table 7.2 – Boundary conditions for FLUENT modeling of LAUCHLAN (2001) experiments

Sinusoidal bed forms have been placed upstream of the weir, with constant amplitude and wavelength, corresponding with the average bed form dimensions as reported in LAUCHLAN (2001). The grain-related roughness is taken into account by a Nikuradse roughness height of $3D_{90}$.

When the flow is in a steady state, particles have been released and tracked. A one-way coupling discrete phase model has been used, in which the random walk model calculates the influence of the steady state turbulence on the particle trajectories. For more information, see section 3.3.3. The particles release locations are uniformly distributed over the inlet boundary (particle injection type “group”).

A Rosin-Rammler sediment distribution has been applied to represent the sediment characteristics from the experiment. A minimum, maximum and mean diameter should be defined, as well as a spread parameter. For the calculation procedure of the spread parameter, reference is made to the FLUENT User Guide (FLUENT INC., 2005).

7.3. Delft3D model set-up

The experiments of Lauchlan have been modeled on a 200x16 grid with square grid cells. Different simulation methods have been tested, to compare the performance of these methods for sediment transport over hydraulic structures.

Case of a vertical wall weir:

- Depth-averaged simulation, weir taken into account in a depth file.
- Depth-averaged simulation, weir taken into account by a 2D-weir.
- 3D simulation, weir taken into account in a depth file.
- 3D simulation, weir taken into account by a local weir.

Case of a sloped weir:

- Depth-averaged simulation, weir taken into account in a depth file.
- 3D simulation, weir taken into account in a depth file.

In the 3D simulations, the vertical has been subdivided into 10 layers. Firstly, a hydrodynamic simulation has been performed, to create steady state flow. This steady flow has been introduced as an initial condition for the flow in the morphological simulation by a restart file. The details of the modeling in Delft3D are summarized in table 7.3.

Component	**File**	**Description**
Length simulation	mdf	Equal to length experiment
Time step	mdf	0.048 s
Inlet boundary, flow conditions	bct	Total discharge, equal to value of experiment logarithmic distribution over the vertical
Outlet boundary, flow conditions	bct	Water level, equal to value of experiment
Suspended sediment concentration at inlet boundary	bcc	Equal to suspended-load / total discharge from experiment, uniformly distributed
Bed-load transport	bcm	Transport excluding pores, equal to bed-load transport from experiment
Sediment transport formula	tra	Van Rijn (1993)
Roughness, Chezy values	rgh	Values from experiment, including bed forms
Side-wall roughness	mdf	Partial slip, roughness length 0.2 mm
Horizontal eddy viscosity / diffusivity	mdf	Both 0.005 m^2/s
Background vertical eddy viscosity / diffusivity	mdf	Both 1e-6 m^2/s (kinematic viscosity)
Model for 3d turbulence	mdf	k-epsilon model
Specific density sediment	sed	2650 kg/m^3
Sediment diameter	sed	D_{50} = 164 μm, D_{10} = 112 μm, D_{90} = 238 μm
Sediment bed thickness	sdb	As in experiment
Morphological scale factor	mor	1 (no morphological acceleration applied)
Morphological updating during FLOW simulation	mor	Yes
Equilibrium sand concentration profile at inflow boundaries	mor	No
Minimum depth for sediment calculation	mor	1 mm
Threshold sediment thickness	mor	1 mm

Table 7.3 – Details of the modeling in Delft3D of the LAUCHLAN (2001) experiments

The values from the experiment can be found in section 7.1 or more extensively in LAUCHLAN (2001).
A 2D-weir is introduced in the *.wr-file, in which the location and the crest height of the weir are specified. A local weir is defined in the *.lwl-file. The energy loss by a local weir is partly calculated by the momentum equations and partly parameterized by an additional loss coefficient. Some test runs have been performed to investigate the correct value of this additional loss coefficient. The velocity difference over the weir in the 3D simulation with local weir resembles the results of all other simulations when this coefficient approaches zero.

7.4. Results

Sediment transport over the vertical and sloped weirs of LAUCHLAN (2001) has been modeled in Delft3D with the sediment transport formulation of Van Rijn (1993) combined with continuous bed level updating. Such morphological computations cannot be performed with FLUENT. In this model, the sediment transport is analyzed by particle tracking, as described in section 3.3.3.

7.4.1. Vertical wall weir, FLUENT

Firstly, a hydraulic computation has been carried out to create a steady state flow field and turbulence properties. LAUCHLAN (2001) observed a gyre upstream of the weir, which entrained all the sediment approaching the weir. Downstream of the weir, a strong recirculation cell is found, causing large deposition rates in this zone. Lauchlan also performed a numerical hydraulic simulation with a 2DV non-hydrostatic model. The results of this model did agree with the observations of the experiment, except the gyre upstream of the weir, which is of great importance for the sediment transport over the weir.

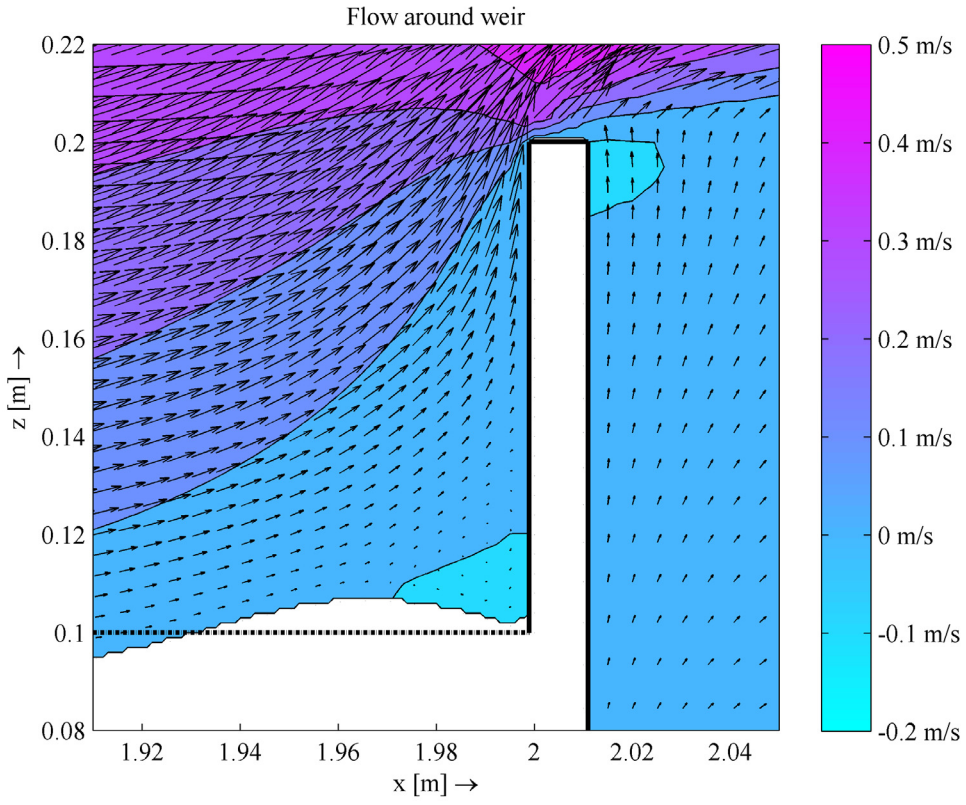

Figure 7.1 – Flow around a vertical wall weir in FLUENT, 3D, k-epsilon turbulence model

FLUENT also does not reproduce this gyre in 2DV or 3D with the k-epsilon or Reynolds Stress turbulence model; see figure 7.1. In addition, this result confirms the conclusion made in section 5.4 that using the Reynolds Stress turbulence model yields no significant improvement of the results. For this reason, a Large Eddy Simulation (only possible in 3D mode of course) has been carried out.

A gyre is visible in the Large Eddy Simulation; see figure 7.2. Unfortunately, Large Eddy Simulation in combination with Discrete Phase modeling is not implemented in FLUENT. The particle trajectories should therefore be analyzed using a statistical turbulence model like the k-epsilon model. LAUCHLAN (2004) suggests that the results of the 2DV computation with the non-hydrostatic flow model of BUSNELLI (2001) could be improved by a more detailed grid representation in the weir vicinity, better boundary condition definition especially at the weir, an improved turbulence model, and a move to 3D numerical flow models for such a situation. The FLUENT simulation performed in this study shows that the 2D k-epsilon turbulence formulation in the flow model of Busnelli can be indicated as the main cause of the poor representation of the flow upstream of the weir.

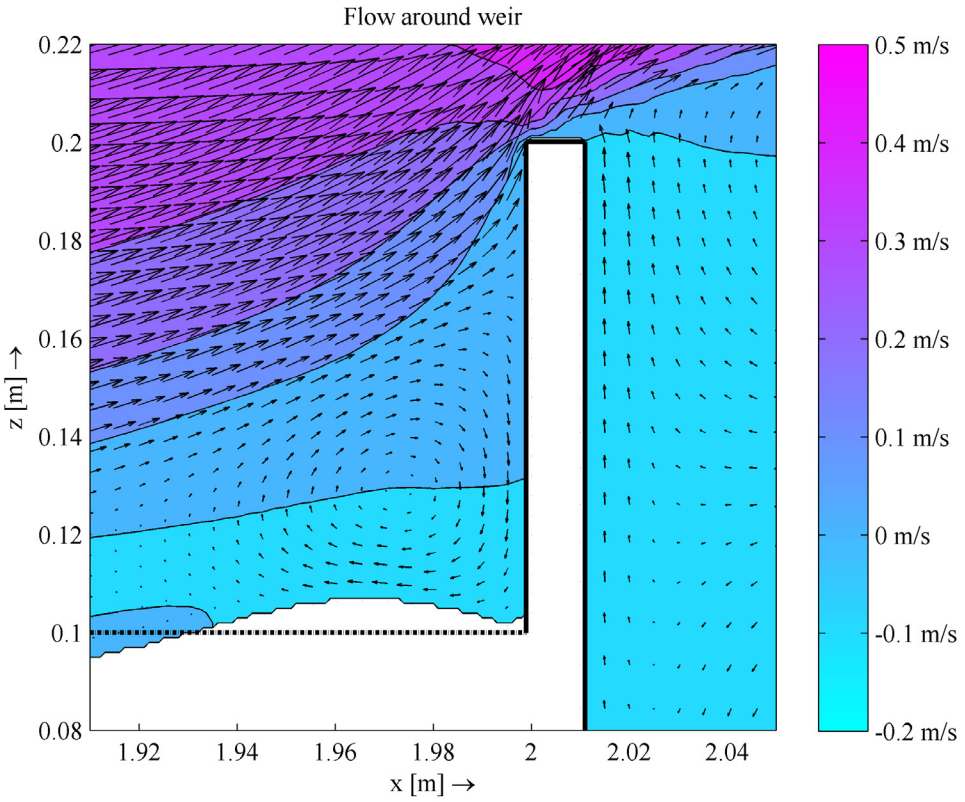

Figure 7.2 – Flow around a vertical wall weir in FLUENT, Large Eddy Simulation

The strong recirculation cell downstream of the weir is visible in all simulations. However, the LES simulation gives a more pronounced recirculation cell, with near zero velocities in the center. When the computation is finished, particles are released at the upstream boundary. Every result can be seen as a realization of a stochastic process, because the particle trajectory is determined by a probabilistic analysis of the turbulent forces on a particle. For more information, reference is made to section 3.3.3. One realization is shown in figure 7.3.

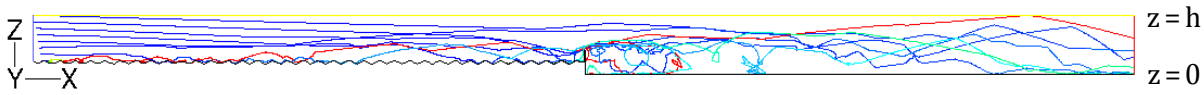

Figure 7.3 – Example of a realization of 10 particle trajectories in FLUENT. The color of the particle trajectories represent elapsed time, varying from blue (0 seconds) via green and yellow to red (210 seconds).

The difference between suspended-load transport and bed-load transport is clearly visible. Because the distance from the upstream boundary to the weir is just 5 meter, the sediment transport is not in equilibrium. The adaptation length of the suspended sediment profile $L_a \approx UH / w_s$ (in which w_s is calculated using the formula of VAN RIJN (1993) for natural sediment) equals approximately 8 meter. This should be taken into consideration in the analysis of the results. Several particles are entrained into the recirculation zone downstream of the weir.

Another way of visualizing the trajectories is using an x-t-diagram, in which the longitudinal position (in x-direction) of a particle is shown as a function of time. The x-t diagram of one realization is shown in figure 7.4.

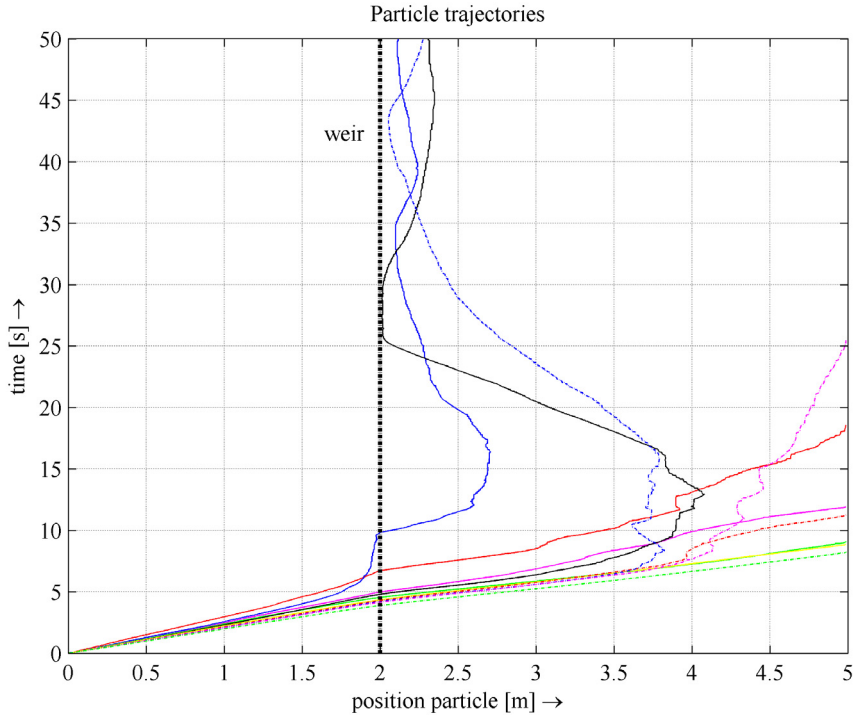

Figure 7.4 – Example of a realization of 10 particle trajectories in FLUENT, x-t-diagram

Most particles can pass the weir without any retardation. The reversed motion of some trajectories downstream of the weir indicates the entrainment of a part of the sediment by the recirculation zone. A small part of the sediment is retarded in the zone upstream of the weir. A strong interaction between bed material and suspended material is visible. After considering 100 particle trajectories, no particle remains upstream of the weir. The maximum observed retardation is 18 seconds. On average, a particle experiences a retardation of 0.4 seconds. The conclusion that all the sediment finally goes over the weir agrees with the observation of Lauchlan.

However, this conclusion does not guarantee that no sedimentation is found upstream of the weir. To estimate the sedimentation rate upstream of the weir, an analysis using the sediment balance principle (continuity) is used. Arbitrary mean particle trajectories are shown in figure 7.5.

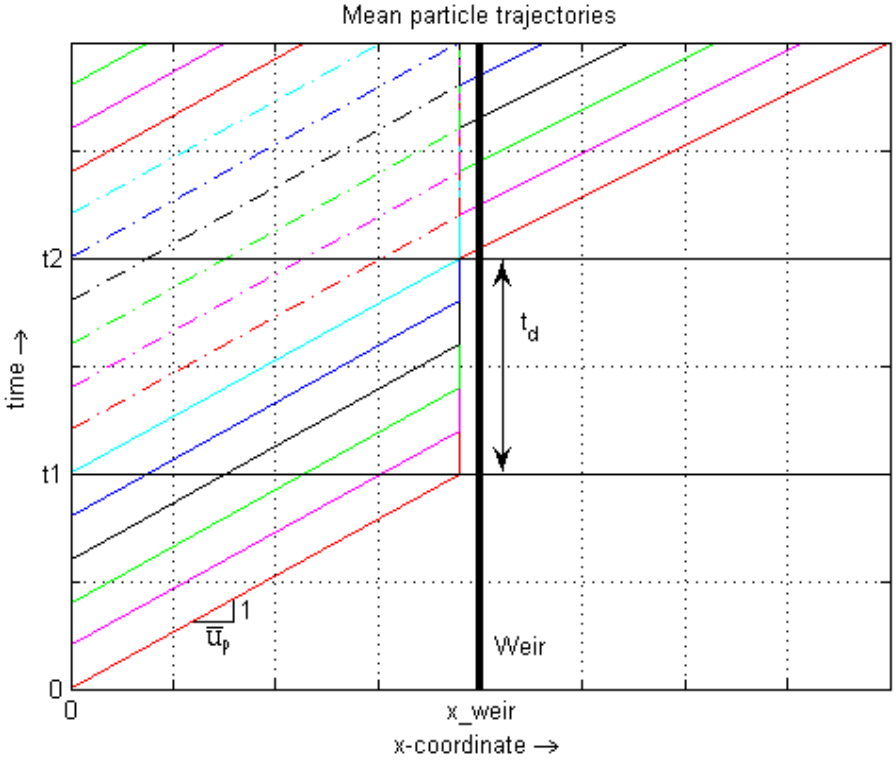

Figure 7.5 – Arbitrary mean particle trajectories shown by an x-t-diagram. The slope of the trajectories is equal to the mean particle velocity $\bar{u}_p$. Upstream of the weir, particles are retarded on average a time t_d.

The sediment balance reads:

$$\frac{1}{B}\frac{S_{out}-S_{in}}{\Delta x}=\frac{-\Delta z_b}{\Delta t}. \tag{7.1}$$

The following intervals can be discerned:

$0 \le t \le t_1$	$S_{in}=0$	$S_{out}=0$	$\Delta z_b=0$	No transport	
$t_1 \le t \le t_2$	$S_{in}=S$	$S_{out}=0$	$\Delta z_b=\frac{S\cdot(t_2-t_1)}{B\cdot\Delta x}$	Deposition	(7.2)
$t \ge t_2$	$S_{in}=S$	$S_{out}=S$	$\Delta z_b=0$	Equilibrium	

In which $t_d=t_2-t_1$ is the average delay upstream of the weir of an arbitrary particle. The zone where the delayed particles are found has a length of approximately $\Delta x \approx 0.05$ m. With the given values of $S=40$ kg/h and $B=0.8$ m, the total deposition due to the average delay of $t_d=0.4$ s equals 0.04 mm. It can be concluded that hardly any sedimentation occurs upstream of the weir. Inaccuracies in this analysis and the non-equilibrium state of the suspended sediment transport in FLUENT are not able to change this conclusion.

7.4.2. *Vertical wall weir, Delft3D*

Four different modeling methods have been assessed, as mentioned in section 7.3. The depth-averaged velocity at both sides of the weir for the four different modeling methods is shown in figure 7.6. The difference in velocity over the weir is approximately equal for all cases. The main difference between the cases is the absence of the enlarged velocity on top of the weir when a 2D-weir is used. In the depth-averaged simulations, only a depth-averaged velocity is calculated. This implies the absence of gyres and recirculation zones. In the 3D simulations, no gyre upstream of the weir and no recirculation zone downstream of the weir are visible at all. At both sides of the weir, unrealistically high vertical velocities are shown, both when the weir is taken into account in the bed level and when the weir is parameterized as a local weir. Clearly, Delft3D is not able to reproduce the flow pattern around a vertical wall weir. This was expected, because Delft3D is meant for flows where the horizontal components of the velocity are significantly larger than the vertical components.

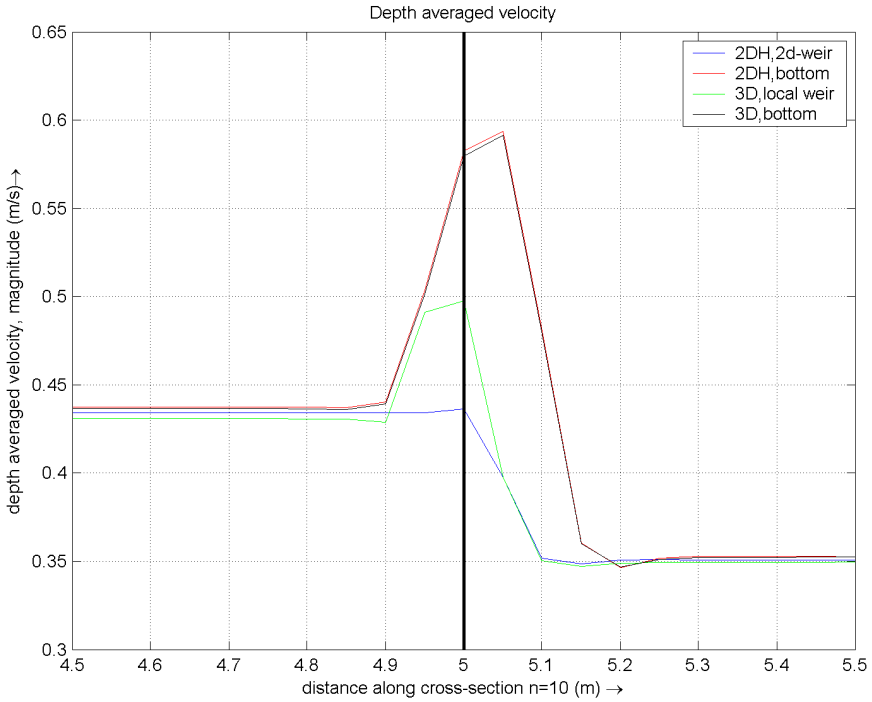

Figure 7.6 – Depth-averaged velocity (m/s) along the flume axis in different Delft3D simulations

The next step is the assessment of the morphological predictions of the model, in spite of the poor reproduction of the hydrodynamic aspects. The formula of VAN RIJN (1993) calculates both sediment transport modes as a function of the flow and the sediment characteristics. Both sediment transport modes ($m^3s^{-1}m^{-1}$) are shown along the flume axis in figure 7.7. Bed-load transport is given by the solid line, suspended-load transport by the dashed line. As in the experiment, a sediment bed with a thickness of 0.10 meter was located upstream of the weir. Downstream of the weir, no sediment is initially available at the bed. These lines show the initial sediment transport rates, so bed level changes do not affect the transport.

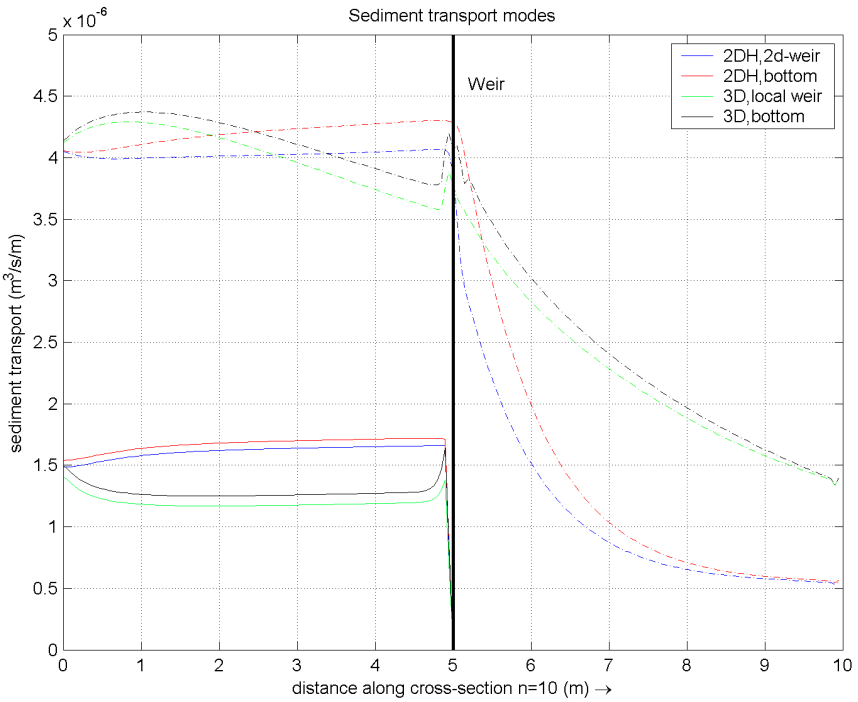

Figure 7.7 – Suspended-load transport (dashed lines) and bed-load transport (solid lines) ($m^3s^{-1}m^{-1}$) along the flume axis in different Delft3D simulations

Delft3D gives a bed-load transport of approximately $1.5 \cdot 10^{-6}$ $m^3s^{-1}m^{-1}$, which corresponds to 0.0032 kg/s. The suspended-load transport is approximately $4.1 \cdot 10^{-6}$ $m^3s^{-1}m^{-1}$, which corresponds to 0.0087 kg/s. These values are in good agreement with the measured values of Lauchlan (0.0026 and 0.0086 kg/s respectively, total transport rates).

The bed-load transport is fully blocked by the vertical wall weir. The bed material is not brought into suspension and taken over the weir, as observed in the experiment. It becomes not clear from this simulation if this blockage is caused by the decreased velocities or by the structure itself. The suspended transport rates are locally increasing due to the acceleration of the flow on top of the weir. Downstream of the weir, the sediment transport rates are rapidly declining, because the depth is suddenly increased, which causes decreased flow velocities.

The bed level change after 7 hours (equal to the length of the experiment) is shown in figure 7.8. Note that the scaling of both axes is different. A two-dimensional example is given in figure 7.9.

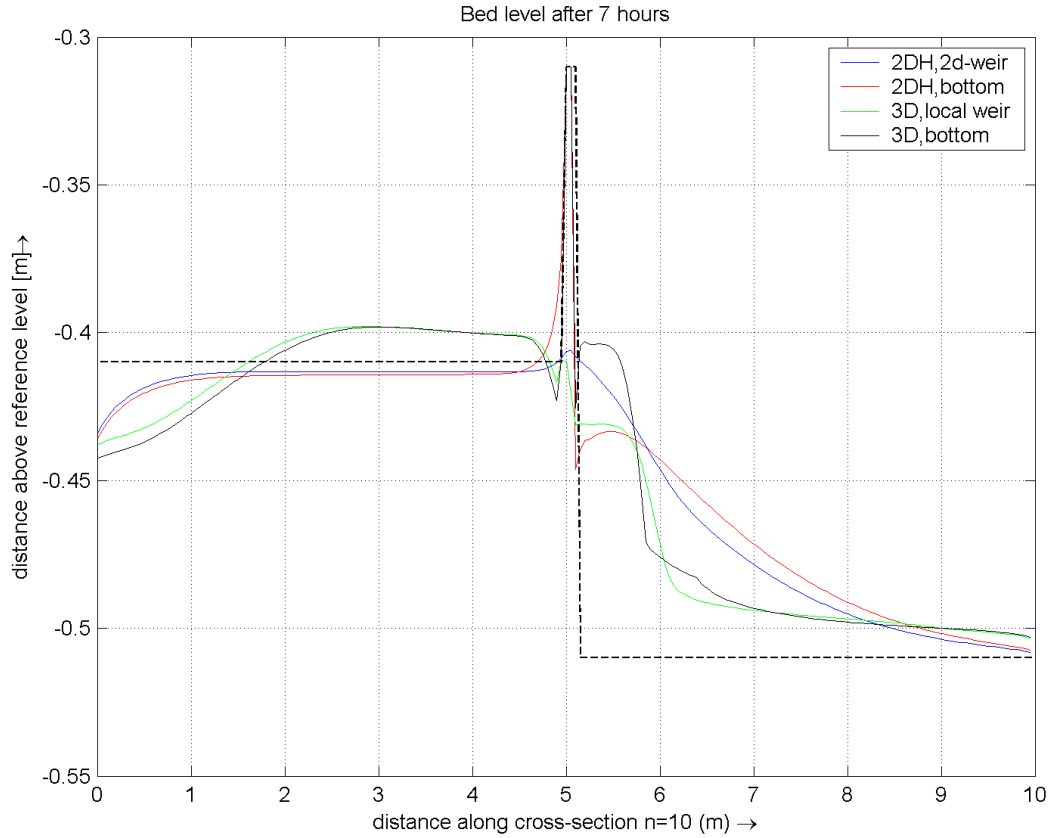

Figure 7.8 – Initial and final bed level along the flume axis in different Delft3D simulations

All simulations show erosion near the upstream boundary. Apparently, the imposed transports are not equal to the equilibrium conditions as calculated by Delft3D. Both 3D simulations give a deposition zone upstream of the weir, because the amount of suspended sediment decreases in streamwise direction, as shown in figure 7.7. Both results are caused by boundary effects, not by the effect of the weir.

Some erosion is found directly upstream of the weir due to the spurious flow accelerations, as mentioned before. This incorrect flow pattern shows that also the morphological results directly next to the weir are not reliable. Downstream of the weir, deposition is found in all cases. The deposited volume in the experiment has a height of approximately 0.1 m next to the weir and a total length of approximately 0.6 m. The 3D simulations are representing this volume best.

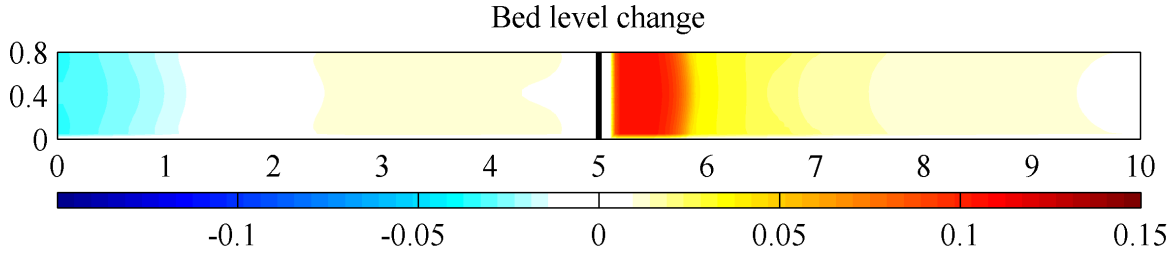

Figure 7.9 – 2D bed level change (m) in case of 3D modeling with a weir in the depth file

It can be concluded that the morphological results of Delft3D qualitatively agree with the experimental results, in spite of the incorrect representation of the flow around the weir.

7.4.3. Sloped weir, FLUENT

Because the geometry of a sloped weir is considerably less extreme than the geometry of a vertical wall weir, the flow over the weir is easier to calculate by the numerical models. FLUENT shows the flow pattern in figure 7.10.

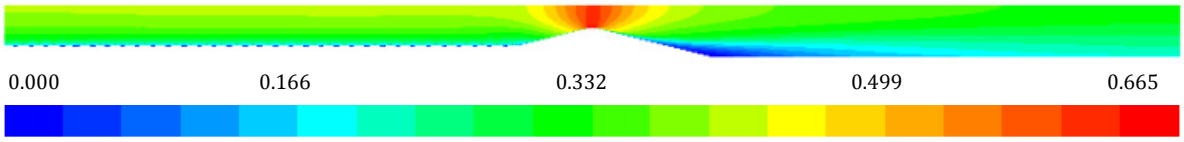

Figure 7.10 – Contours of velocity magnitude (m/s) in FLUENT for the case of a sloped weir

A small separation zone is visible at the toe of the downstream slope. The velocity on top of the weir equals approximately 1.8 times the velocity upstream of the weir. This is the result of the decrease in depth from 0.35 to 0.20 meter.
The particle trajectories are analyzed in the same way as in the case of a vertical wall weir. One realization of the particle trajectories is given in figure 7.11. Ten particle trajectories are shown in an x-t-diagram in figure 7.12.

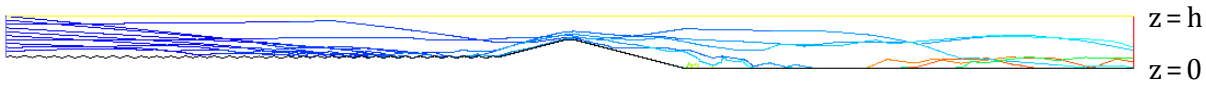

Figure 7.11 – Example of a realization of 10 particle trajectories in FLUENT. The color of the particle trajectories represent elapsed time.

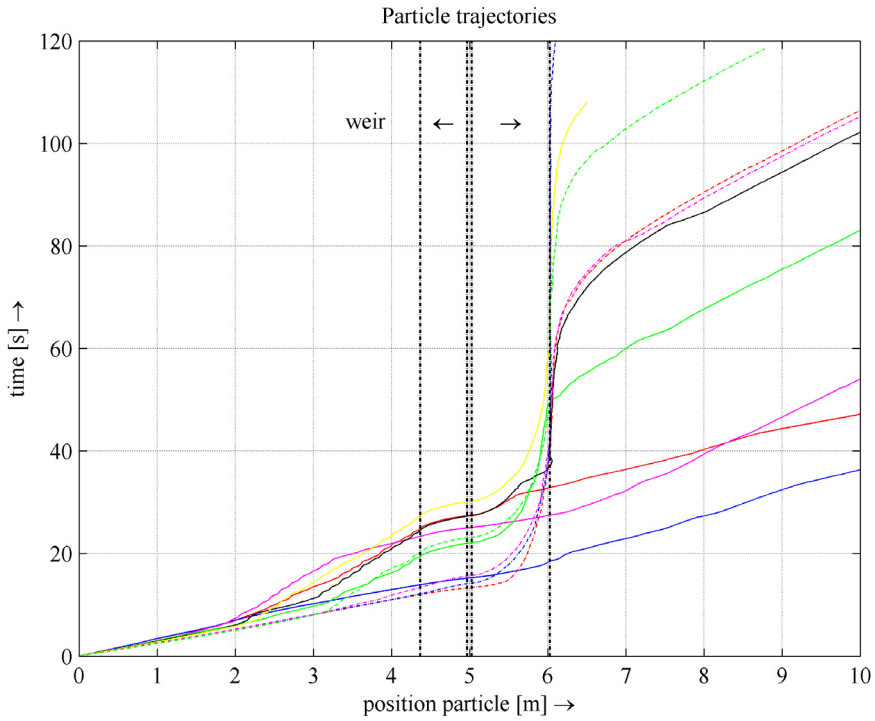

Figure 7.12 – Example of a realization of 10 particle trajectories in FLUENT, x-t-diagram

Also in this case, some particles are slightly retarded upstream of the weir. The average delay of a single particle is calculated on 6 seconds. The retardation occurs gradually in this case, over a distance of approximately 0.5 m. With the value of the sediment transport from the experiment (9 kg/h) the thickness of the deposited layer upstream of the weir is estimated on 0.014 mm. Also the deposition upstream of the weir in this sloped weir case is negligible. This conclusion corresponds to the observations from LAUCHLAN (2001).

A considerable part of the particles slides along the downstream slope in bed-load transport mode. These particles enter the small zone with low velocities at the toe of the downstream slope, as shown in figure 7.10. In figure 7.12, the motion of several particles is delayed at this point. However, eventually all particles leave this zone. It is expected that already a small accumulation of particles changes the flow pattern at the toe of the slope in such a way, that the retardation of particles stops. This conclusion agrees with the observation of Lauchlan, who observed small deposition rates at the downstream slope.

7.4.4. Sloped weir, Delft3D

In Delft3D, the maximum velocity magnitude on top of the weir equals 0.68 m/s. This agrees with the FLUENT results. In the report of Lauchlan, no quantitative description is given.

Both sediment transport modes along the flume axis are shown in figure 7.13.

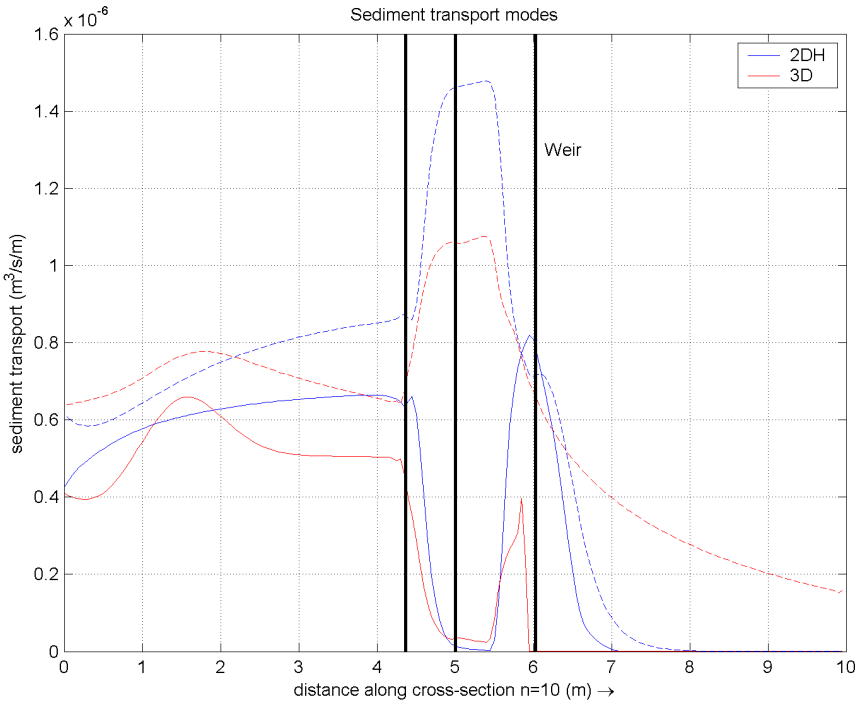

Figure 7.13 – Bed-load transport and suspended-load transport ($m^3s^{-1}m^{-1}$) along the flume axis. Bed-load transport is given by the solid lines, suspended-load transport by the dashed lines.

Upstream from the weir, some erosion occurs. As in the case of a vertical wall weir, the imposed boundary conditions are apparently not equal to the equilibrium conditions, calculated by the VAN RIJN (1993) formula in Delft3D. The transport rates in the 3D case are larger than in the 2DH case. The bed-load transport is brought into suspension by the accelerating flow above the weir. At the downstream slope, the bed-load transport magnitude rises again.

Downstream of the weir, deposition occurs in both simulations. In the 3D case, the bed-load transport is stopped at the toe of the downstream slope. This is also observed in FLUENT, as described in the previous section. The suspended transport gradually declines. In the 2DH case, both transport modes are rapidly disappearing.

In figure 7.14, the initial bed level and the final bed level after 8 hours for both simulation types are shown. Note that the scaling of both axes is different. The deposition qualitatively agrees with the experimental results in both cases (3D and 2DH). The deposition pattern looks more realistic in the 3D case, although the discontinuity halfway the downstream slope seems strange. The qualitatively right reproduction of the deposition is logical, because the depth downstream of the structure is larger than upstream.

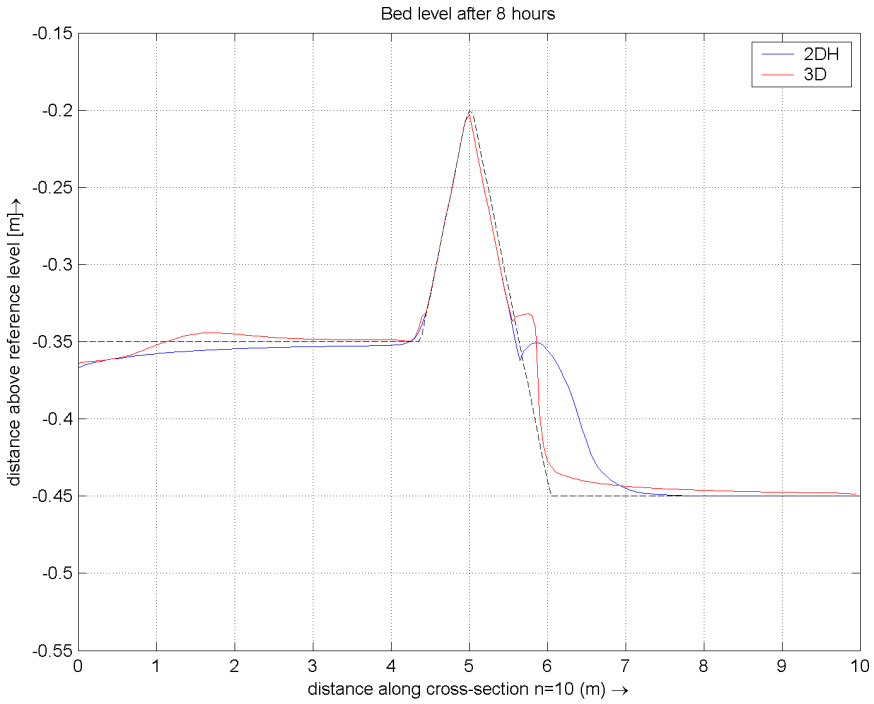

Figure 7.14 – Initial bed level (dashed line) and final bed level (solid lines) in different Delft3D simulations

It can be concluded that the hydraulic and morphological results of Delft3D qualitatively agree with the experimental observations.

7.5. Sediment transport over a weir in Delft3D

It becomes not clear from the simulations with the vertical wall weir of Lauchlan whether the bed-load transport reduction in Delft3D is caused by the decreased velocities due to the larger depth or by the structure itself. Therefore, the behavior of weirs has been investigated in a simplified situation in this section.

To investigate the behavior of a 2D-weir, a comparison has been made between a 2D-weir and the same weir when taken into account by a locally increased bed level (also in a 2DH model). Some properties of this arbitrary two-dimensional situation are given in table 7.4.

Variable	Magnitude
Upstream water depth (m)	2.014
Downstream water depth (m)	2.000 (boundary condition)
Upstream depth-averaged velocity (m/s)	0.5000 (boundary condition)
Downstream depth-averaged velocity (m/s)	0.5035

Table 7.4 – Properties of the simulation of flow over a weir

The bed level weir is shown in figure 7.15. The bed level in water level points is analogue to the 2D-weir parameterization.

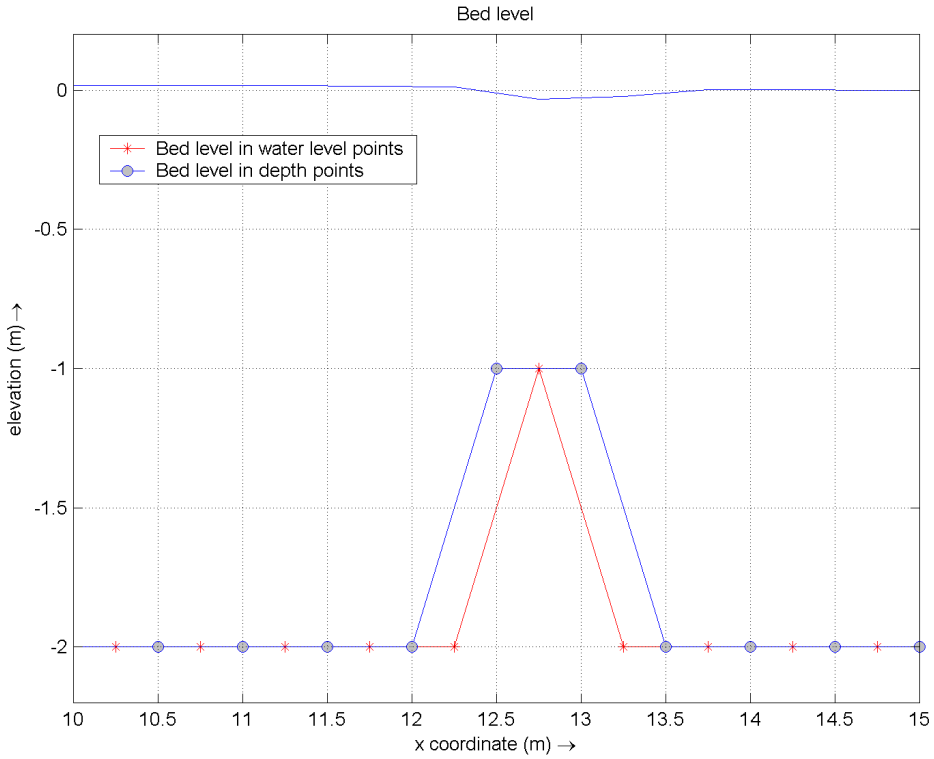

Figure 7.15 – Interpolation of bed level points to water level points in Delft3D

The bed level in bed level points and the interpolation of bed level points to water level points are shown in figure 7.15. The interpolation of bed level points to water level points at the staggered grid is performed with the interpolation method max (DPSOPT = MAX in the master definition file of Delft3D). This interpolation technique sets the depth at a water level point equal to the maximum water depth in the surrounding depth points.

Water levels and flow velocities upstream and downstream (as given in table 7.4) are nearly equal in both ways of modeling. These values correspond with the values as calculated with the analytical conservation laws as given in section 2.6. The only difference is the absence of the increased velocity on top of the weir when using the 2D-weir parameterization. This is shown in figure 7.16.

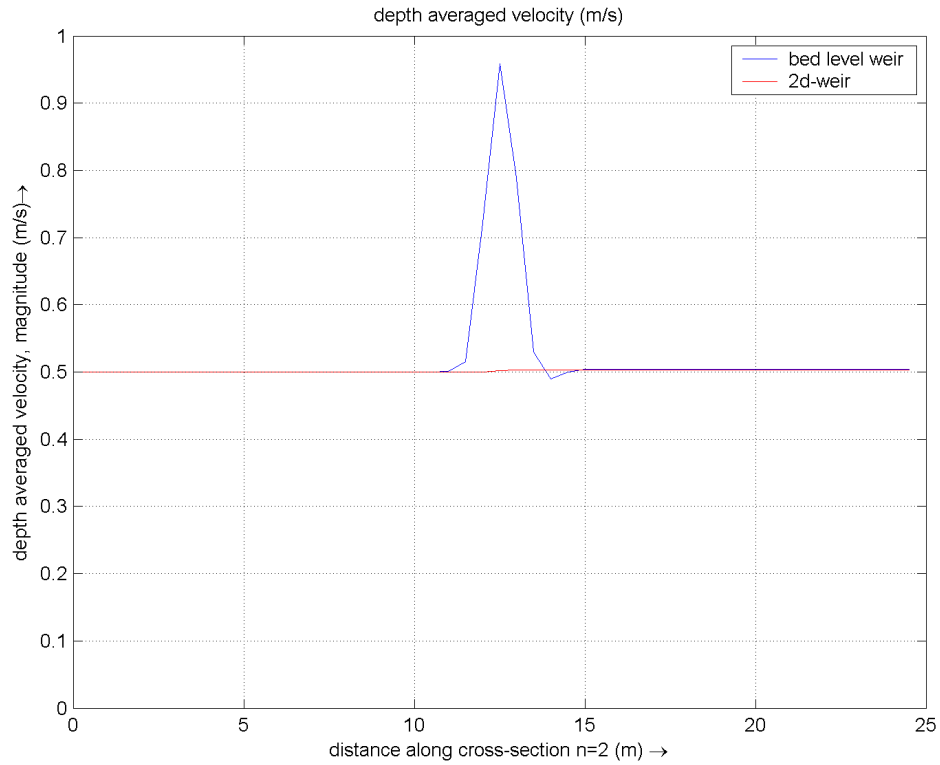

Figure 7.16 – Flow over a weir, depth-averaged velocity (m/s) for a 2D-weir (red line) and a bed-level weir (blue line)

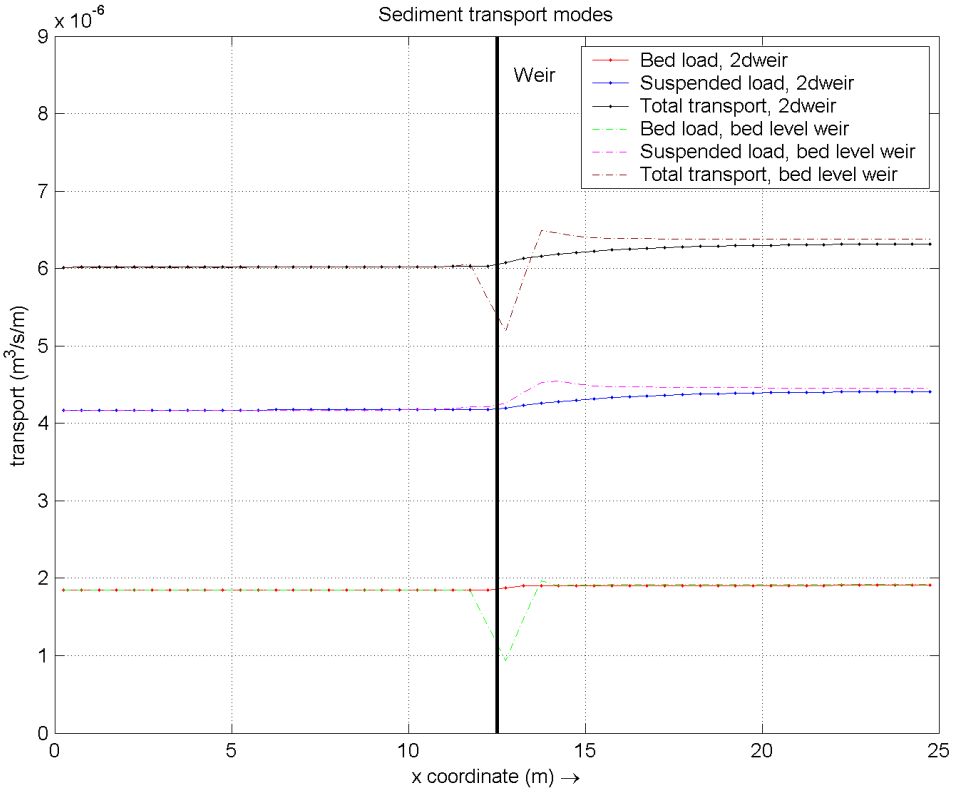

Figure 7.17– Bed-load transport and suspended-load transport ($m^3s^{-1}m^{-1}$). Transport rates in case of the 2D-weir are given by the solid lines with dots. The dashed lines show the transport rates in case of a weir in the bed level.

Sediment with $D_{50} = 200$ µm is added to the simulation. Sediment transport is calculated with the formulation of Van Rijn (1993), so both bed-load transport and suspended-load transport are taken into account separately. Both transport modes and the total transport are given in figure 7.17.

Sediment transports around the 2D-weir show a continuous coarse through the weir. The small change in transport is caused by the difference in velocity over the weir. Lauchlan shows that it is possible that in a two-dimensional situation all the sediment passes the weir. But she observed a strong gyre upstream of the structure, which entrained all bed-load transport, which is carried in suspension over the weir. The continuous line for bed-load transport is physically not possible.
Interpolation deforms the weir in bed level points into the sloped weir, as shown in figure 7.15. This slope causes a reduction in bed-load transport. Also this reduction is not able to block all bed-load transport. The increased velocity on top of the weir causes a spatially retarded increase in suspended sediment transport.

7.6. Conclusions

Sediment transport over weirs has been modeled by analyzing particle trajectories in FLUENT, and by sediment transport formulations and bed level updating in Delft3D. This essential difference makes quantitative comparison difficult. LAUCHLAN (2001, 2004) performed laboratory experiments of sediment transport over vertical wall weirs and sloped weirs. These experiments have been modeled with FLUENT en Delft3D in this study.

Regarding the reproduction of the experiments of the vertical wall weir can be concluded:

	Experiment	**FLUENT**	**Delft3D**
Flow	Lauchlan observed a gyre upstream of the vertical wall weir and a recirculation zone downstream of the weir.	FLUENT does reproduce the recirculation zone, but the gyre upstream of the weir is absent. This deficiency is caused by the shortcomings of k-ε turbulence modeling, because this gyre is present when Large Eddy Simulation is used.	In 3D simulations with Delft3D, unrealistically large vertical velocities are visible, which is the result of the shortcomings of hydrostatic modeling. Gyres and recirculation zones are not found in Delft3D at all.
Sediment transport	All bed-load and suspended-load sediment transport is entrained by the gyre and brought into suspension over the weir.	Particle trajectories in FLUENT show that all particles pass the weir.	Sediment transports are rapidly decreasing downstream of the structure. Bed-load transport reduces to zero in front of the weir.
Deposition	In front of the weir, no deposition has been observed. Deposition has been found	The deposition, caused by the retardation of some particles in the zone upstream of the	No deposition occurs upstream of the weir. Sedimentation has been observed downstream

	downstream of the weir.	weir, is negligible. Deposition does occur in the recirculation zone downstream of the weir.	of the weir. This holds in 3D and 2D with a weir in the bed level and in 2D with a 2D-weir parameterization.

Table 7.5 – Conclusions regarding the reproduction of the experiments of the vertical wall weir

It becomes not clear from these simulations whether the bed-load transport reduction in Delft3D is caused by the decreased velocities due to the larger depth or by the structure itself. For this reason, a simulation has been performed with a flat bottom and a 2D-weir. The magnitudes of both sediment transport modes show a continuous line along the flume axis and over the 2D-weir. It is possible that bed-load transport is entrained and brought into suspension over the weir, but the continuous line for bed-load transport is physically not possible.

Regarding the reproduction of the experiments of the 1:4 sloped weir can be concluded:

	Experiment	**FLUENT**	**Delft3D**
Flow	An acceleration zone and a deceleration zone have been observed.	In agreement with the experiments.	In agreement with the experiments. The velocities are equal to the values of FLUENT.
Sediment transport	All bed-load and suspended-load sediment transport is entrained by the accelerating flow and brought into suspension over the weir.	Particle trajectories in FLUENT show that all particles pass the weir.	Bed-load transport is brought into suspension over the weir by the accelerating flow.
Deposition	No deposition upstream of the weir has been observed. Deposition occurred at the downstream slope.	The deposition, caused by the retardation of some particles in the zone upstream of the weir, is negligible. Bed-load transport is partly interrupted at the toe of the downstream slope.	Also in agreement with the experiments.

Table 7.6 - Conclusions regarding the reproduction of the experiments of the 1:4 sloped weir

The final conclusions from this chapter are:

- The flow and transports around vertical wall weirs are poorly reproduced by Delft3D.
- The hydraulic and morphological aspects of a sloped weir are correctly reproduced by Delft3D where the grid is fine enough to resolve the shape of the sloped weir.
- The 2D-weir parameterization in Delft3D is completely permeable for sediment transport. This is physically not correct.
- The results of FLUENT are satisfying, and give confidence to use FLUENT also in situations that are more complex.

8. Three-dimensional flow and transport over hydraulic structures

In the previous chapter has been concluded that the results of FLUENT are satisfying, and give confidence to use FLUENT also in situations that are more complex. This also follows from simulations of the other situations from literature, as described in the previous chapters.

Because no appropriate experimental data are available, a three-dimensional situation has been designed and modeled with Delft3D and FLUENT. FLUENT has been used to judge the performance of Delft3D in this case.

The situation is described, the model set-up in FLUENT and Delft3D is treated and the results are presented, analyzed and compared. In addition, alternative ways of modeling with Delft3D are discussed.

8.1. Simulation description

Contrary to all previous situations, the situation as described in this section is not based on a laboratory experiment. Three-dimensional flow and transport in an imaginary situation has been modeled with FLUENT and Delft3D. This section deals with the design of this situation.

The background of the design is the situation in the Lek river near Vianen, as described in section 1.2.1. In this design, the river width is locally doubled. At low river discharges, the flow is concentrated in the main channel by an emerged longitudinal weir. At high discharges, the weir is submerged, and sediment is taken over the weir. Sediment settles both in the main channel and in the zone behind the structure, due to decreasing flow velocities, caused by the increased width. At low river discharges, the main part of the deposited sediment in the main channel is eroded again. In contrast to this, the sediment behind the weir stays at its location. During every flood period, the deposited volume behind the weir is increased.

The Vianen case during high discharges has been highly simplified and scaled down to make modeling with FLUENT possible. The schematization of the case is shown in figure 8.1.

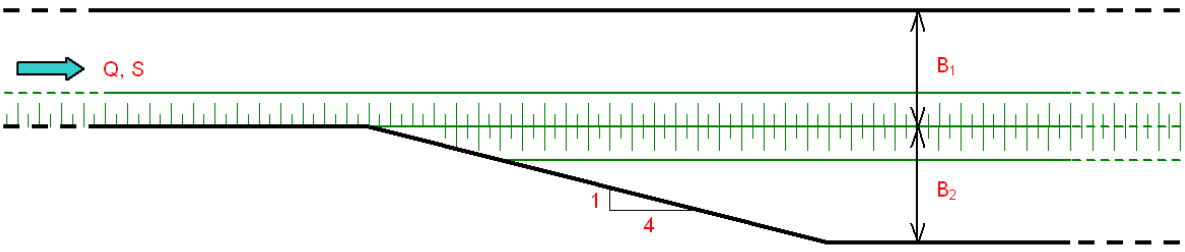

Figure 8.1 – Design of a three-dimensional situation, top view

To make sure that the design resembles a realistic situation, the proportions and properties from Vianen are roughly taken into account in the design situation.

Variable	Vianen	Design	Scaling
Original river width (m)	± 140	10	Practical reasons
Increased river width (m)	± 280	20	Proportional
Water depth (m)	± 8.5	1	Roughly proportional
Flow velocity (m/s)	± 1.5	0.5	Froude scaling
Roughness height (m)	± 0.32	0.038	Same Chezy value
Shear velocity (m/s)	0.1057	0.0353	Calculated with (2.14)
Particle diameter (μm)	± 500	200	Same w_s / u_*
Weir height (m)	6.46	0.75	Proportional
Weir slopes	Unknown	1:4	Standard value

Table 8.1 – Values of variables in the Vianen case and in the design situation

No differences in bed level are present, neither a longitudinal bed level gradient. Another important difference with the Vianen case is the absence of the curvature of the channel.

8.2. FLUENT model set-up

A three-dimensional simulation has been performed in FLUENT. The distance of the upstream boundary to the start of the increase in width equals 60 meter. The adaptation length of suspended sediment transport is approximately $U \cdot d / w_s \approx 20$ m, so the sediment transport is in equilibrium when it reaches the expansion zone. The increase in width of 10 meter gives with the 1:4 ratio a length of the expansion zone of 40 meter. The widened zone has been extended over 60 meter until the downstream boundary. A rigid-lid computation has been performed, to save computation time. This approximation does not result in large errors when the deformation of the free surface is relatively small; see section 5.4. The deformation of the free surface will be checked later on. A structured grid has been used, containing 1.8 million grid cells. A detailed description of the generation of the geometry, mesh, and boundary conditions is given in appendix A.

The settling velocity of spherical particles with a diameter of 200 micrometer equals 0.0245 m/s, as calculated with equation (2.22) combined with the analytical formulation of KAZANSKIJ (1981), as described in RAUDKIVI (1998). This value differs only 5% with the settling velocity of natural sediment (0.0257 m/s) as calculated with the equations of VAN RIJN (1993), as given in (2.23).

Wall treatment is important for the correct calculation of the turbulence near the wall. This turbulence modeling is essential for bed-load transport predictions. The flow near the wall is best represented by enhanced wall treatment. Enhanced wall treatment requires $z^+ \leq 5$, and preferably $z^+ \leq 2$. In addition, the aspect ratio of the cells should be limited to acceptable values. Too large aspect ratios result in flow alignment: the flow tends to follow the direction of the longest edge of the cells. These restrictions result in enormous amounts of grid cells, which is not feasible, even with the use of a large calculation cluster. Furthermore, the combination of enhanced wall treatment and a roughness height is not available in FLUENT. For these reasons, wall functions will be applied.

VAN BALEN (2010) performed LES simulations of curved open-channel flows. Also in this study, wall functions have been used. It appears that the use of wall functions results in a correct reproduction of the turbulence near the wall. Also the results for uniform flow, as described in section 4.4, give confidence in the use of the wall function approach. In this way, the same Nikuradse roughness height can be defined in FLUENT and Delft3D.

The boundary conditions used are shown in table 8.2. The turbulence inflow quantities estimation is based on a turbulent viscosity $\nu_t = \kappa u_* h / 6$. Sediment transport is calculated using a Discrete Particle Model with the Random Walk method to take the effect of turbulence into account. A default roughness constant $C_s = 0.5$ at the bed is assumed, which seems to correspond with analytical shear stress formulations for uniform flow, as described in section 4.4.1.

A second-order upwind scheme is used for momentum and turbulence, to ensure accurate results. First-order upwind is used in the first stage of the simulation, because the calculation converges faster with this simpler scheme.

Location	Type	Characteristics
Sediment bed	WALL	$k_s = 0.038$ m, $C_s = 0.5$
Weir surface	WALL	$k_s = 0.038$ m, $C_s = 0.5$
Inlet	VELOCITY INLET	U = 0.5 m/s, $k = 0.0017$ m^2/s^2, $\varepsilon = 1.136 \cdot 10^{-4}$ m^2/s^3
Outlet	OUTFLOW	
Rigid-lid water surface	SYMMETRY	
Side walls	WALL	$k_s = 0$ m

Table 8.2 – Boundary conditions for FLUENT modeling of 3D flow and transport

The simulations are performed in parallel mode (8 processors) at the Linux calculation cluster of the Laboratory for Aero & Hydrodynamics at Delft University of Technology.

8.3. Delft3D model set-up

To investigate the quality of the current way of morphological modeling with Delft3D, model settings of the Vianen project have been adopted in this study. The geometry is equal to the geometry as described in FLUENT, but in this case, the sloped weir has been removed and replaced by a 2D-weir parameterization. This 2D-weir parameterization only contains a location (equal to the location of the weir crest) and a crest height. Because Delft3D imposes an equilibrium transport condition at the upstream boundary, the length between the upstream boundary and the expansion zone (which is 60 meter in FLUENT) has been reduced to 20 meter. The total length of the domain is 125 m.

The horizontal mesh contains 500x160 grid cells. Because Delft3D is applied in depth-averaged mode, the vertical has not been divided in layers. The length of the hydrodynamic simulation is two hours. A morphological acceleration factor of 60 has been applied. This results in a morphological simulation time of 120 hours (5 days), which is a realistic duration of a river flood.

At the upstream boundary, a current velocity (0.5 m/s) has been defined. Downstream, the water level has been set to zero, which is equal to reference level. The depth of 1 meter has been defined positive below this reference level. A reflection coefficient (which changes a reflective boundary into a weakly reflective boundary) has been imposed at the water level boundary:

$$\alpha = T_d \sqrt{\frac{d}{g}}. \tag{8.1}$$

The time scale T_d is equal to the time in which a surface wave propagates from the upstream to the downstream boundary. A surface wave with a shallow water propagation velocity $c = \sqrt{gd}$ propagates in a time L/c over a distance L. This leads to $\alpha = L/g = 13\ \mathrm{s}^2$. This coefficient prevents reflection of spin-up waves, resulting in faster convergence of the solution.

The constant horizontal eddy viscosity and diffusivity are both equal to 0.01 m^2/s. A total sediment transport is calculated with the transport formula of Engelund & Hansen. Sediment concentrations at the upstream boundary are calculated by Delft3D with a Neumann boundary condition; see section 3.2.6. A no-slip condition has been defined at the sidewalls, analogously to the FLUENT simulations.

8.4. Results

All relevant aspects for this study of the considered situations from literature are satisfying reproduced by FLUENT. This gives confidence to compare the results of Delft3D with the results of FLUENT for a three-dimensional case, with the purpose to assess the performance of Delft3D in such situations.

8.4.1. FLUENT

The figures 8.2, 8.3 and 8.4 show the flow velocities at different locations in the domain. The flow is distributed over the new channel width in the expansion zone and approximately 20 meter downstream. In this zone, sediment distribution between both sides of the longitudinal weir is possible. The maximum transverse velocities are in the order of 0.25 m/s. Downstream of the expansion a new equilibrium situation arises. A no-slip condition has been defined at the sidewalls (wall type boundary condition).

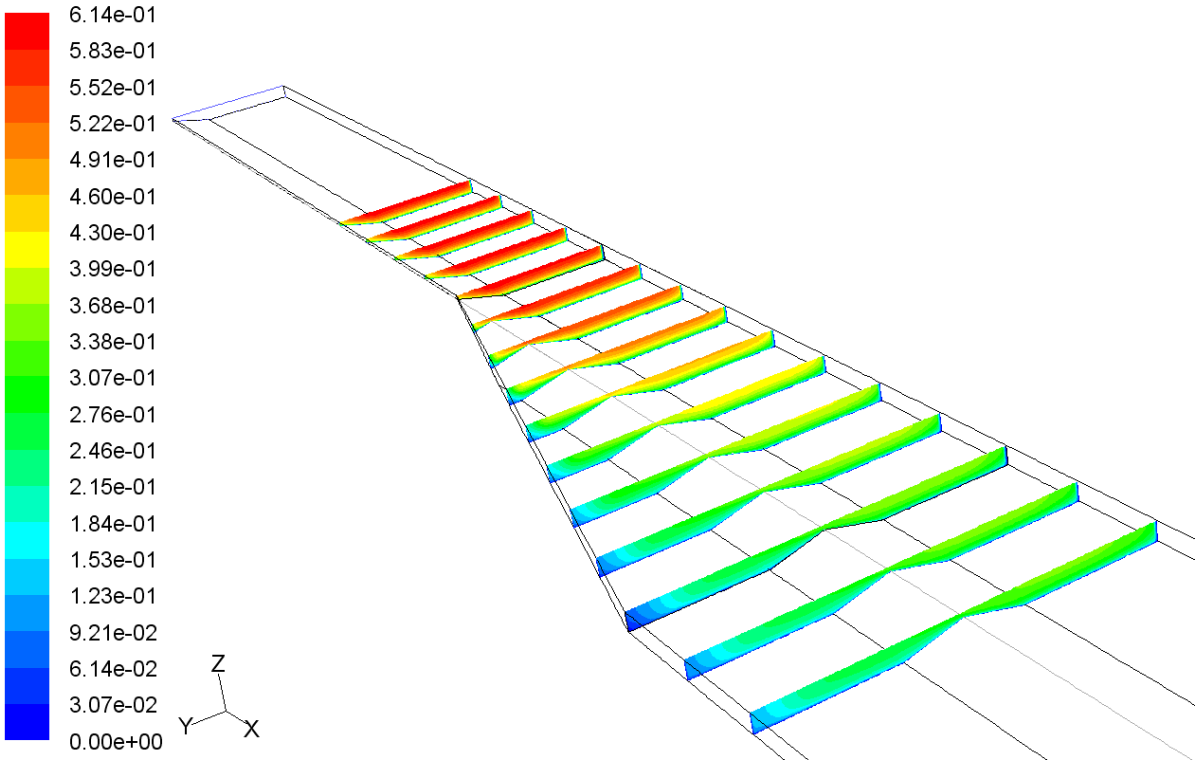

Figure 8.2 – Cross-sections with velocity magnitude (m/s) in FLUENT

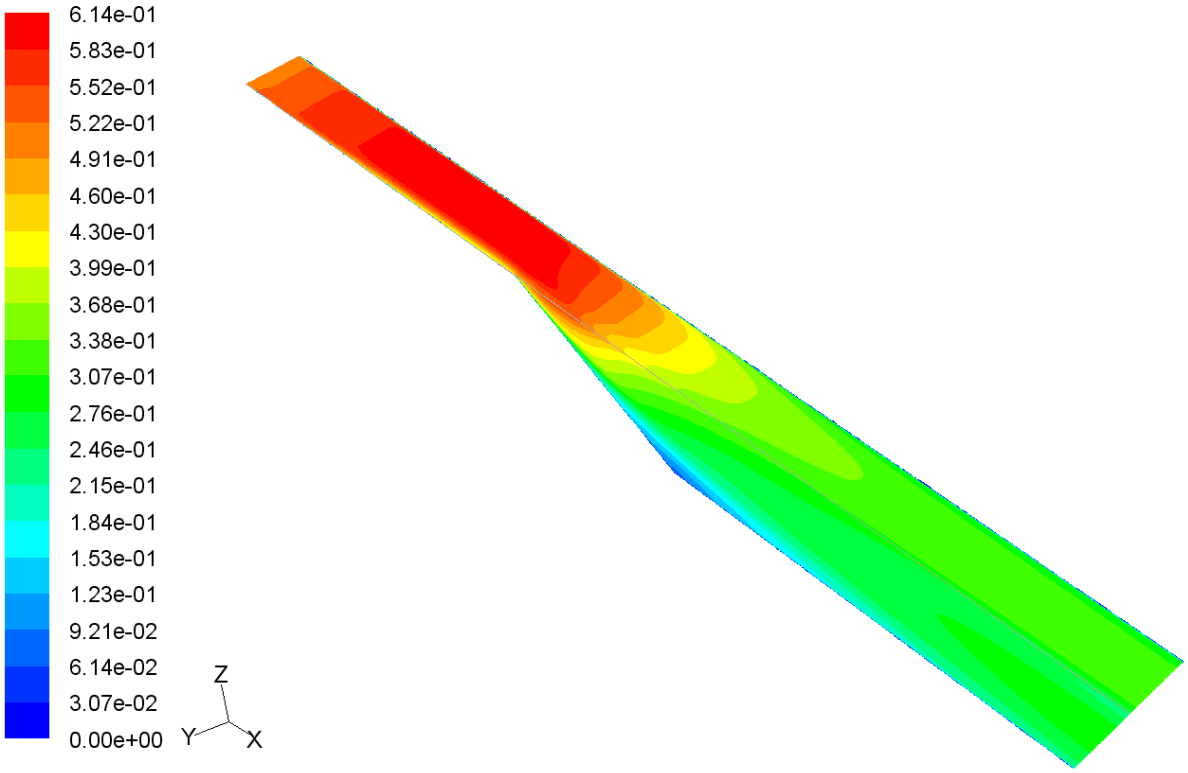

Figure 8.3 – Velocity magnitude (m/s) at the water surface in FLUENT

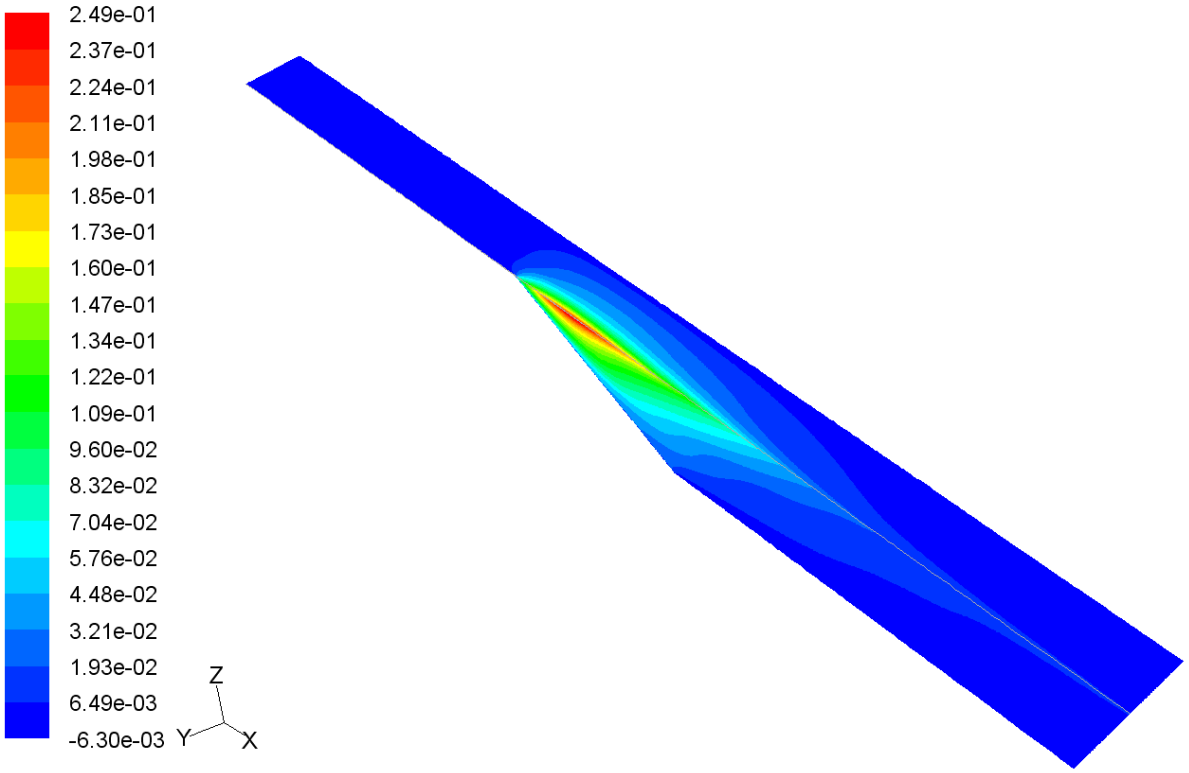

Figure 8.4 – Velocity (m/s) in y-direction at the water surface in FLUENT

When the flow is in a steady state, particles are released at the upstream boundary. Different particle diameters have been investigated. The settling velocity has been determined using equation (2.22) combined with the empirical formulation of Kazanskij (1981) for the drag coefficient. The ratio w_s / u_* is based on the upstream shear velocity of 0.035 m/s.

Diameter D (µm)	Settling velocity w_s (m/s)	Ratio w_s / u_*	Transport mode
100	0.008	0.22	Suspension
150	0.016	0.45	Suspension
200	0.025	0.69	Saltation/Suspension
300	0.043	1.18	Saltation
400	0.059	1.62	Saltation
500	0.078	2.14	Saltation/Bed-load
600	0.096	2.63	Bed-load
700	0.113	3.09	Bed-load

Table 8.3 – Particle diameters and corresponding transport modes in FLUENT simulations

Particles are released uniformly distributed over the vertical at the upstream boundary at distinct locations. These locations are characterized by the transverse coordinate, y, which is zero at the left wall and 10 m at the right wall. $y = 10$ m is also equal to the position of the weir crest. An example is given in figure 8.5, where particles with $D_{50} = 500$ µm are released

at $y = 5$ m. In figure 8.6, the starting position y is shown on the horizontal axis. The figure shows the probability that an arbitrary particle that starts at y moves over the weir crest, which gives a final transverse position $y > 10$ m. The probabilities are simply obtained by counting. For every combination of diameter and starting location, approximately 50 particles are tracked on average.

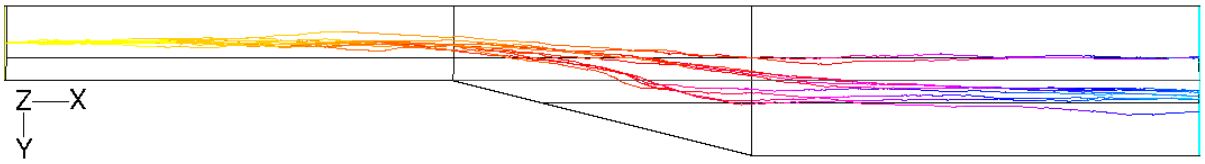

Figure 8.5 – Example of particle trajectories for particles with D_{50} = 100 µm, released at y = 5 m

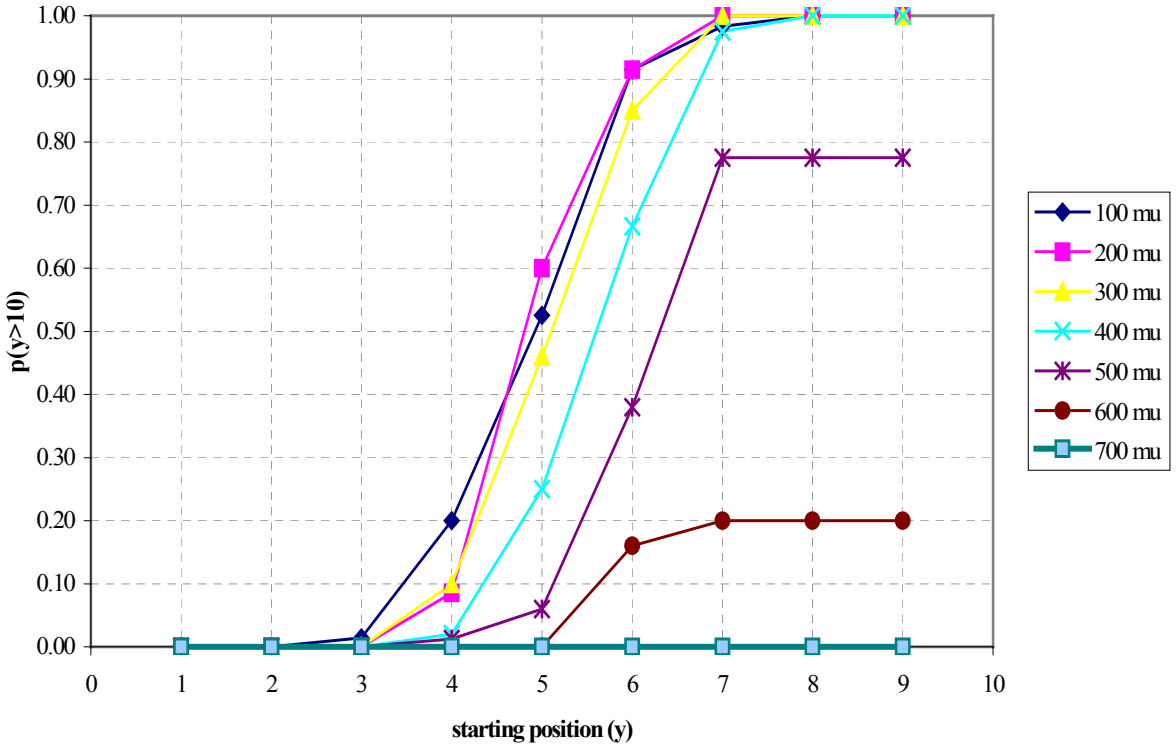

Figure 8.6 – Probability of a final position behind the weir (y > 10) for different particle diameters as a function of the y-coordinate of the release position at the upstream boundary

This probability curves can be used to give an indication of a relation:

$$\frac{S_2}{S_1} = C \cdot \frac{Q_2}{Q_1} \tag{8.2}$$

for different particle diameters. An index 2 stands for the fluxes over the weir, an index 1 for the fluxes in the main channel. A weighted average of the probabilities is used, in which the weight is related to the cross-sectional area around a starting point. For $D > 200$ µm, the probabilities of the positions $y = 8$ m and $y = 9$ m are neglected, because particles at the

slope reach the expansion zone also at the toe of the slope ($y = 7$ m). The final ratio Q_2 / Q_1 is equal to 0.852. This is determined in the zone where hardly any lateral exchange of discharge takes place.

The weighted average of the probabilities $p(z > 10)$ and the corresponding coefficients C are listed in table 8.4. The coefficient C is calculated by:

$$C = \frac{p(z > 10)}{1 - p(z > 10)} \cdot \frac{Q_1}{Q_2} . \tag{8.3}$$

However, both for $D = 100$ µm and for extremely small particles of $D = 1$ µm a value of $C = 0.96$ has been found. For $D = 1$ µm, a value of $C = 1$ should be valid. Apparently, the weighted average, based on surface area at the upstream boundary, is not fully correct. For this reason, all values of C, as calculated by (8.3), have been multiplied by $1/0.96$. The coefficient C for $D = 150$ µm becomes 1.04 in this way. It is possible that the particles higher in the suspension range of $0 < w_s / u_* \leq 0.6$ have a greater probability to move over the structure, due to relatively large velocities near the weir surface. Another possibility is the influence of uncertainty in the probabilities, caused by the limited number of particles tracked or by too large a weight of the release position at the slope ($y = 9$ m) with respect to $D = 100$ µm. Because the second reason is considered more likely, the value of C is bounded to 1.00 for this particle diameter.

Particle Diameter (µm)	w_s / u_*	Weighted average probabilities	Coefficient C
100	0.22	0.45	1.00
150	0.45	0.46	1.00
200	0.69	0.40	0.81
300	1.18	0.32	0.57
400	1.62	0.25	0.41
500	2.14	0.16	0.23
600	2.63	0.05	0.06
700	3.09	0.00	0

Table 8.4 – Distribution of sediment for different particle diameters, given by the coefficient C of equation (8.3)

Bed-load transport has a strong tendency to move along the toe of both slopes of the weir. This is (partly) caused by the abrupt change in geometry at this location, resulting in relatively low shear stresses at the toe of the slopes. These shear stresses are too low to move particles that are entrained in this zone up the slope.

The maximum pressure differences are found at the start of the expansion zone. The maximum difference in pressure over the width at the rigid-lid surface is approximately 100 Pa, which corresponds to 1 cm. The rigid-lid approximation appears to be valid.

8.4.2. Delft3D

The depth-averaged velocity, as calculated by Delft3D is shown in figure 8.7. The ratio Q_2 / Q_1 at the downstream boundary is equal to 0.99.

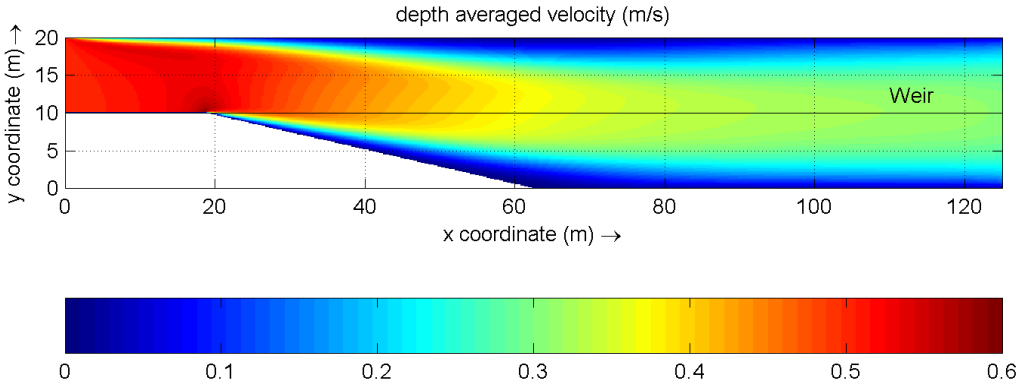

Figure 8.7 – Depth-averaged velocity (m/s) in the 3D situation

Sediment transport has been calculated by the formulation of Engelund & Hansen and Van Rijn (1993). In the first case, only a total transport is calculated. The transport is set equal to the transport capacity. In the latter, a distinction is made between bed-load transport and suspended-load transport. For suspended-load transport, the transport equation for suspended material is solved, including advection and diffusion processes. The results for $D = 200$ µm are shown in figure 8.8 to 8.10. Note that the scaling of the figures differs. The sediment transports occur before bed level changes have taken place.

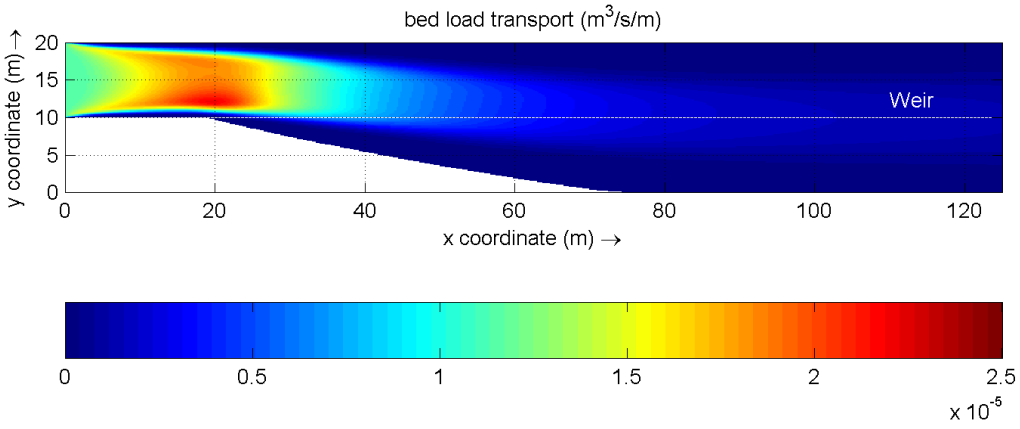

Figure 8.8 – Total transport ($m^3s^{-1}m^{-1}$) by Engelund & Hansen for D = 200 µm

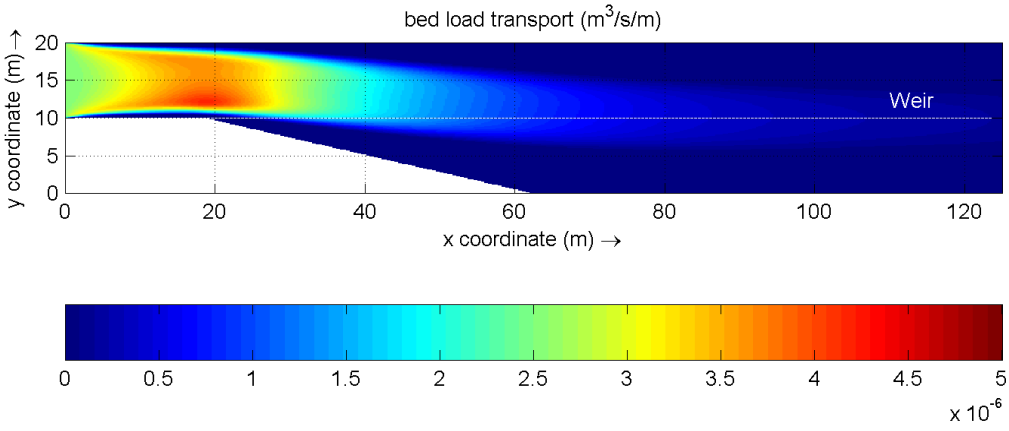

Figure 8.9 – Bed-load transport ($m^3s^{-1}m^{-1}$) by Van Rijn (1993) for D = 200 µm

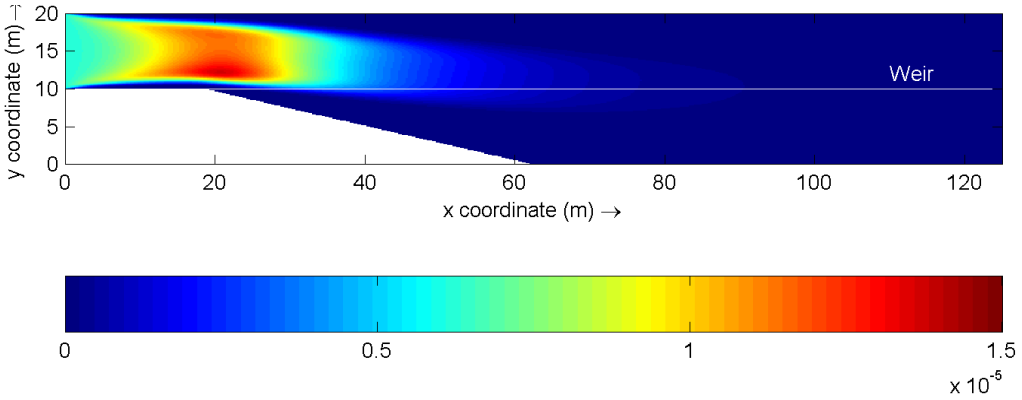

Figure 8.10 – Suspended-load transport ($m^3s^{-1}m^{-1}$) by Van Rijn (1993) for D = 200 µm

Both sediment transport formulations show the same trend. Sediment that reaches the weir, can pass the weir unhindered. The formula of Van Rijn gives a ratio of bed-load and suspended-load of approximately 1:3. The sediment transport as calculated by van Rijn (1993) leads to an erosion and sedimentation pattern after 5 days (120 hours) as shown in figure 8.11.

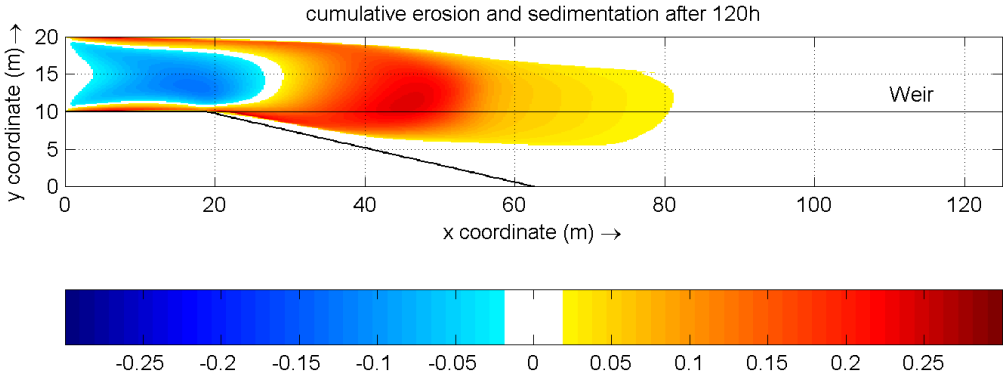

Figure 8.11 – Erosion and sedimentation (m) after 120 hours by Van Rijn (1993) for D = 200 µm

The sedimentation patterns go through the weir in a continuous way. The same figure can be given for $D = 100$ µm and $D = 500$ µm for which the ratio between bed-load and suspended-

load is approximately 1:5 and 3:2 respectively. The total transport magnitude differs for different particle diameters, because the transport is calculated in Delft3D by a Neumann boundary condition. The scaling of both figures below is equal to figure 8.11.

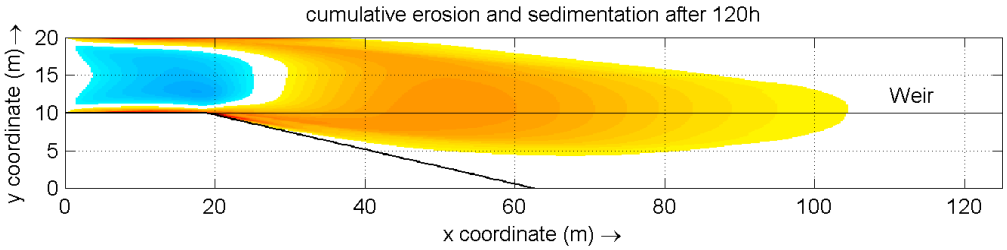

Figure 8.12 – Erosion and sedimentation (m) after 120 hours by Van Rijn (1993) for D = 100 µm

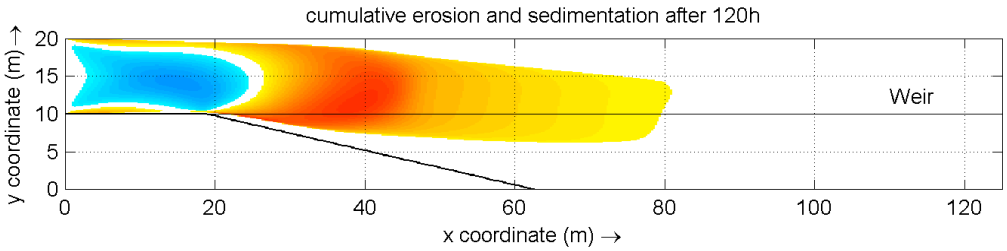

Figure 8.13 – Erosion and sedimentation (m) after 120 hours by Van Rijn (1993) by D = 500 µm

Also coarse sediment passes the weir unhindered. In this situation, sediment with $D = 500$ µm is transported as bed-load; see table 8.3. The decreased flow velocities in the expansion zone strengthen this bed-load transport character. Relatively fine sediment propagates further downstream due to smaller settling velocities and diffusion effects. This is visible in figure 8.12. An overview of the hydrodynamic and morphological results of all simulations can be found in appendix B.

8.5. Comparison

The discharge is fully spread over the width in the zone with the weir in Delft3D. The ratio $Q_2 / Q_1 = 0.99$. FLUENT gives $Q_2 / Q_1 = 0.85$. The 2D-weir in Delft3D has clearly too little influence on the flow. This is also visible in the velocity plots 8.3 and 8.7, respectively. FLUENT keeps the discharge more concentrated in the 'main channel'.

Sediment transport is modeled in a different manner in Delft3D and FLUENT. In FLUENT the motion of an individual particle is shown. In Delft3D, the origin of the sediment at some location is not clear. For that reason, a simulation with two identical sediment fractions is carried out, one located in front of the weir ($10 < y \leq 20$) and one behind the weir ($0 \leq y < 10$). Bed-load transport of sediment from one of these fractions is only found on top of the sediment bed of the concerned fraction. When making use of suspended transport modeling, including diffusion, sediment is also able to reach the domain where the other fraction is present.

In Delft3D, all the sediment that reaches the weir also goes over this obstacle, independent of the transport mode. This has also been concluded in section 7.5. From the FLUENT simulations, it becomes clear that for larger particle diameters, a greater part of the sediment

moves parallel to the upstream slope. The sediment diameter clearly influences the distribution of sediment between main channel and zone behind the structure.

8.6. Analysis

In the previous sections, two main deficiencies of the Delft3D simulation are mentioned:

- The weir has too little effect on the discharge distribution between main channel and the zone behind the weir.
- All sediment that reaches the weir also passes the weir, independent of the grain diameter.

To examine the influence of a 2D-weir on the overall flow, a simulation of the same geometry has been performed, but without weir. The results are shown in the figures 8.14 and 8.15, respectively with and without weir. The scaling of both plots is identical.

It can be concluded that the influence of the weir on the flow is negligible. The weir does not affect the velocity component parallel to the weir. An energy loss is calculated, based on the velocity component parallel to the weir. To assess the effect of this energy loss, the difference in velocity magnitude in y-direction between both situations is calculated and shown in figure 8.16. The figure gives the y-velocity with weir minus the y-velocity without weir. This is equal to the effect of the 2D-weir on the transverse component of the depth-averaged velocity.

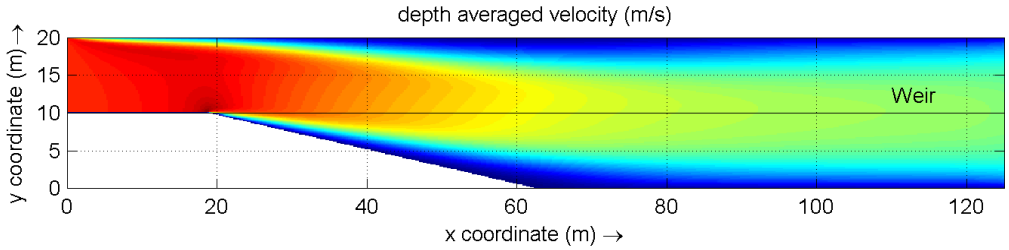

Figure 8.14 – Depth-averaged velocity (m/s) with 2D-weir

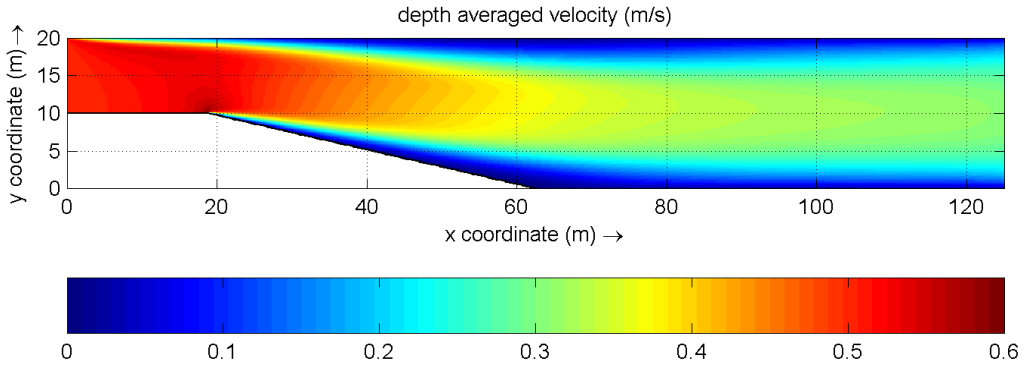

Figure 8.15 – Depth-averaged velocity (m/s) without 2D-weir

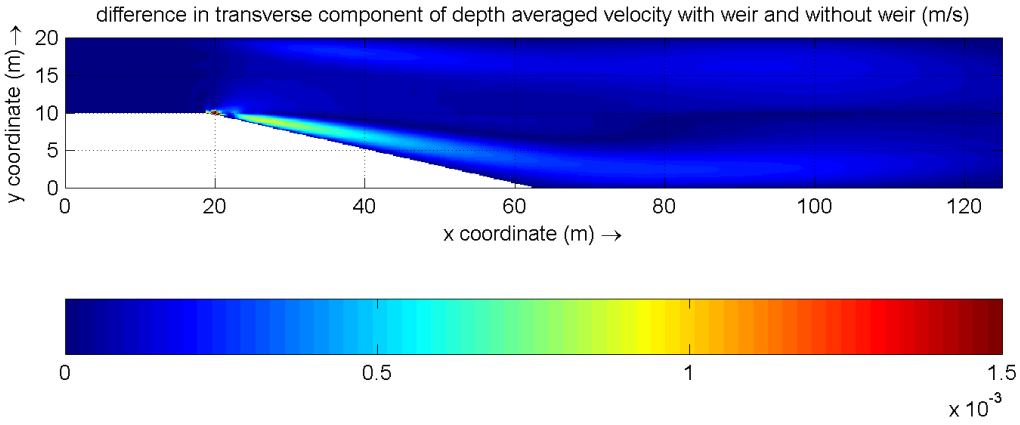

Figure 8.16 – Effect of a 2D-weir on the transverse component of the depth-averaged velocity (m/s)

The maximum transverse velocity is approximately 0.06 m/s. The effect of the weir is in the order of $1 \cdot 10^{-3}$ m/s, that is only 1.5% of the transverse velocity. Intuitively it can be known that this is much too low for a weir that covers 75% of the depth. The FLUENT simulation affirms this statement.

The weir has no direct effect on sediment transport, and because the hydraulic effect is much too small, also the indirect effect of the weir on the sediment transport is negligible. The resulting erosion and sedimentation in both situations is identical, see figures 8.17 and 8.18 for the situations with and without weir respectively. $D = 200$ µm has been used in this comparison. The scaling of both plots is the same.

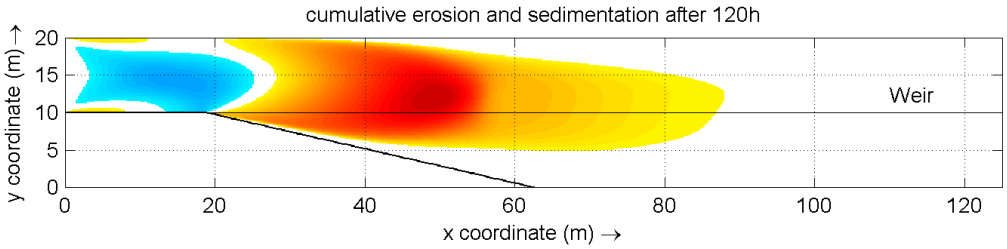

Figure 8.17 – Cumulative erosion and sedimentation (m) with 2D-weir

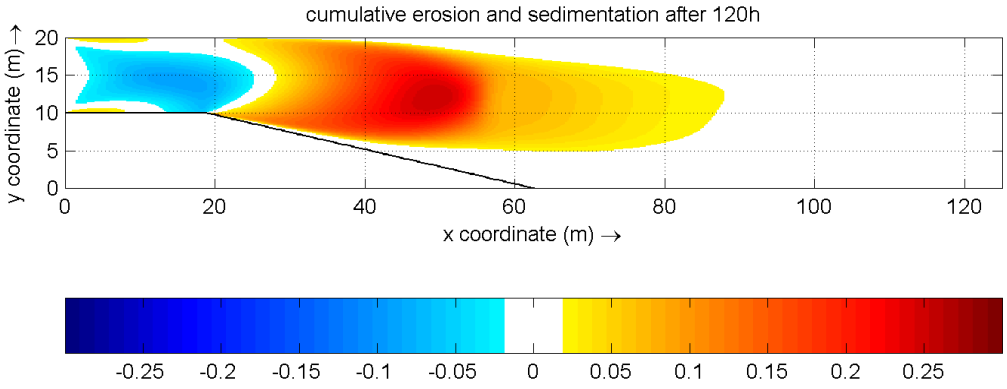

Figure 8.18 – Cumulative erosion and sedimentation (m) without 2D-weir

The weir parameterization is meant for flow perpendicular to the weir crest. In this situation, the flow is oriented almost parallel to the weir crest. This is one cause of the incorrect influence on the flow. Another reason could be the user-defined constant horizontal eddy viscosity. This choice is discussed in the next section.

8.7. Other ways of modeling with Delft3D

Three other ways of modeling have been investigated:

- Depth-averaged modeling with increased bed level points at both sides of the 2D-weir.
- Modeling with five computational layers, in which the 2D-weir is substituted by a local weir with $c_{loss} = 0$, as explained in section 7.3.
- Modeling with five computational layers, in which the 2D-weir is substituted by a locally increased bed level.

8.7.1. 2DH with increased bed level points

The resulting flow is given in figure 8.19. The flow is more concentrated in the main channel than in the case with only a 2D-weir. Compare figure 8.19 with figure 8.14. However, the ratio Q_2 / Q_1 at the downstream boundary is equal to 0.99, against 0.85 in FLUENT. The distribution of discharge between the main channel and the zone behind the weir takes place over a larger distance than in the situation with a 2D-weir.

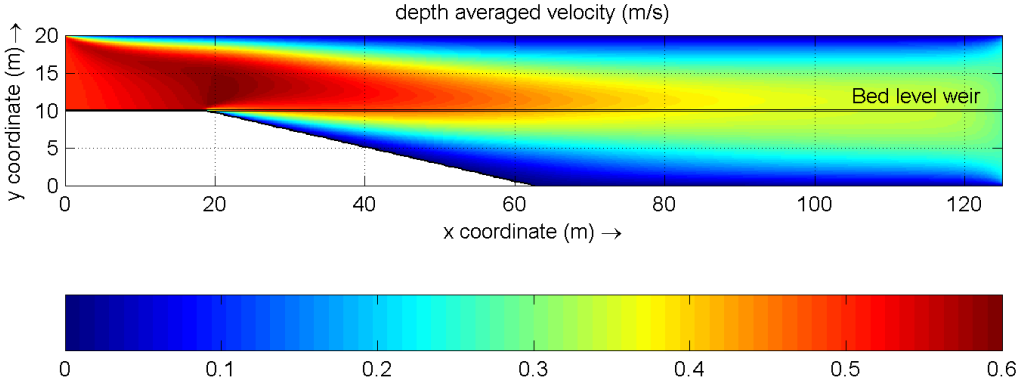

Figure 8.19 – Depth-averaged velocity (m/s), 2DH modeling with increased bed level points at both sides of the 2D-weir

Six simulations are performed.

- Transport formulations Engelund & Hansen and Van Rijn (1993)
- Mean particle diameter $D_{50} = 100$ µm, $D_{50} = 200$ µm, $D_{50} = 500$ µm

The resulting erosion and sedimentation patterns are given in Appendix B. Bed-load transport is fully blocked by the bed level weir. All sediment settles upstream of the weir when the bed-load type formula of Engelund & Hansen is used. The sedimentation behind the weir balances the erosion in the same zone. The bed-load fraction from Van Rijn (1993) is also blocked, but the suspended-load fraction is partly able to pass the weir. This results in more continuously shaped sedimentation patterns, especially in case of small particle diameters. A bed-load formula is only applicable when suspended-load is hardly present.

This approach leads to an underestimation of the sediment transport over the weir. FLUENT shows that not all bed-load transport is blocked by the hydraulic structure. This is also concluded in the work of LAUCHLAN (2001).

8.7.2. 3D with a local weir or with increased bed level points

The effect of a local weir is hydraulically approximately identical to the effect of locally increased bed level points in a 3D simulation. The depth-averaged velocity of the simulation with locally increased bed level points is given in figure 8.20. The ratio $Q_2 / Q_1 = 1.05$, against 0.85 in FLUENT. This deviation is present in all Delft3D simulations.

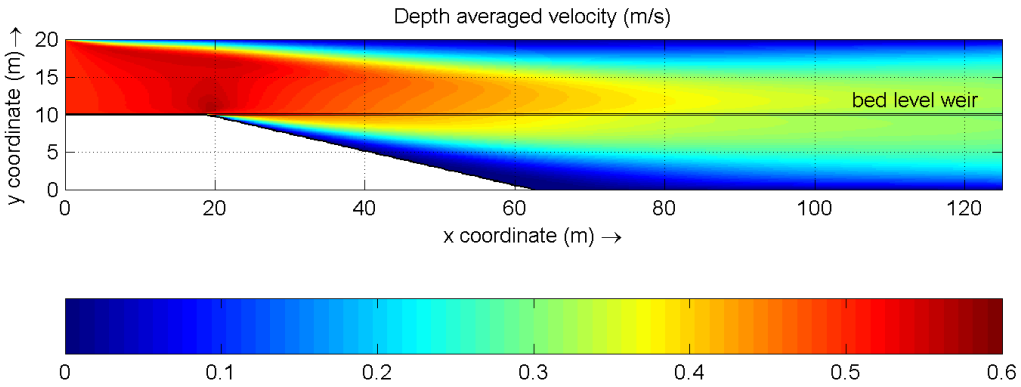

Figure 8.20 – Depth-averaged velocity (m/s), 3D modeling with a weir in bed level points

A possible reason is a wrong value of the user-defined horizontal eddy viscosity, as briefly mentioned before. This parameter should be chosen dependent on flow characteristics (Reynolds number and anisotropy of the flow) and grid interval size. There is no clear guideline how to choose this value. When this value is chosen too high, the flow behavior is too coherent, because the horizontal eddy viscosity is governing for the horizontal transfer of momentum. In this study, the current way of modeling in river engineering practice is analyzed, so constant horizontal eddy viscosities are defined.

A hydraulic test simulation with HLES of the 3D simulation with bed level weir has been performed, to check whether the order of magnitude of the user-defined constant value of the horizontal eddy viscosity is correct. The horizontal eddy viscosity in the upper layer of the grid is given in figure 8.21. The value of the horizontal viscosity appears to be approximately 0.001 m^2/s. This is 10 times smaller than the user-defined constant value of 0.01 m^2/s in the other simulations. The horizontal transfer of momentum is indeed overestimated by the user-defined viscosity. However, also the HLES-simulation gives $Q_2 / Q_1 = 1.04$. It seems that the overestimated value of the horizontal eddy viscosity is not the cause of the difference in the distribution of discharge between FLUENT and Delft3D.

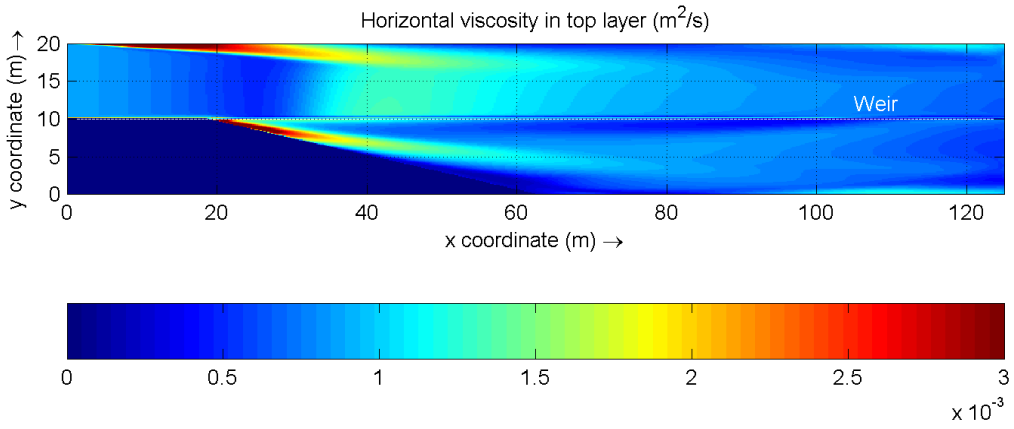

Figure 8.21 – Horizontal viscosity (m^2/s) in the top layer as calculated by HLES in Delft3D

It should be mentioned that the results of FLUENT are also not infallible. FLUENT makes use of a three-dimensional k-epsilon turbulence model. An important shortcoming of this model in shallow flows is the assumption of isotropy of the turbulence properties. The effect of the walls is treated separately, using wall functions or enhanced wall treatment.

Besides that, several studies have shown that unsteady processes are important for the exchange of sediment between for instance the main channel and the floodplains. FLUENT gives a steady state flow, in which discrete particles are released. Unsteady solving of water motion and particle trajectories is also possible, but this takes too much time when morphological time scales should be resolved.

In a 2DH simulation, all vertical velocities are set to zero. In a 3D simulation, vertical velocities are calculated. The error made by the hydrostatic model is shown in figure 8.22, in which the vertical velocities in the lowest layer (layer number 5) at x = 25 meter are shown.

All vertical velocities are zero, except the vertical velocities in the two points at both sides of the weir. In this point, huge vertical velocities are found. This corresponds to the findings in section 7.4.2 about the Delft3D modeling of the flow over the vertical wall weir from the experiments of Lauchlan. The morphological behavior directly around the weir is therefore doubtful.

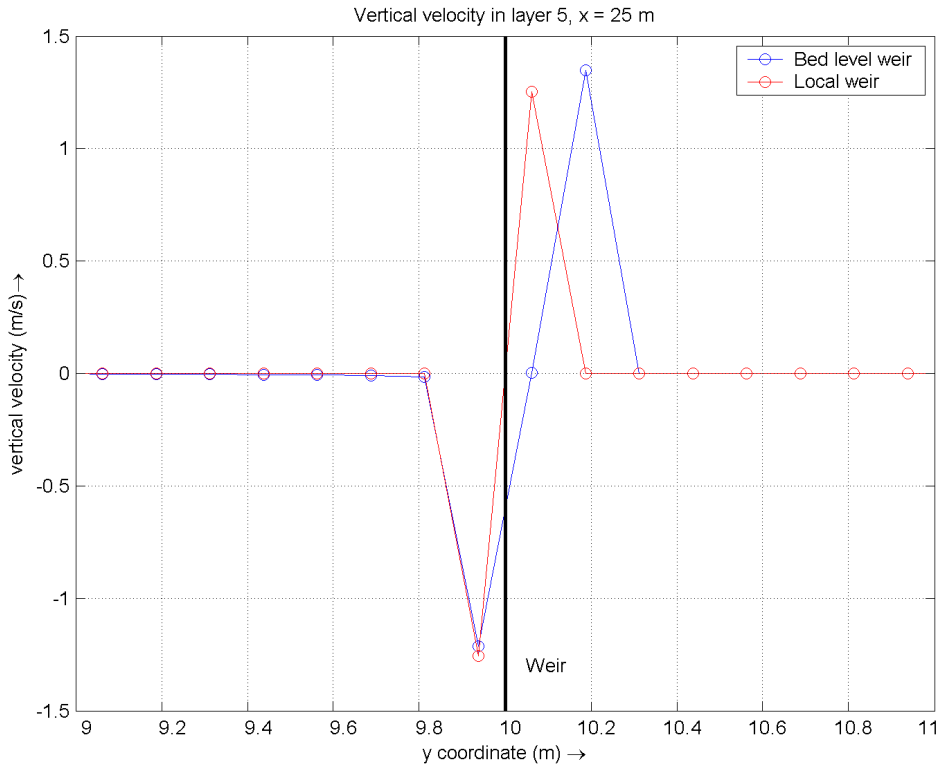

Figure 8.22 – Vertical velocity (m/s) in the lowest computational layer at x = 25 meter

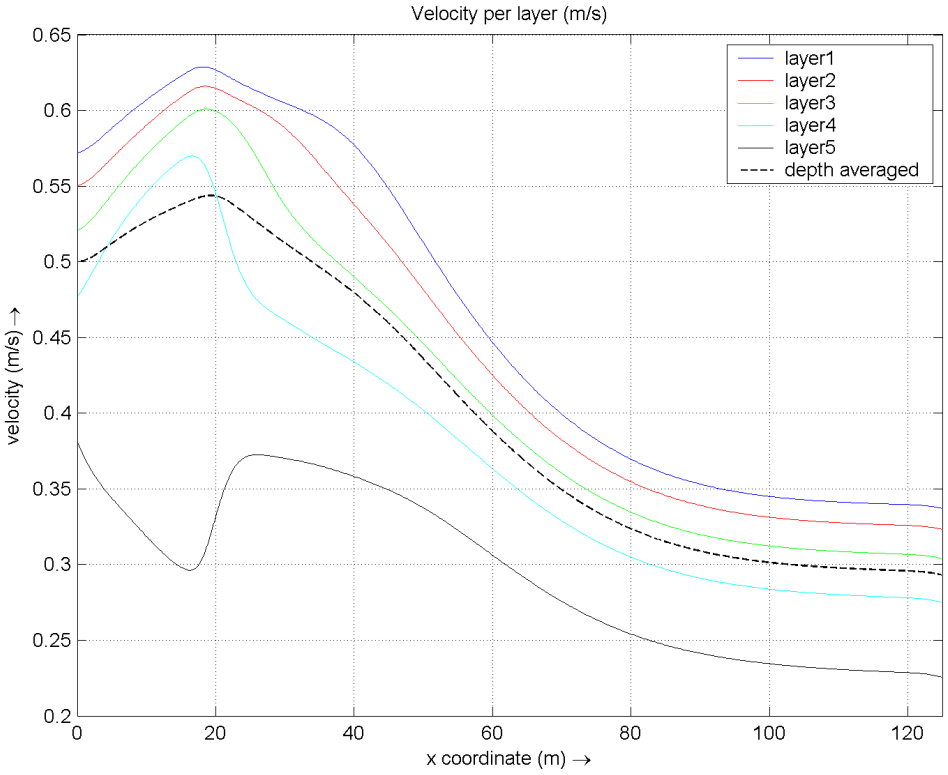

Figure 8.23 – Velocity magnitude (m/s) along the axis of the main channel (y = 15 m) for different computational layers. The depth-averaged velocity is also included.

The resulting erosion and sedimentation patterns for $D_{50} = 500$ µm are given in Appendix B. An erosion zone is found in the main channel. This is caused by an increase in the velocities in the layer adjacent to the bed, as shown in figure 8.23 for the simulation with a weir in bed level points. In this figure, the velocity magnitude per computational layer in the axis of the main channel is shown ($y = 15$ m). Also the depth-averaged velocity is included.

The velocity in the lowest layer (layer 5) is governing for bed-load transport. Bed-load transport is dominant in the case with $D_{50} = 500$ µm. The increased velocity concerns the x-component of the velocity. The cause of this behavior is not clear. The resulting erosion zone looks counterintuitive.

Boundary effects have influence in all simulations. The Neumann boundary condition for sediment transport and (in three dimensional computations) the logarithmic velocity profile give no equilibrium state behavior upstream of the domain of interest. Looking back, it would have been better to choose the boundary further away. However, this shortcoming does not affect the conclusions in any sense.

8.8. Conclusions

After analyzing the FLUENT simulations, it turns out that suspended-load transport is distributed between the main channel and the zone behind the weir in the same ratio as the discharge. This is not the case for bed-load transport, where for larger ratios of w_s / u_* the amount of sediment that passes the weir becomes smaller.

The same 3D situation has been modeled with Delft3D. The weir has been represented by a 2D-weir parameterization. It appears that this parameterization has hardly any influence on the flow. The model concept is meant for perpendicular flow. The mainly parallel oriented flow in this case is not calculated correctly by Delft3D. This results in a ratio $Q_2 / Q_1 = 0.99$ against $Q_2 / Q_1 = 0.85$ in FLUENT, in which the index 1 stands for the main channel and the index 2 for the zone behind the weir.

The 2D-weir parameterization has no direct influence on sediment transport. All mobile sediment that reaches the weir also passes the weir, independent of transport mode. The results of FLUENT show that this assumption is correct in case of suspended-load transport. For bed-load transport, this assumption results in significant errors.

The weir has no direct effect on sediment transport, and because the hydraulic effect is much too small, also the indirect effect of the weir on the sediment transport is negligible. The consequence is that it makes no difference whether the weir is present or not.

In order to improve the performance of Delft3D for this situation, three other ways of modeling have been investigated.

1. Depth-averaged modeling with increased bed level points at both sides of the 2D-weir.
2. Modeling with five computational layers, where the 2D-weir is substituted by a local weir
3. Modeling with five computational layers, where the 2D-weir is substituted by a locally increased bed level.

The results are summarized below.

	Flow	Sediment transport
2DH, bed-level weir	The discharge is distributed between the main channel and the zone behind the weir over a larger distance with respect to the situation with 2D-weir. However, the final ratio $Q_2 / Q_1 = 0.99$.	Bed-load transport is fully blocked and suspended-load transport is partially blocked by the weir. Large amounts of sedimentation are visible in the main channel.
3D, local weir or bed-level weir	The results of the simulations with a local weir and a bed-level weir strongly resemble each other. Unrealistic vertical velocities are visible at both sides of the weir, caused by the hydrostatic pressure assumption. The ratio $Q_2 / Q_1 = 1.05$	An erosion zone is found in the main channel due to increased velocities in the bed-adjacent layer. These increasing velocities are not found in other computational layers. Bed-load transport and suspended-load transport are partially blocked by the weir.

Table 8.5 – Results of the simulations of flow and sediment transport in case of 2DH modeling with a bed-level weir and in case of 3D modeling with a local weir or a bed-level weir

The 3D simulations performed give no rise to recommend this way of modeling when the details of the hydraulic structure are not resolved on the horizontal grid. Unrealistic hydraulic behavior around the weir, caused by the application of hydrostatic modeling on steep slopes, makes the results unreliable.

As concluded before, 2DH modeling with a 2D-weir gives an overestimation of bed-load transport over hydraulic structures. When the bed-level points at both sides of the weir are increased to crest level of the weir, all bed-load transport is blocked in the simulations performed in this study. This gives an underestimation of bed-load transport over hydraulic structures.

9. Discussion

The parameterization of hydraulic structures is introduced in Delft3D for taking the energy loss into account, which is caused by their presence in the flow. The aim is the correct representation of the influence of such a structure on the total flow pattern. The local details of the flow are assumed subgrid, and therefore kept out of the calculation. Just these local details are of great importance for sediment transport around hydraulic structures. Slope-effects, turbulent structures, interaction between transport modes (LAUCHLAN, 2001), deformation of vertical velocity profiles and other non-hydrostatic effects determine the exact motion of the particles.

A scale-problem arises. Sediment transport around hydraulic structures should be parameterized in large-scale models. Only large-scale variables are available as parameters. It is very difficult, or maybe even impossible, to make a fully valid direct link between large-scale hydraulic parameters (like depth, depth-averaged velocity and hydraulic roughness) and sediment transport around hydraulic structures. Also the numerical implementation is difficult, because a large accumulation of sediment in one grid cell directly upstream of a weir is physically not correct. The question is if it is possible to model sediment transport over hydraulic structures correctly on a grid with an interval size in the order of meters.

A pragmatic view is needed, combined with expert judgment. In the current way of modeling, the weirs have no direct influence on sediment transport at all. This leads to an overestimation of the sediment flux over the hydraulic structure, mainly in the case of bed-load transport. This has been shown by the comparison between sediment transport in FLUENT and Delft3D in a situation with three-dimensional flow and transport over a weir.
An often-used solution for this problem is increasing the bed level points at both sides of the weir to crest level. The hydraulic effect of this increased bed level should be equal to the effect of the 2D-weir parameterization, because this is validated (for flow perpendicular to the structure). In this way, suspended-load transport is reduced and hardly any bed-load transport is able to pass the weir. This approach gives an underestimation of sediment transport over the weir.

The correct parameterization is located somewhere in between. Knowledge of sediment transport in non-uniform flow situations is lacking. In addition, experimental data or field measurements are hardly available. Therefore, there is a need for a rule of thumb, to judge the amount of sediment that goes over a weir in Delft3D. The magnitude of the sediment transport can be ‘tuned’ by increasing the bed level points to a certain level between zero and crest height. The slope effect reduces the amount of sediment that is transported over the weir. A non-erodible layer should be applied on top of the weir, to ensure that the crest height is maintained during the simulation.

When Delft3D is applied in three dimensions in the current hydrostatic mode, the flow around the weir becomes unrealistic. This has been shown in the previous section. A better representation of sediment transport is therefore not expected in this way. The reliability of the results can probably be improved by non-hydrostatic modeling on a three-dimensional grid with a sufficiently high resolution. This will result in larger computation times. In addition, non-hydrostatic modeling using Delft3D is currently only available in Z-grid mode. The combination of Z-grid and morphological computations is not preferable, because staircases arise at the bed. When the code of Delft3D would be parallelized in an efficient way (like in FLUENT), the first problem could be reduced.

The 3D simulations performed give no rise to recommend this way of modeling instead of 2DH modeling when the details of the hydraulic structure are not resolved on the horizontal grid.

10. Conceptual model

Because it is not fully possible to parameterize sediment transport around hydraulic structures in a correct way in a coarse model like Delft3D, there is need for a method to estimate the influence of a structure on the sediment. This chapter attempts to give such a method.

Bed-load transport and suspended-load transport are treated in different ways. It should be noted that from Lauchlan's experiments, it becomes clear that the interaction between both transport modes is also important for sediment transport over a weir. Bed-load transport can be entrained by a gyre or an accelerating flow, and be carried in suspension over the structure.

10.1. Suspended-load transport

Suspended-load transport can be characterized by $w_s / u_* < 0.6$, or in terms of the Rouse parameter $w_s / \kappa u_* < 1.5$. The Rouse parameter is a measure of the shape of the concentration profile over the vertical. Small values of the Rouse parameter give more uniform distributions over the vertical, large values of the Rouse parameter give relatively high concentrations near the bed. A Rouse distribution for $w_s / u_* = 0.2$ is given in figure 10.1.

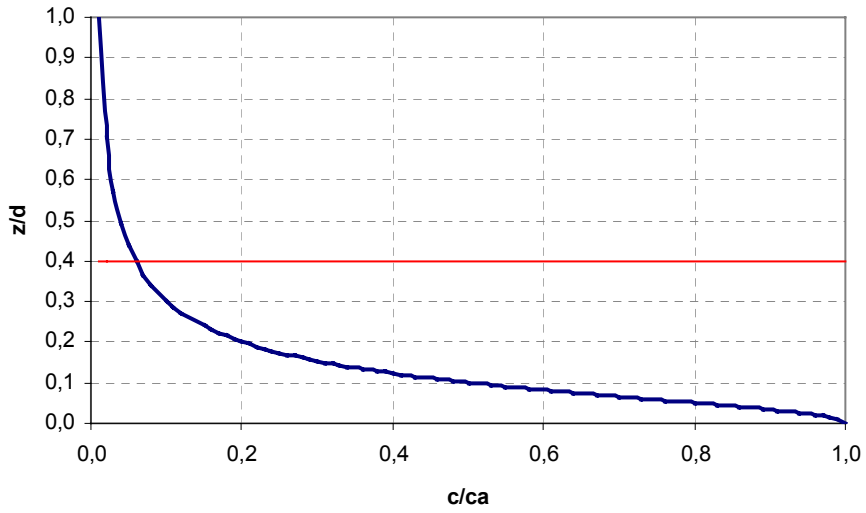

Figure 10.1 – Concentration profile (in blue) of suspended-load transport and a dividing line (in red) for sediment distribution around a hydraulic structure

A dividing line is defined: z_{div} / d. Al sediment above this line goes over the structure, all sediment below this line stays in the main channel.

$$S_1 = \int_a^{z_{div}} c(z)\, dz$$
$$S_2 = \int_{z_{div}}^{d} c(z)\, dz \qquad (10.1)$$

The dividing line is dependent on the relative height of the structure h_{weir}/d and the oblique angle of the flow over the weir to the weir crest φ.

$$\frac{z_{div}}{d} = f\left(\frac{h_{weir}}{d}, \varphi\right) \tag{10.2}$$

Data should be analyzed to check this relation and to formulate a function f. The shear velocity directly upstream of the structure is used in this analysis. This shear velocity can be determined by integration of the logarithmic velocity profile; see (2.14).

10.2. Bed-load transport

Both bed-load transport and saltation are both considered as bed-load transport, so $w_s/u_* > 0.6$. An analysis of bed-load transport is based on the Shields parameter:

$$\theta = \frac{u_*^2}{\Delta g D} \approx \frac{4}{3C_D\left(w_s/u_*\right)^2}. \tag{10.3}$$

Sediment is able to move up when the Shields parameter exceeds the critical shear stress, adjusted for slope effects. VAN RIJN (1993) gives the implicit relation of Shields in explicit form. Therefore the dimensionless grain diameter should be used:

$$D_* = \left(\frac{\Delta g}{\nu^2}\right)^{1/3} D. \tag{10.4}$$

The Shields-curve for incipient motion reads analytically:

$$\begin{aligned}
&\theta_{cr} = 0.24/D_* && 1 < D_* \le 4\\
&\theta_{cr} = 0.14/D_*^{0.64} && 4 < D_* \le 10\\
&\theta_{cr} = 0.04/D_*^{0.1} && 10 < D_* \le 20\\
&\theta_{cr} = 0.013D_*^{0.29} && 20 < D_* \le 150\\
&\theta_{cr} = 0.055 && D_* > 150
\end{aligned} \tag{10.5}$$

The critical Shields values should be adjusted for slope effects, for instance with the empirical relation of DEY (2001), as given in (2.34):

$$\frac{\tau_{b,cr}}{\tau_{b,cr,0}} = \left(1-\frac{\tan\alpha}{\tan\phi}\right)^{0.75}\left(1-\frac{\tan\gamma}{\tan\phi}\right)^{0.37}. \tag{10.6}$$

The longitudinal bed slope α and the transverse bed slope γ can be written in terms of the geometry of the weir and the oblique angle of the flow φ (not to confuse with the angle of internal friction ϕ), in case of a triangular weir with a width B_{weir} and a height h_{weir}:

$$\tan\alpha = -\frac{2h_{weir}\sin\varphi}{B_{weir}}$$
$$\tan\gamma = -\frac{2h_{weir}\sin\varphi}{B_{weir}\tan\varphi} \qquad (10.7)$$

The slope influences the critical shear stress, but also the actual shear stress is affected. The influence of slopes on critical shear stress can be adequately described, but the influence of slopes on actual shear stress is less clear (LAUCHLAN, 2001). For this reason, FLUENT simulations have been carried out with enhanced wall treatment and a very high grid resolution near the wall ($z_p^+ < 2$), to give a rough estimation of this effect. The actual shear stress along the slope (τ_2) can be described by the depth-dependent shear stress in uniform flow conditions, multiplied by a slope-dependent factor $f(\alpha)$.

Relationship (2.14), combined with (2.9) and multiplied with $f(\alpha)$ gives:

$$\tau_2(x) = \tau_1 \cdot \left(\frac{d_1\left[\ln\{d_1/z_0\}-1\right]}{d_2(x)\left[\ln\{d_2(x)/z_0\}-1\right]} \right)^2 \cdot f(\alpha), \qquad (10.8)$$

in which d_1 and τ_1 are the upstream water depth and shear stress. The depth along the slope is given by $d_2(x) = h_1 - x\tan\alpha$ for $0 \le x \le L$, in the case of a straight slope. The multiplication factor $f(\alpha)$ has been investigated for four different values of α and for two values of h_{weir}/d.

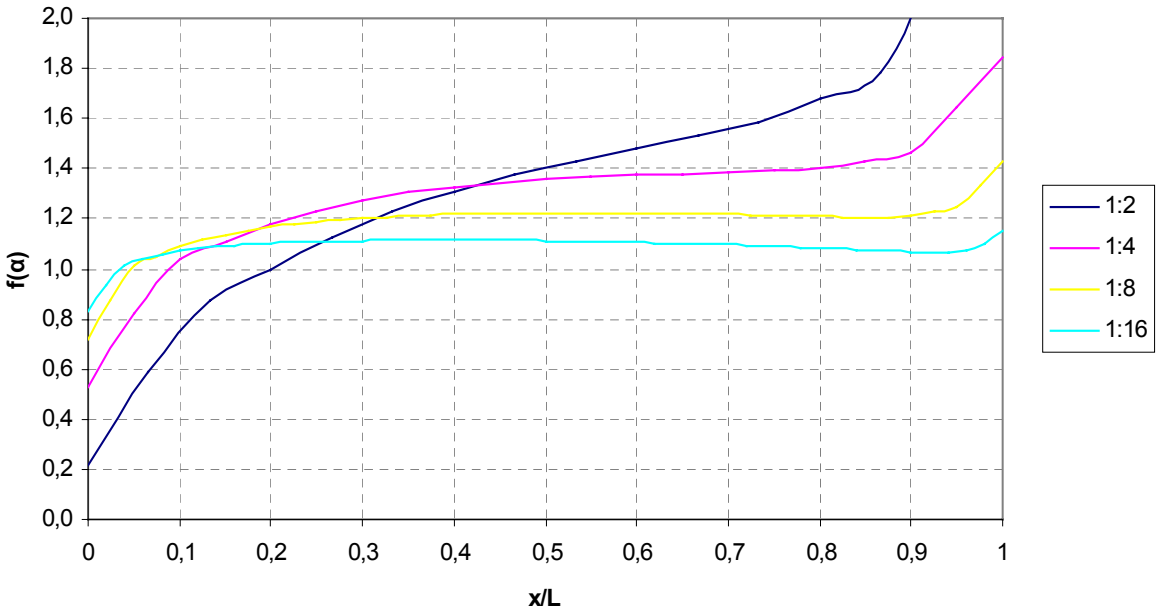

Figure 10.2 – The value of the slope dependent factor f(α) as a function of the position at the slope divided by the length of the slope for $h_{weir}/d = 0.5$

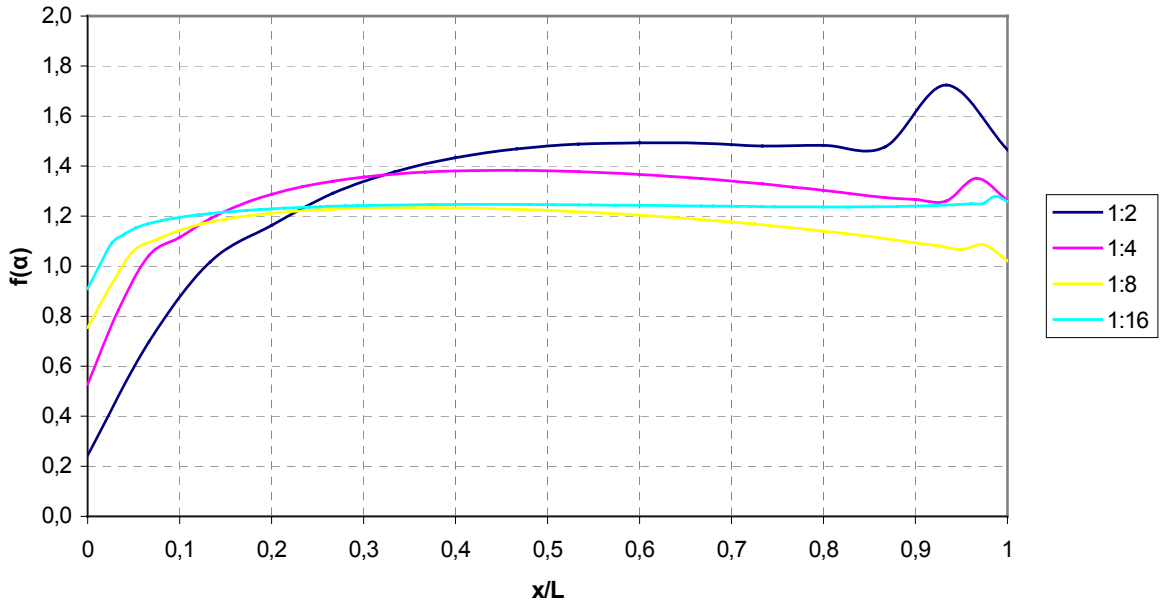

Figure 10.3 – The value of the slope dependent factor f(α) as a function of the position at the slope divided by the length of the slope for $h_{weir}/d = 0.75$

The values $f(\alpha) < 1$ at the toe of the slope are caused by the abrupt change in slope. The flow separates from the bed, resulting in decreased shear stresses. This effect is larger for steeper slopes. In reality, the transition from river bed to the slope of the hydraulic structure will be more gradual. The effect of decreased shear stresses will be less pronounced in that case.

Mainly the shear stresses at the lower part of the slope are important for sediment transport over weirs. It seems that the shear stress goes to a constant value when the slope is long enough. The deviation near the crest is not able to increase the bed-load transport over the weir anymore. The constant value for $f(\alpha)$ is given as a function of the slope α in figure 10.4.

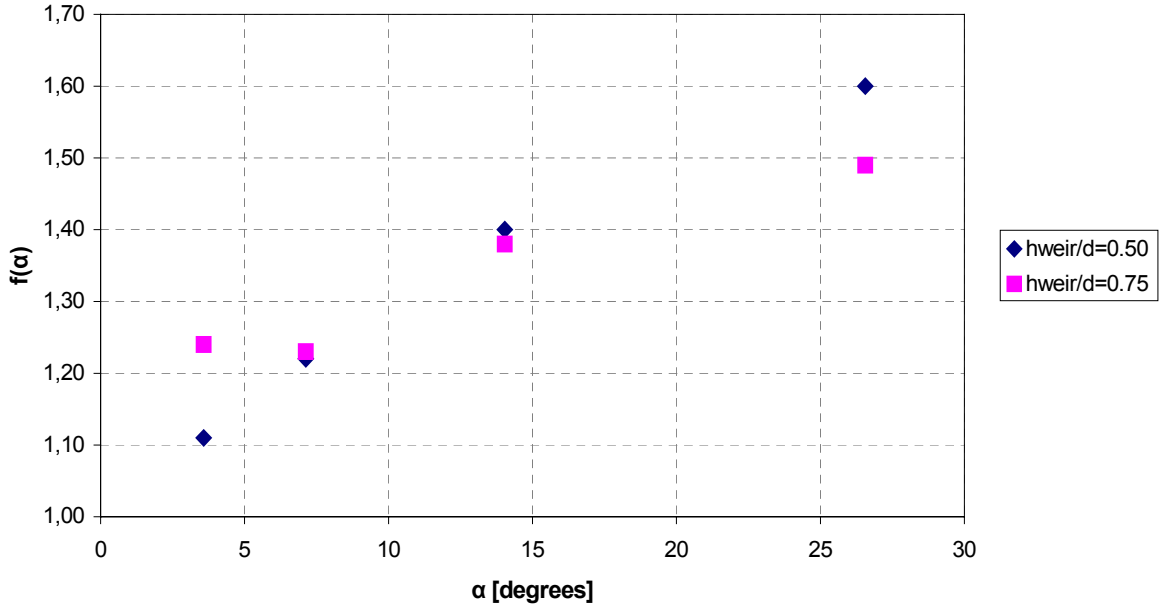

Figure 10.4 – Constant value of the slope dependent factor f(α) as a function of slope angle α

The results for $h_{weir}/d = 0.5$ look more realistic than the results of $h_{weir}/d = 0.75$. The decreasing values of $f(\alpha)$ for larger values of x/L in figure 10.3 are strange. Also the value of $f(\alpha)$ for $h_{weir}/d = 0.75$ and slope 1:16 deviates from the other values. A possible reason for the better results of $h_{weir}/d = 0.5$ is that the rigid-lid approximation yields better results than for higher weirs.

Because the flow needs some time to change, the flow at the toe of the slope has a nearly uniform character ($f(\alpha) = 1$). Also the depth-averaged velocity has the smallest value at this point. Bed-load transport from the river bed should pass this zone, to be able to move over the weir. Therefore, $f(\alpha) = 1$ is governing for bed-load transport over the weir. The upstream Shields parameter (based on uniform flow conditions) will be used in the analysis. When the oblique angle of the flow φ changes along the slope, also other places should be considered.

The amount of transport over the weir for $\theta > \theta_{cr}$ can be formulated in terms of either the transport stage $T_* = \theta/\theta_{cr}$ or the excess shear stress $S_\tau = (\theta - \theta_{cr})/\theta_{cr}$ (HARRIS, 2003). In this analysis, the latter is used, so:

$$C = \frac{S_2/S_1}{Q_2/Q_1} = g\left(\frac{\theta - \theta_{cr}}{\theta_{cr}}\right). \tag{10.9}$$

10.3. Application

The theory for suspended-load transport and bed-load transport, as developed in the previous sections, will be applied to the situation with three-dimensional flow and transport over weirs, as described in section 8.1. This situation will be modeled with FLUENT to give an indication of the functions f and g in (10.2) and (10.9) respectively.

Suspended-load transport gives for both $D = 100$ µm and $D = 150$ µm a coefficient $C = 1$ (table 8.4). This means that suspended sediment is distributed in the same ratio as the discharge. This corresponds to the findings of LAUCHLAN (2001). A dividing line, as suggested in section 10.1 is not needed.

Pathlines of the flow over the weir at the surface are given in figure 10.5.

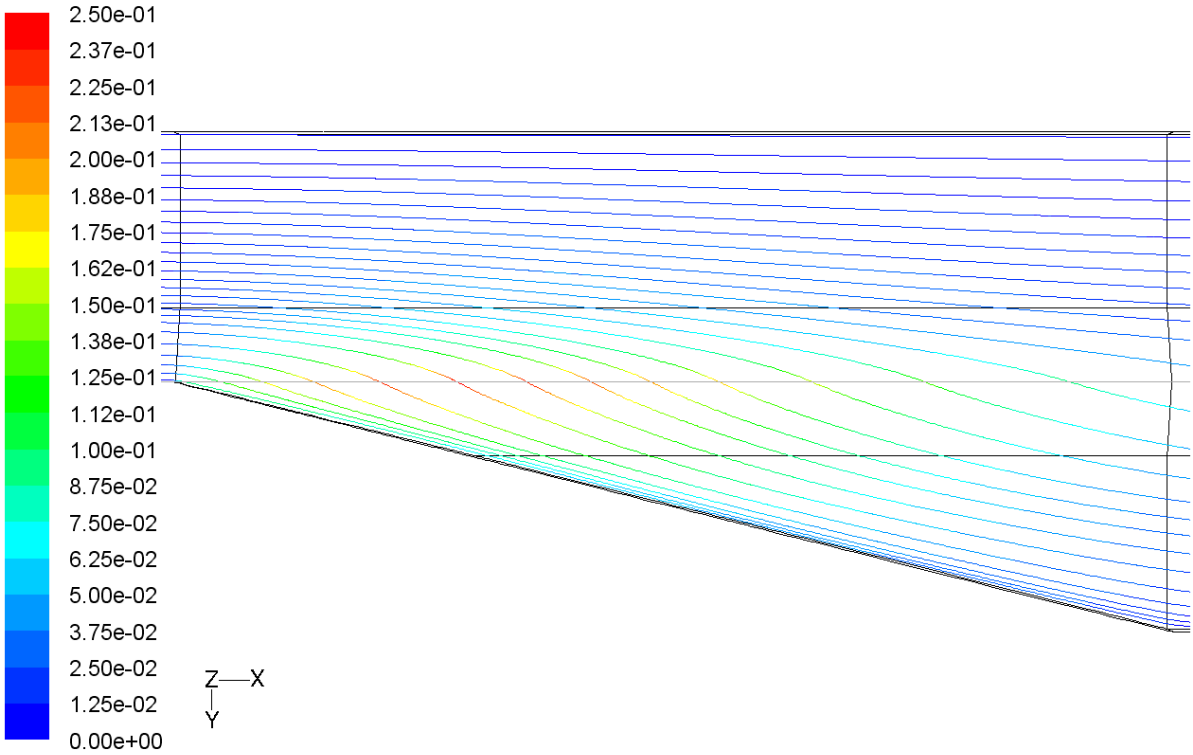

Figure 10.5 – Pathlines of the flow in FLUENT, colored by relative y-velocity [-]

The color of the pathlines represents the relative y-velocity (which is a dimensionless number: the y-velocity divided by the velocity magnitude), which is equal to the tangent of the angle of the flow with respect to the weir crest. This angle varies from approximately $\tan\varphi = 0.06$ at the toe of the slope to $\tan\varphi = 0.25$ at the weir crest.

Two points are considered to analyze equation (10.9) for bed-load transport: the toe of the slope and the weir crest. It is assumed that $f(\alpha) = 0$ at the toe of the slope and $f(\alpha)$ is equal to the constant value from figure 10.4 at the weir crest.

The magnitude of the depth-averaged velocity at the toe of the slope and on top of the weir crest is given as a function of the x-coordinate in figure 10.6. The pathlines in figure 10.5

show that a representative value at the toe is found near $x = 60$ m and on top of the weir crest near $x = 75$ m. This gives depth-averaged velocities of 0.53 m/s and 0.47 m/s respectively.

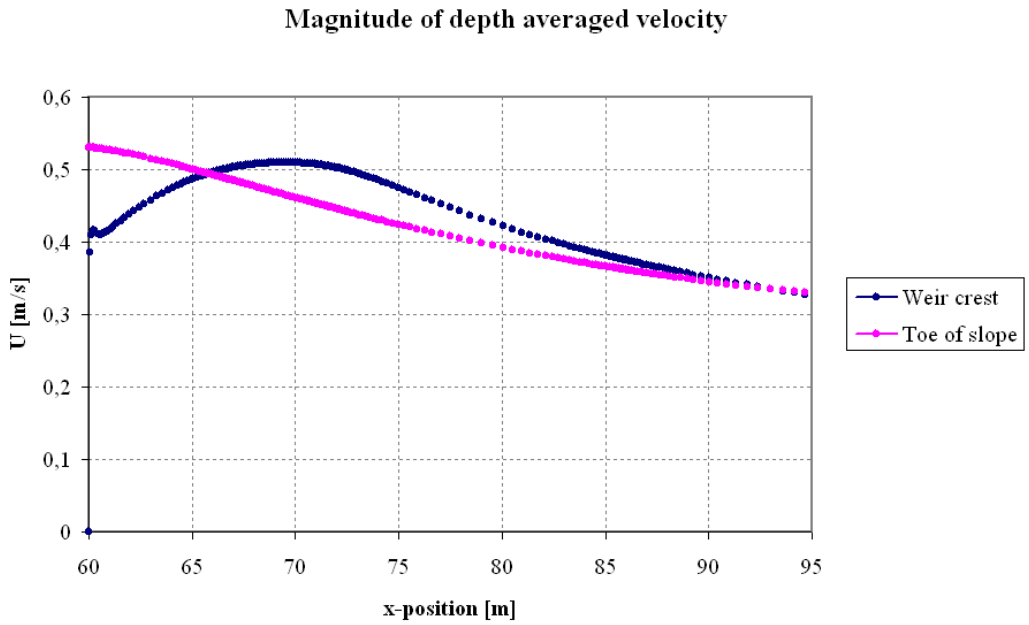

Figure 10.6 – Depth-averaged velocity (m/s) along the toe of the slope and along the weir crest

The oblique angle of the flow is equal to 3.43 degrees at the toe of the slope. Equation (10.7) gives $\alpha = -0.86°$ and $\gamma = -14.30°$ for $h_{weir} = 0.75$ m and $B_{weir} = 6$ m. This results in a correction factor for the critical shear stress (10.6) of 1.167.

The results of FLUENT for the toe of the slope are listed in table 10.1. The dimensionless grain diameter D_* is used to determine the critical shear stress on a flat bed $\theta_{cr,0}$, as given by (10.5). The actual shear stress on a flat bed θ_0 is based on the particle diameter, the depth-averaged velocity of 0.53 m/s and the depth of 1 meter directly upstream of the slope via (2.14) and (10.3). Equation (2.14) gives a local shear velocity $u_* = 0.0374$ m/s. The excess shear stress is calculated by $S_\tau = (\theta - \theta_{cr}) / \theta_{cr}$.

D (μm)	w_s / u_*	C	D_*	$\theta_{cr,0}$	θ_{cr}	θ_0	$\theta=\theta_0$	S_τ
200	0.67	0.81	5.0592	0.0496	0.0579	0.4321	0.4321	6.4637
300	1.15	0.57	7.5888	0.0383	0.0447	0.2881	0.2881	5.4500
400	1.58	0.41	10.1184	0.0317	0.0370	0.2160	0.2160	4.8330
500	2.09	0.23	12.6480	0.0310	0.0362	0.1728	0.1728	3.7717
600	2.57	0.06	15.1776	0.0305	0.0356	0.1440	0.1440	3.0496
700	3.02	0	17.7072	0.0300	0.0350	0.1235	0.1235	2.5250

Table 10.1 – FLUENT data of bed-load transport over weirs, position: toe of the slope

The same equations give $\varphi = 14.04°$, $\alpha = -3.47°$, $\gamma = -13.88°$ and a correction factor for the critical shear stress of 1.230. The Shields parameter for flat beds θ_0 is based on the local shear velocity on top of the weir u_*. With $d = 0.25$ m and $U = 0.47$ m/s follows $u_* = 0.0439$ m/s. The Shields parameter at the slope $\theta = \theta_0 \cdot f(\alpha)$. From figure 6.17, $f(\alpha) = 1.13$ is estimated.

***D* (µm)**	w_s / u_*	**C**	D_*	$\theta_{cr,0}$	θ_{cr}	θ_0	θ	S_τ
200	0.57	0.81	5.0592	0.0496	0.0610	0.5953	0.6727	10.0289
300	0.98	0.57	7.5888	0.0383	0.0471	0.3969	0.4485	8.5311
400	1.34	0.41	10.1184	0.0317	0.0390	0.2977	0.3364	7.6193
500	1.78	0.23	12.6480	0.0310	0.0382	0.2381	0.2691	6.0510
600	2.19	0.06	15.1776	0.0305	0.0375	0.1984	0.2242	4.9840
700	2.57	0	17.7072	0.0300	0.0369	0.1701	0.1922	4.2088

Table 10.2 – FLUENT data of bed-load transport over weirs, position: weir crest

The excess shear stress at the toe of the slope is significantly lower than on top of the weir crest. This means that the conditions at the toe of the slope are governing for the distribution of bed-load transport between main channel and the zone behind the weir.
The coefficient C is plotted against the excess shear stress S_τ at the toe of the slope (corrected for slope effects) in figure 10.7, to investigate the relation (10.9).

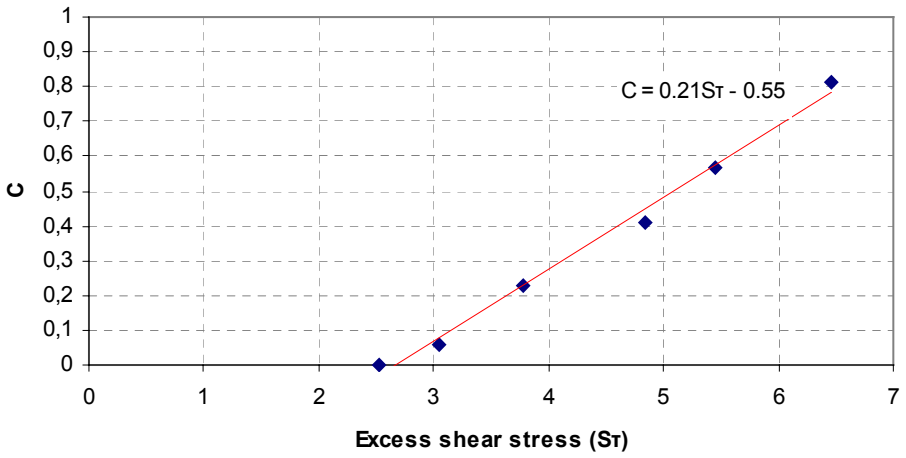

Figure 10.7 – Relation between excess shear stress S_τ at the toe of the slope and the coefficient C of equation (10.9)

The coefficient C is linearly related to the excess shear stress at the toe of the slope. The red line is obtained by linear regression. Equation (10.9) can be written as:

$$C = \frac{S_2/S_1}{Q_2/Q_1} = 0.21 \cdot \left(\frac{\theta - \theta_{cr}}{\theta_{cr}} \right) - 0.55 \qquad (10.10)$$

The correlation coefficient of the regression line equals 0.996. The amount of data supporting (10.10) is very limited. It is also not known whether the model concepts regarding bed-load transport (at sloped beds) in FLUENT are fully correct. The relation can therefore be seen as a rough rule of thumb to judge the amount of bed-load transport over a hydraulic structure.

For the sloped weir case of LAUCHLAN (2001), a value of $S_\tau = 2.09$ can be calculated for the location at the toe of the upstream slope. Equation (10.10) gives no transport over the weir for this value, which fully contradicts the conclusions of Lauchlan. In two-dimensional cases, all water and sediment is forced over the structure. This shows that the theory of this section is only applicable in three-dimensional situations, in which water and sediment can either go over the weir or move along the weir. It would be nice to perform laboratory experiments of three-dimensional flow and transport over hydraulic structures, to check the validity of the theory of this section.

11. Conclusions and recommendations

The two main objectives of this study have been defined in section 1.3. In this chapter, conclusions and recommendations are given regarding both objectives.

11.1. Conclusions

The first objective has been defined as:

A. *Assessing the performance of the current way of Delft3D modeling of sediment transport around hydraulic structures in three-dimensional flows.*

Delft3D is meant to model flow phenomena of which the horizontal length and time scales are significantly larger than the vertical scales. Near hydraulic structures, this is generally not the case. These structures are parameterized as 2D-weirs in a depth-averaged Delft3D model in engineering practice. 2D-weirs are included in the momentum equation as local energy losses. The parameterization of hydraulic structures by 2D-weirs aims at representing the influence of the weirs on the flow at larger scales. The partly empirical formulations are based on perpendicular flow over weirs. The local flow around the structures is not correctly modeled.

The performance of the current way of Delft3D modeling of sediment transport around hydraulic structures has been assessed by parallel simulation with Delft3D and FLUENT of both laboratory experiments and a three-dimensional design situation. FLUENT is an advanced software system for flow modeling, with which sediment transport can be studied by analyzing the trajectories of discrete particles.

Regarding the modeling of laboratory experiments, it can be concluded that:

Uniform flow	FLUENT is able to reproduce wall shear stresses in uniform flow conditions at hydrodynamically smooth and rough beds correctly. Also the difference between suspended-load transport and bed-load transport is reproduced in the right way.
Flow over weirs	The flow over the upstream slope of a 1:4 sloped groin section (STOLKER, 2005) is modeled correctly by FLUENT and Delft3D. In the separation zone downstream of the crest, the results of both models show significant deviations from the laboratory measurements. The results are very sensitive to the turbulence model used, wall treatment and the exact geometry of the weir. The reproduction of flow at upstream slopes is of greater importance for the magnitude of sediment transport over structures than the flow at downstream slopes.
Sediment transport over weirs *FLUENT*	FLUENT is able to reproduce the gyres upstream and downstream of a vertical wall weir, as observed in the experiments of LAUCHLAN (2001), when Large Eddy Simulation is used. The gyre upstream of the weir is absent when the k-epsilon turbulence model is chosen. Large Eddy Simulation cannot be combined with particle tracking. The analysis of particle trajectories with k-epsilon turbulence modeling shows that FLUENT gives only sedimentation downstream of the weir, which corresponds to the experimental observations. The same holds for sediment transport over a sloped weir.

Sediment transport over weirs *Delft3D*	Delft3D gives non-physical vertical velocities at both sides of the vertical wall weir. This is mainly caused by the hydrostatic pressure assumption. Gyres and recirculation zones are not found in Delft3D at all. The morphological results of Delft3D qualitatively agree with the experimental results, in spite of the incorrect representation of the flow around the weir. The hydraulic and morphological results of Delft3D for the sloped weir are approximately right.

The modeling of the laboratory experiments gives confidence in using FLUENT as an instrument to judge the performance of Delft3D in modeling three-dimensional flow and transport over hydraulic structures. A three-dimensional flow situation has been designed, which resembles the flow over a longitudinal weir.

After analyzing the simulations of this design situation of three-dimensional flow and transport over hydraulic structures, it can be concluded that:

Sediment distribution in FLUENT	It turns out that *suspended-load transport* is distributed between the main channel and the zone behind the weir in the same ratio as the discharge. This is not the case for *bed-load transport*, where for larger ratios of w_s / u_* the amount of sediment that passes the weir becomes smaller.
Parallel flow over a weir in Delft3D	The same 3D situation has been modeled with Delft3D. The longitudinal weir has been represented by a *2D-weir parameterization*. It appears that this parameterization has hardly any influence on the flow. The model concept is meant for perpendicular flow. The *mainly parallel oriented flow* in this case is not calculated correctly by Delft3D.
Sediment transport over a weir in Delft3D	The *2D-weir parameterization* has no direct influence on *sediment transport*. All mobile sediment that reaches the weir also passes the weir, independent of transport mode. The results of FLUENT show that this assumption is correct in case of suspended-load transport. For bed-load transport, this assumption results in significant errors. The weir has no direct effect on sediment transport, and because the hydraulic effect is much too small, also the indirect effect of the weir on the sediment transport is negligible. The consequence in this case is that it makes no difference whether the longitudinal weir is present or not.
3D modeling with Delft3D	*3D simulations* with five computational layers have been performed. These simulations give no rise to recommend this way of modeling when the details of the hydraulic structure are not resolved on the horizontal grid. Unrealistic hydraulic behavior around the weir, caused by the application of *hydrostatic modeling* on steep slopes, makes the results unreliable.
2D-weir parameterization and surrounding bed level	2DH modeling with a 2D-weir gives an overestimation of bed-load transport over hydraulic structures. When the *bed-level points* at both sides of the weir are increased to crest level of the weir, all bed-load transport is blocked in the Delft3D simulations performed in this study. This gives an underestimation of bed-load transport over hydraulic structures.

11.2. Recommendations

The second objective has been defined as:

B. Making recommendations on the modeling of sediment transport around hydraulic structures in hydraulic engineering practice.

A 2D-weir without increased bed level points overestimates the sediment transport over the structure. When the bed level points are increased until crest level of the 2D-weir, the sediment transport over the weir is underestimated. The sediment transport over the weir can be tuned by an increased bed level somewhere between zero and crest level.

The distribution of sediment between the main channel (index 1) and the area behind the weir (index 2) can be described with a relation:

$$\frac{S_2}{S_1} = C \cdot \frac{Q_2}{Q_1} \tag{11.1}$$

The value of C as given by Delft3D can be judged with the following rules of thumb:

Suspended-load transport Suspended-load transport is distributed between the main channel and the zone behind the weir in the same ratio as the discharge, so $C = 1$.

Bed-load transport For bed-load transport in three-dimensional situations with clearly oblique flow over the weir, the coefficient C can be related to the excess shear stress S_τ at the upstream slope, in which the actual Shields parameter θ and the critical Shields parameter θ_{cr} are adjusted for slope effects. The relation based on the data of this study can be written as:

$$C = \frac{S_2/S_1}{Q_2/Q_1} = 0.21 \cdot \left(\frac{\theta - \theta_{cr}}{\theta_{cr}} \right) - 0.55 \tag{11.2}$$

Perpendicular flow In situations where the flow is directed almost perpendicular to the crest of the structure, the conclusions of LAUCHLAN (2001) are recommended. Nearly all mobile sediment is transported over the structure in these situations.

The coefficient C in Delft3D can be influenced by giving the bed level points near the weir the right height. In river engineering applications, a representative hydrograph with a limited number of discharge levels is frequently used. Hydraulic structures like longitudinal weirs, groins and weirs in the inlet of side channels are in most cases only submerged in the period with the highest discharge. When the structure is submerged during different discharge levels, a discharge-dependent bed level can be used.

Regarding the model concepts of Delft3D, the following is recommended:

Parameterization of parallel flow over weirs	The implementation of another model concept for situations with mainly parallel flow over hydraulic structures than the model concept for perpendicular flow. Currently, the 2D-weir, which is meant for perpendicular flow, is used in both cases.
Parallelization of the Delft3D code	Sediment transport around hydraulic structures is dependent on relatively small-scale processes. These processes are subgrid at coarser grids. A correct parameterization based on large-scale parameters seems to be nearly impossible. The grid resolution should be enlarged in these situations. The 3D hydraulic and morphological modeling with Delft3D of 1:4 sloped structures on a relatively fine grid shows that satisfactory results can be obtained for practical applications. When this is needed in simulations of large-scale problems, the grid becomes large. This results in increased computation times. Efficient parallelization of the Delft3D code (like in FLUENT) can reduce this problem.
Non-hydrostatic morphological modeling	Delft3D simulation of hydraulic structures, using different computational layers, gives no distinct benefits with respect to depth-averaged modeling. The main reason is the occurrence of errors caused by the hydrostatic pressure assumption. Possibly, better results could be obtained when it is possible to combine non-hydrostatic modeling with morphological computations on a sigma grid.

11.3. Challenges

Studying physical processes using Reynolds Averaged Numerical Simulation (RANS) is clearly not perfect. The following aspects of this study could be better founded in further studies:

Bed-load transport in FLUENT	Bed-load transport is treated in the same way as suspended-load transport in FLUENT. The motion of a particle is dependent on the balance of acceleration forces of gravity and the flow. The turbulent flow is taken into account in a statistical way. Incipient motion is not reproduced correctly with this method. Bed-load transport is related to incipient motion. The reproduction of bed-load transport by FLUENT should be more comprehensively investigated to obtain a higher reliability of the results of this study.
Parallel flow and perpendicular flow	In this study, perpendicular flow (STOLKER, 2005 and LAUCHLAN, 2001) and flow over a longitudinal weir has been considered. These are two extreme cases. Situations in between should be studied to bridge this gap.
Continuation of this study *Numerical modeling* *Laboratory experiments*	The rule of thumb describing bed-load transport over hydraulic structures in three-dimensional flows is based on a very limited amount of data. More data could improve the founding of equation (11.2). The model concepts underlying this rule of thumb can be investigated better, using a more advanced numerical simulation technique, like Large Eddy Simulation or Detached Eddy Simulation, or when a laboratory experiment is performed. Possibly, other processes are also of importance, which are not taken into account in chapter 10.

References

ALBERTSON, M. (1953): "*Effects of Shape on the Fall Velocity of Gravel Particles*", Proceedings of the 5th Iowa Hydraulics Conference, Iowa City, Iowa

BALEN, W. VAN (2005): "*Large-scale coherent structures in turbulent shallow flows*", MSc. thesis, Delft University of Technology

BALEN, W. VAN (2010): "*Curved open-channel flows, a numerical study*", PhD. thesis, Delft University of Technology

BATTJES, J.A. (2002): "*Vloeistofmechanica*" (in Dutch), lecture notes, Delft University of Technology

BUSNELLI, M. M. (2001): *"Numerical simulation of free surface flows with steep gradients"*, PhD. thesis, WL | Delft Hydraulics, Delft, The Netherlands.

COURANT, R. AND D. HILBERT (1962): "*Methods of mathematical physics*", Interscience, New York.

DELTARES (2009): "*Delft3D-FLOW User Manual*", Delft

DEY, S. (2001): "Experimental study on incipient motion of sediment particles on generalized sloping fluvial beds", *Int. Journal of Sediment Research, Vol. 16, No. 3*, pp. 391-398

DN URBLAND (2009): "*Ruimte voor de Lek: variantenstudie*" (in Dutch), Delft

ENGELUND, F. AND E. HANSEN (1967): "*A monograph on sediment transport in alluvial streams*", Teknisk Forlag, Kopenhagen

FLUENT INC. (2005): "*FLUENT 6.2 User's Guide*", Lebanon, NH, United States

GALAPPATTI, R. AND C.B. VREUGDENHIL (1985): "*A depth integrated model for suspended sediment transport*", Journal of Hydraulic Research, Vol. 23, No. 4 (1985), pp. 359–377.

HARRIS, C.K. (2003): "*Sediment transport processes in coastal environments*", Virginia Institute of Marine Science, Gloucester Point, United States.

JAGERS, H.R.A. & D. SCHWANENBERG (2003): "*CFD for Hydraulic Structures*", WL | Delft Hydraulics, report Q3429, Delft

LAUCHLAN, C.S. (2001): "*Sediment transport over steep slopes, an experimental investigation; results and analysis*", RWS RIZA, Delft Cluster

LAUCHLAN, C.S. (2004): "*Experimental investigation of bed-load and suspended-load transport over weirs*", Journal of Hydraulic Research, Vol. 42, No. 5 (2004), pp. 549-555

MEIJER, D.G. (1994): "*Sediment distribution in a channel bifurcation*", WL | Delft Hydraulics, report Q1941, Delft

MEYER-PETER, E. AND R. MÜLLER (1948): "*Formulas for bed-load transport*", Proceedings IAHR, Stockholm, Vol. 2, paper 2, pp. 39-64

MORSI, S. A. AND A. J. ALEXANDER (1972): "*An Investigation of Particle Trajectories in Two-Phase Flow Systems*", Journal of Fluid Mechanics, Vol. 55, No. 2, pp. 193-208

MOSSELMAN, E. (1998): "*Transport van sediment over steilranden en overlaten*" (in Dutch), WL | Delft Hydraulics, report for RWS RIZA, Q2423, Delft

MOSSELMAN, E. (2001): "*Morphological development of side channels*", CFR project report 9, IRMA-SPONGE en Delft Cluster, Delft

NGUYEN, B.T. (2006): "*Flow over oblique weirs*", MSc. Thesis, Delft University of Technology

NIEUWSTADT, F.T.M. (1998): "*Turbulentie*" (in Dutch), Epsilon uitgaven Utrecht

RAUDKIVI, A.J. (1998): "*Loose Boundary Hydraulics*", Third Edition; Pergamon Press, Oxford, United Kingdom

RIJN, L. C. VAN, (1993): "*Principles of Sediment Transport in Rivers, Estuaries and Coastal Seas*", Aqua Publications, The Netherlands.

RUPPRECHT, R. (2004): "*Modeling of the morphological interaction between a river and its groyne fields*", MSc. thesis, Delft University of Technology

SCHIERECK, G.J. (2004): "*Bed, bank and shore protection*", Second edition, Delft University Press, Delft, The Netherlands

SCHWANENBERG, D. (2006): "*3D Non-hydrostatic flow, 3D CFX simulation of a groyne section*", WL | Delft Hydraulics, report Q3429, Delft

STOLKER, C. (2005a): "*Stroombeelden bij recht aangestroomde kribben*" (in Dutch), WL | Delft Hydraulics, report Q3018, January 2005, Delft

STOLKER, C. (2005b): "*Stroombeelden bij recht aangestroomde kribben*" (in Dutch), WL | Delft Hydraulics, report Q3018, December 2005, Delft

UIJTTEWAAL, W.S.J. (2003): "*Turbulence in hydraulics*", lecture notes, Delft University of Technology

VRIEND, H.J. DE (2006b): "*Sediment transport in complex flows: time for a step forward*", Second Sino-American Workshop on advanced computational modeling in hydroscience and engineering, November 25-26, 2006, Beijing, China

Appendix A – Model set-up of 3D situation in FLUENT

In this appendix, a description is given of the model set-up of the situation with three-dimensional flow and transport in FLUENT.

First, geometry, mesh and boundary conditions have been defined in Gambit, the preprocessor of FLUENT. Firstly, 87 vertices are defined. These vertices are connected by 161 straight edges. This gives 114 faces and 26 volumes. The domain has been divided in these volumes to be able to create a structured grid with only quads, which is preferable to triangles. Triangles should be split up into quads with help of additional points in the middle. This extra point is connected to a point somewhere in the middle of the edges of the triangle. In this way, quads are obtained. This is illustrated in figure A1.

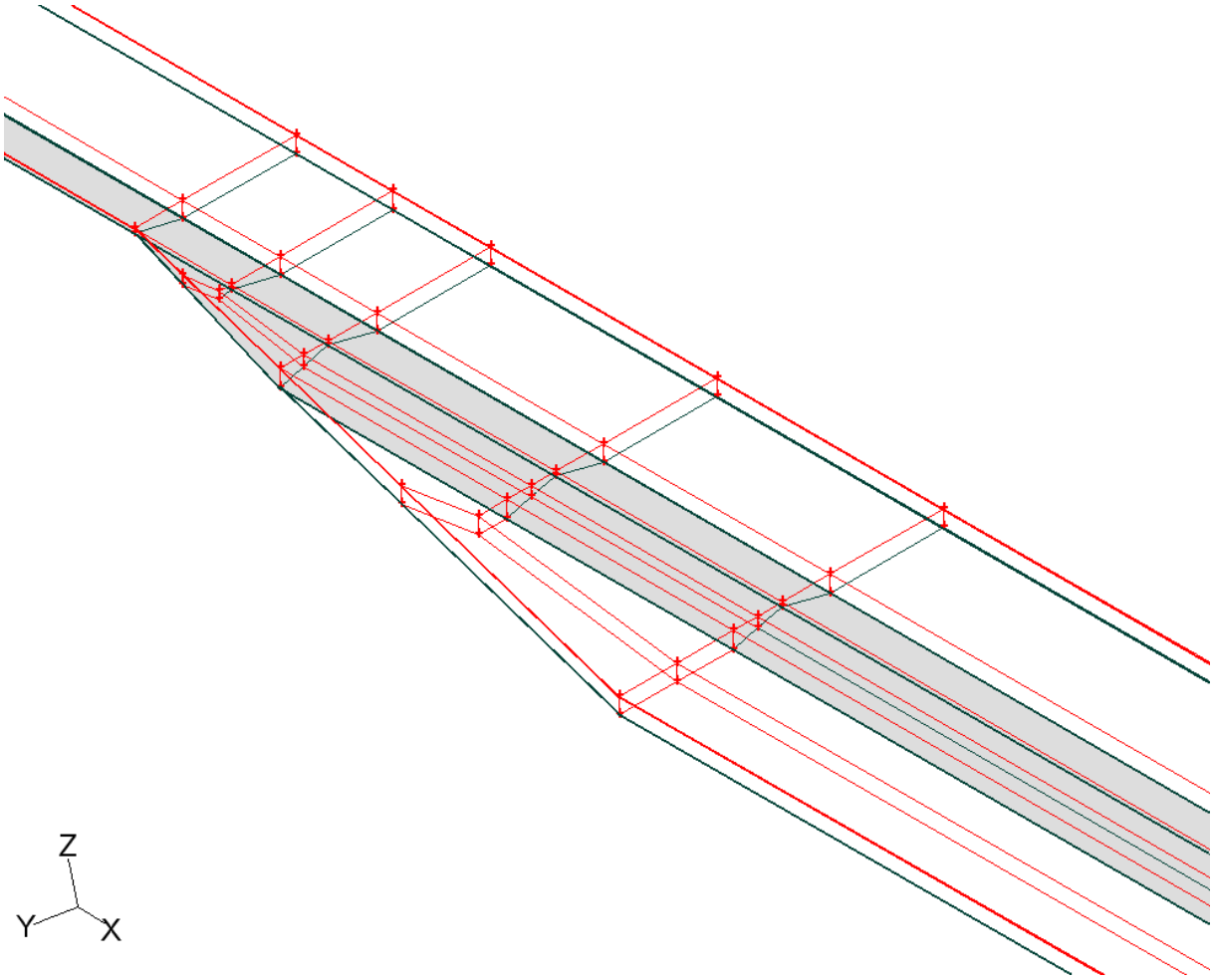

Figure A1 – Geometry and mesh volumes

The vertical (with a height of 1 meter at both sides of the weir) has been divided in 12 intervals. The first length is equal to 0.08 m, which is larger than twice the roughness height of 0.038 m. In this way, the distance of the wall to the velocity point of the wall-adjacent cell is larger than the roughness height. Otherwise, unrealistic results can appear. With this distance to the wall, the z^+ of the first cell is approximately 1400, which is much larger than 20. This means that wall function can be used. Opposite faces all have the same number of grid points. Attention should be paid to the transition of the mesh from one face to the other.

The ratio between two adjacent intervals has to be smaller than 1.3 for correct turbulence modeling. For this reason, first lengths and last lengths of the face meshes have been defined. FLUENT smoothes the mesh between both ends of the face automatically. The mesh density has been enlarged near the expansion zone, the main zone of interest.

When the mesh is finished, boundaries and boundary types have been defined, with the types wall, velocity inlet, outlet and symmetry. Defining boundary conditions is relatively simple in rigid-lid models. The mesh with approximately 1.2 million cells as created in Gambit has been imported in FLUENT. A grid check has been performed in FLUENT 3ddp (which stands for double precision in three dimensions).

The following settings have been applied:

- Solver: implicit steady solver. FLUENT gives a steady state flow at the end of the simulation.
- Viscous model: realizable k-epsilon, with standard wall functions. Model constants have been kept default.
- Materials: water has been chosen.
- Operating conditions: the direction and magnitude of gravity has been defined.
- Boundary conditions:
    - Volumes: water has been specified.
    - Inlet: type velocity inlet, variables inlet velocity, k and ε have been defined.
    - Outlet: type outflow, no parameters are needed.
    - Bottom: type wall, roughness height 0.038 m, roughness constant 0.5, no-slip condition.
    - Water surface: symmetry, no parameters are needed.
    - Side walls: roughness height 0, no-slip condition.
- Solution controls for flow and turbulence:
    - Under-relaxation factors: pressure 0.15, density 1.00, body forces 1.00, momentum 0.35, turbulent kinetic energy 0.40, turbulent dissipation rate 0.40, turbulent viscosity 1.00.
    - Discretizations: pressure: standard (in multiphase computations, PRESTO has been chosen), momentum: second order upwind, turbulent kinetic energy: second order upwind, turbulent dissipation rate: second order upwind.
    - Pressure-velocity coupling: simple. (In multiphase computations, PISO has been chosen)
- Solution initialization: compute from inlet values.
- Solution initialization: patch volumes. Different initial velocities have been defined in the zone with a width of 10 meter and the zone with a width of 20 meter. This gives more stable behavior and faster convergence.
- Monitors: different residuals and the wall drag force are shown during the simulation.
- Iterate: calculate 5000 iterations. The model has been converged before this number is reached. The model stopped.

When the flow was in a steady state, sediment transport has been defined:

- Discrete phase model: no interaction with continuous phase, steady particle tracking.
- Materials: sand has been defined, with density 2650 kg/m^3.
- Injections have been defined, with a starting location, starting velocity vector, material (sand), particle diameter and diameter distribution (linear with two equal values, thus constant).
- Turbulent dispersion, stochastic tracking: discrete random walk model with random eddy lifetime. Time scale constant is equal to 0.15 (default).

Flow and particle trajectories can be analyzed.

Appendix B – Delft3D simulations with different weirs

In this appendix, the results of the Delft3D simulations for three-dimensional flow and transport over weirs are given.

The following results are presented:

- Depth-averaged velocity (m/s): page B-2.
- Erosion and sedimentation after 120 hours (m): page B-3 to B-5.

Depth-averaged velocity

All figures are scaled from 0 to 0.6 m/s, as given in the color bar below.

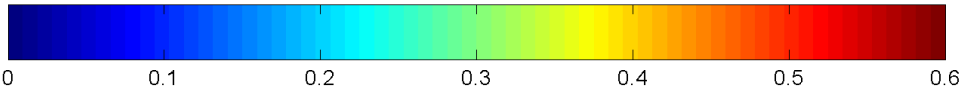

Figure B1 – Scaling of all depth-averaged velocity figures (m/s)

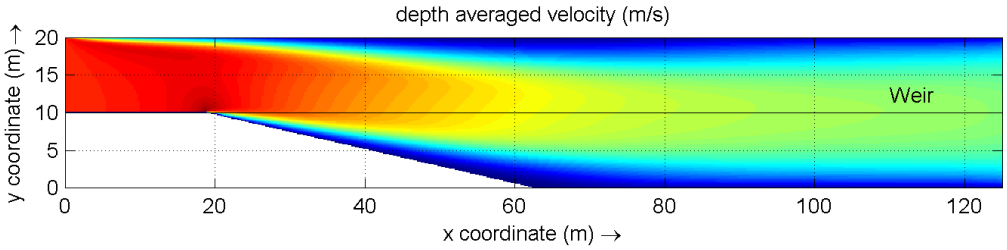

Figure B2 – Depth-averaged velocity (m/s), 2DH, 2D-weir

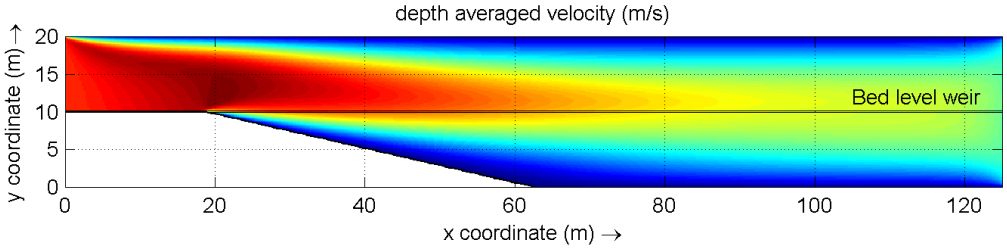

Figure B3 – Depth-averaged velocity (m/s), 2DH, bed level weir

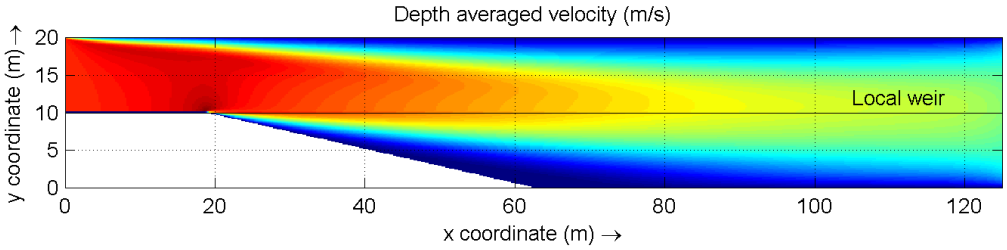

Figure B4 – Depth-averaged velocity (m/s), 3D, local weir

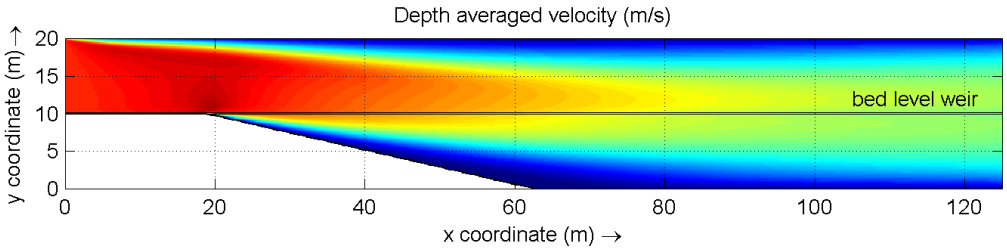

Figure B5 – Depth-averaged velocity (m/s), 3D, bed level weir

Erosion and sedimentation after 120 hours

All figures are scaled from –0.3 m (erosion) to 0.3 m (sedimentation), as given in the color bar below.

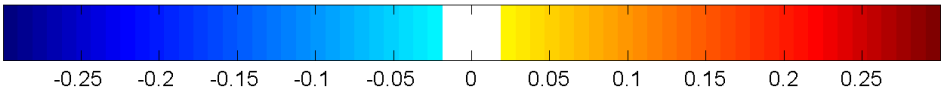

Figure B6 – Scaling of all erosion and sedimentation figures (m)

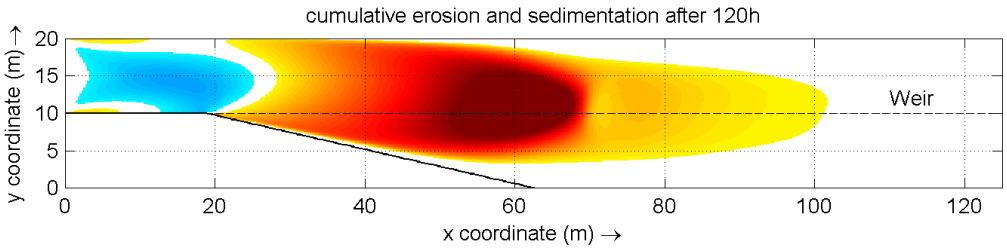

Figure B7 – Erosion & sedimentation (m), D_{50} = 100 µm, 2DH, 2D-weir, Engelund-Hansen

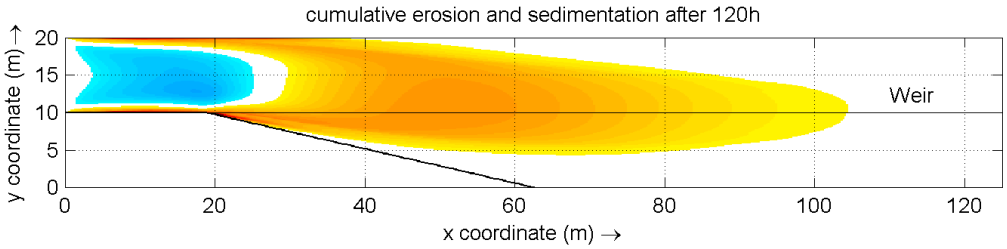

Figure B8 – Erosion & sedimentation (m), D_{50} = 100 µm, 2DH, 2D-weir, Van Rijn (1993)

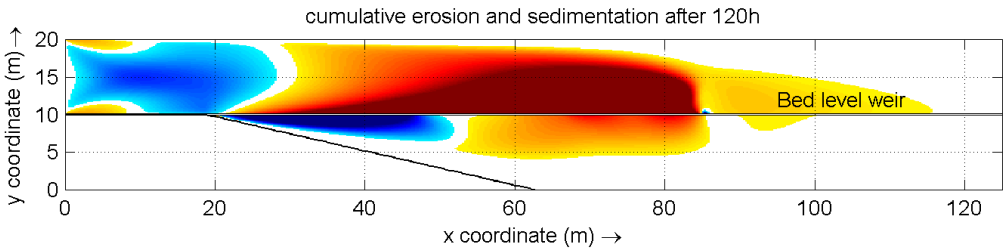

Figure B9 – Erosion & sedimentation (m), D_{50} = 100 µm, 2DH, bed level weir, Engelund-Hansen

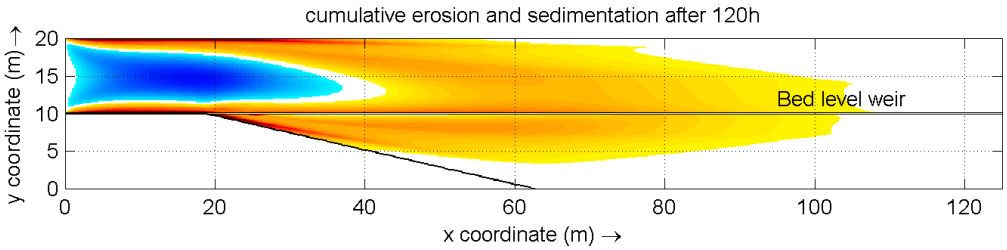

Figure B10 – Erosion & sedimentation (m), D_{50} = 100 µm, 2DH, bed level weir, Van Rijn (1993)

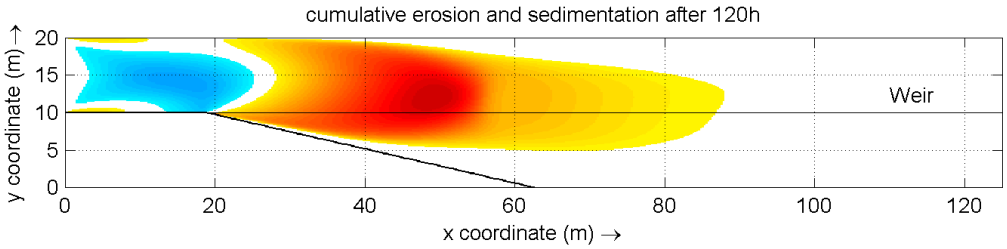

Figure B11 – Erosion & sedimentation (m), D_{50} = 200 µm, 2DH, 2D-weir, Engelund-Hansen

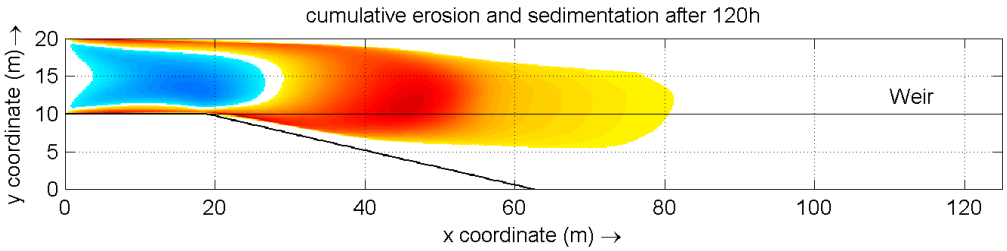

Figure B12 – Erosion & sedimentation (m), D_{50} = 200 µm, 2DH, 2D-weir, Van Rijn (1993)

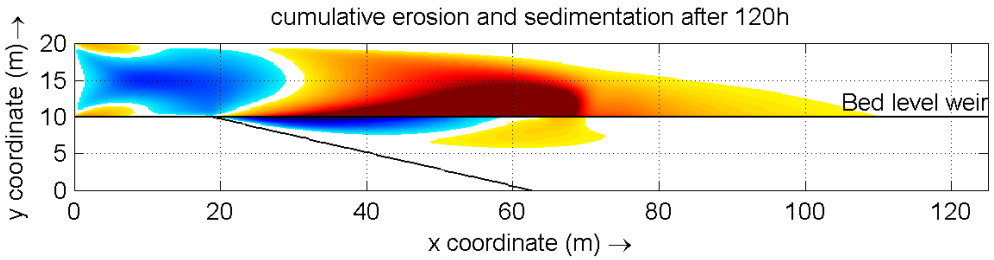

Figure B13 – Erosion & sedimentation (m), D_{50} = 200 µm, 2DH, bed level weir, Engelund-Hansen

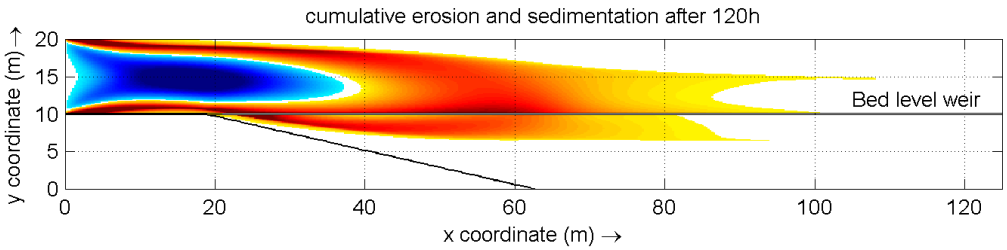

Figure B14 – Erosion & sedimentation (m), D_{50} = 200 µm, 2DH, bed level weir, Van Rijn (1993)

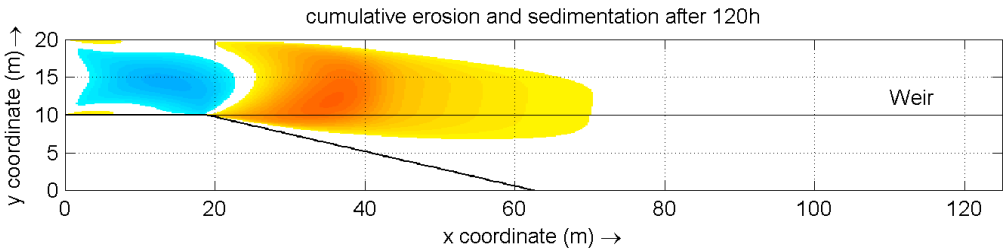

Figure B15– Erosion & sedimentation (m), D_{50} = 500 µm, 2DH, 2D-weir, Engelund-Hansen

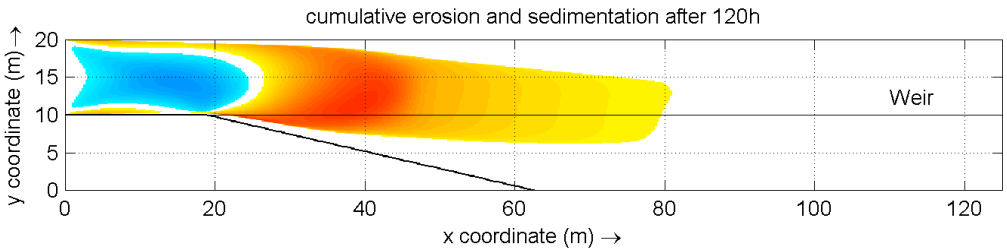

Figure B16– Erosion & sedimentation (m), D_{50} = 500 µm, 2DH, 2D-weir, Van Rijn (1993)

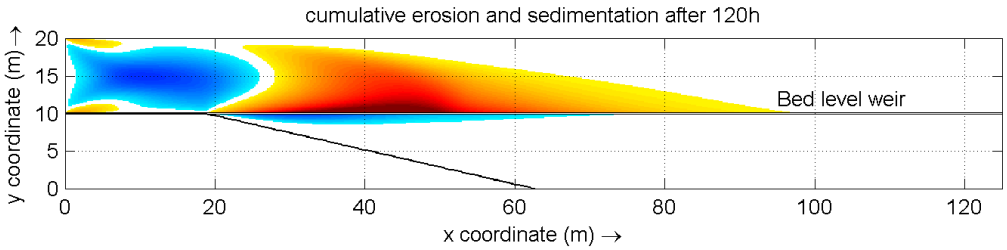

Figure B17– Erosion & sedimentation (m), D_{50} = 500 µm, 2DH, bed level weir, Engelund-Hansen

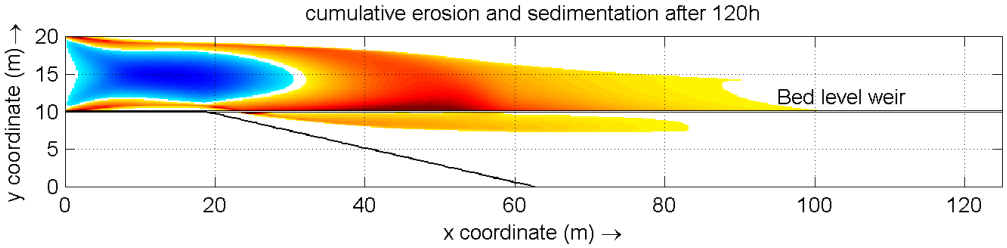

Figure B18 Erosion & sedimentation (m), D_{50} = 500 µm, 2DH, bed level weir, Van Rijn (1993)

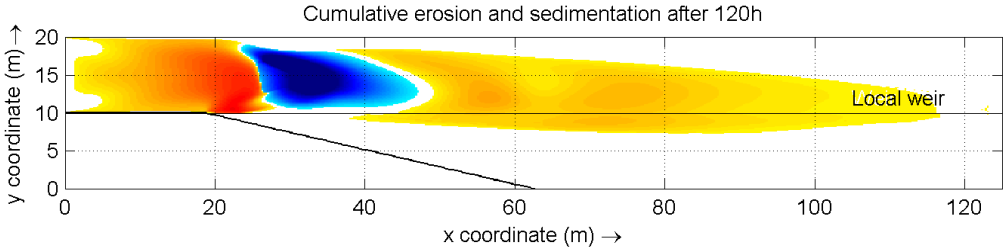

Figure B19– Erosion & sedimentation (m), D_{50} = 500 µm, 3D, local weir, Van Rijn (1993)

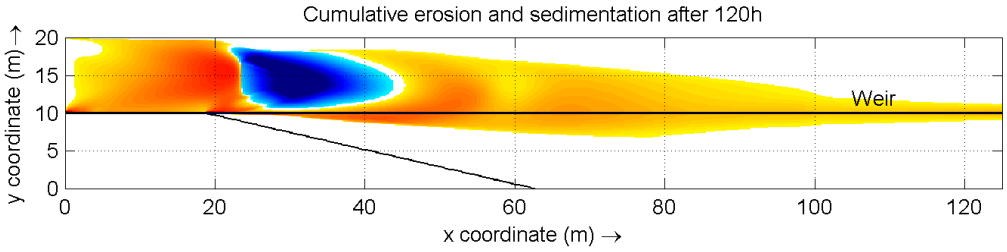

Figure B20– Erosion & sedimentation (m), D_{50} = 500 µm, 3D, bed level weir, Van Rijn (1993)